UCRL-1903 Del

UNIVERSITY OF CALIFORNIA

Radiation Laboratory

Contract No. W-7405-eng-48

NRA QUARTERLY PROGRESS REPORT

March, April, May, 1952

August 7, 1952

Berkeley, California

TABLE OF CONTENTS

1. CAVITY DESIGN

S. W. Kitchen
UCRL

A "final" drift tube table has been prepared for all but the first 30 Mev of A-12, (see UCRL-1859) based upon the design parameters given in the last quarterly report (UCRL-1774). The table is final only in the sense that it contains all the information that can be obtained from half cell studies. Since both the final adjustment of drift tube lengths required for initial field flattening and the determination of the stem positions must be done on a complete model, the table was presented in terms of a tenth scale model. The resonance data necessary to complete the table for the first 30 Mev is being obtained.

The measurements locating the positions of the whole drift tube stem and the gap splitter were completed for the high β (long drift tube) test. (UCRL-1848.) The final geometry in the tenth scale model is shown in Fig. 1.

As there was some doubt as to the accuracy of the Mark I calibration during this period, the ratio of the H field along the wall to the average axial E on the axis, as well as the ratio of the peak axial E to the average was determined by the BB technique. (See Figs. 2 and 3.) The results agreed with the former field measurements by the probe technique to within five percent, the probable error of the measurements. The peak axial E also agreed well with the distribution previously calculated by the Theoretical Group. (See Fig. 4.) It should be emphasized that this axial distribution of E does <u>not</u> represent the E distribution between drift tube surfaces.

The change from thick cylindrical drift tubes to bulbous pipes in A-12 required not only new resonance data, but also a new calculation of the sensitivity of A-12 resonance to dimensional deviations. (See UCRL-1814.) The results shown in Fig. 5 indicate the change in frequency if a cell were to be isolated, not of A-12 as a whole. This data is of interest because the axial field distribution is determined by the cumulative effects of the individual resonant frequencies of each cell.

Since large currents affect the resonant frequency of a cavity, the detuning was re-investigated by Myron Good, with consequent field deflattening effect, of a 0.5 amp beam (UCRL-1817). It was concluded that the maximum effect of the accelerated beam could be greater than 3 percent, which will not affect accelerator performance. The beam lost in the first few gaps might, however, have a noticeable effect.

Experience in Mark I may indicate that it will be advantageous to operate A-12 as a series of electrically short sections rather than as a single long resonant cavity. In a short-section machine, there is no flattening problem. Instead the problem is that of keeping the various sections in phase. This phasing can presumably be done in the absence of beam by a mechanical servo system, but if the small frequency shift caused by the beam causes sizeable rapid phase shifts, they must be tuned out electronically. Examining the phase effects of the accelerated beam, Good found that the shift was $20^\circ \pm 4^\circ$ with a maximum rate of phase shift of 3×10^{-3} degrees per cycle. (UCRL-1858.) The shift due to the lost beam will be in the opposite direction and may be much larger.

Investigation of the beam acceptance in A-12 when parameters are varied has continued on the differential analyzer. In addition to the work reported in the last quarter, the studies of the effect of varying the beam injection energy has been completed. It was found that varying the injection energy by ± 20 percent altered the acceptance by less than 5 percent. The effects of fluctuating rf level and varying the magnetic focusing are currently being examined.

During this period, the group consisted of S. A. Colgate, D. B. Cummings, M. L. Good, B. V. Hill, S. W. Kitchen, D. B. Moore and A. D. Schelberg.

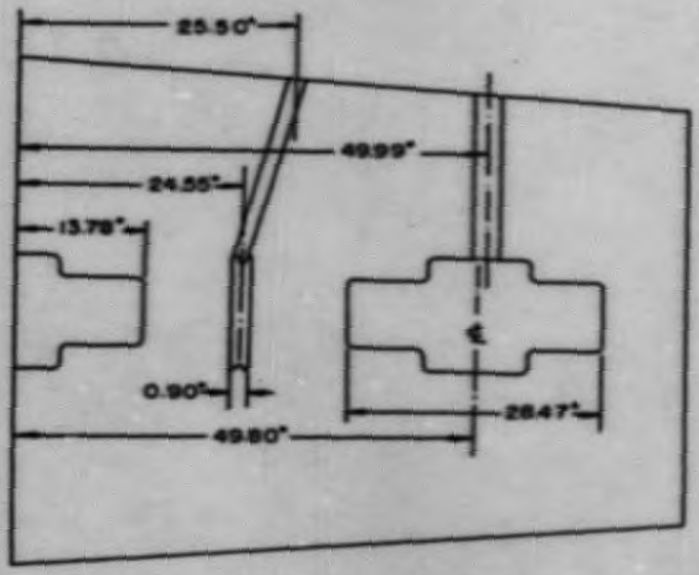

SECRET

FIG. 1 SECTION 1

MU 4118

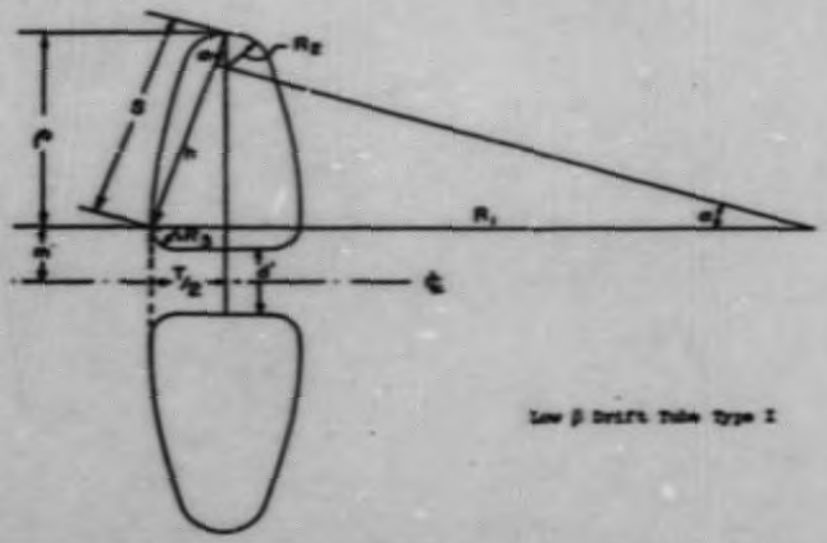

Low β Drift Tube Type I

$d = 2(a + \rho)$ = Drift Tube O.D.

d' = Drift Tube I.D.

T = Drift Tube Length

$\theta = \tan^{-1} T/2\rho$

$s = \rho/\cos\theta$

$R_1 = h/\sin\theta$

$R_2 = (s - h)/\cos\theta$

$R_3 = 0.2008'$

$a = 0.7008'$

$h = 1/2(a + \rho - T/2)$

FIG. 2 SECTION I

MU 4119

1903-7

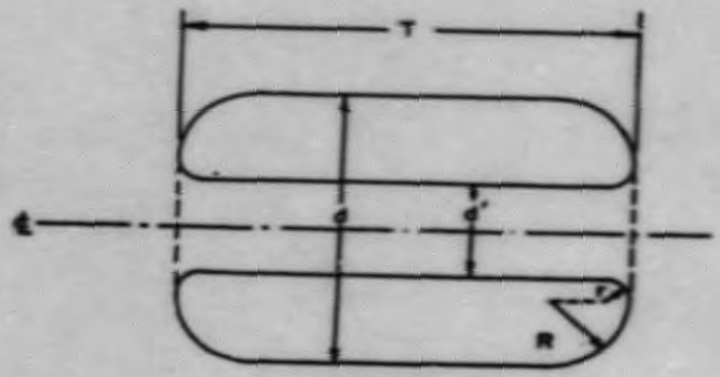

Naval Drift Tube

Dimensions For 1/10 Scale Model

d = 10.000" Drift Tube O.D.

d' = 3.400" Drift Tube I.D.

r = 0.2000" = 0.720"

R = (1/2)(d - d') - r = 2.480"

T = Length of Drift Tube (Refer to D.T. Table)

FIG. 3 SECTION I

MU 4120

1903-8

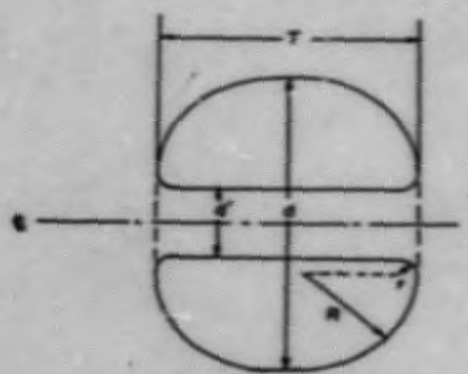

Low β Drift Tube Type II

Dimensioned For 1/10 Scale Model

d = Drift Tube O.D. (Refer to L.T. Table)

d' = Drift Tube I.D.

T = Length of D.T.

r = 0.250d'

R = (1/2)(d - d') - r

FIG. 4 SECTION I

NU 4121

SECRET

1903.9

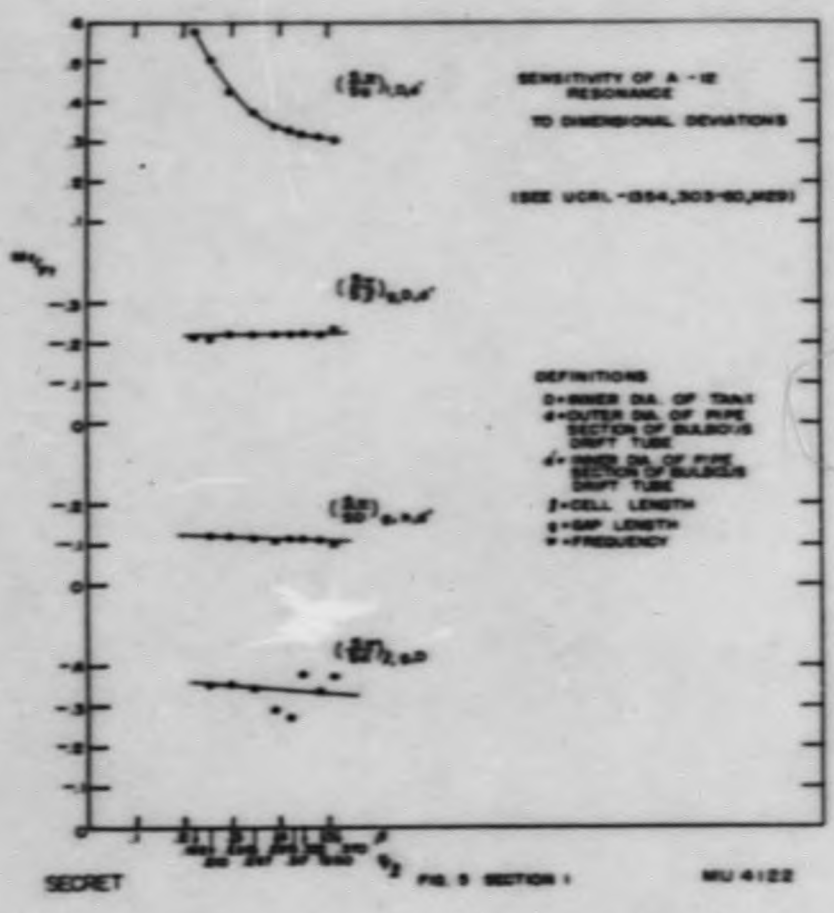

SECRET

FIG. 5 SECTION I

MU 4122

2. SPARKING AND X-RAYS IN A MERCURY PUMPED VACUUM SYSTEM

Wallace Kilpatrick
UCRL

Sparking

The most obvious conclusion about 200 Mc sparking is that it follows strictly surface gradient[1] and does not depend upon total voltage. In order to arrive at this conclusion, a quantitative means for measuring the probability of sparking had to be constructed, since it was clearly evident that the d.c. notion of sparking was inadequate. Counting equipment previously described[2] was used to establish that, at constant gradient

$$\frac{dn}{dt} = n^{-K_1}, \qquad K_1 \gg 0 \tag{1}$$

where K_1 is a constant, n is the number of sparks accumulated prior to time t, and dn/dt is the sparking rate. When sparks occurred using copper electrodes, there was no exception to equation (1) for all surface gradients up to 0.82 Mv/cm, where 3.3 in. < gap < 8.75 in. Higher gradients were not available because of rf power limitation. When dn/dt decreased a few orders to one spark in fifteen minutes, the corresponding n was defined as N. N was then interpreted to be the inherent number of sparks required before sparking ceased to exist at that gradient. It was then found, by using various surface and gap geometries, that N could be calculated for copper on a gradient basis for $1 < N < 10{,}000$, using the expression,

$$N = \left(\frac{E}{E_o}\right)^2 \cdot e^{\alpha\left(1 - \frac{E_o}{E}\right)}, \quad \alpha = 4.9$$

where E is surface gradient in Mv/cm, E_o is defined as the threshold or surface gradient at which sparking first occurs.

If E varies over an electrode surface, Eq. (2) takes the form,

$$N = \frac{1}{A_o}\int \left(\frac{E}{E_o}\right)^2 \cdot e^{\alpha\left(1 - \frac{E_o}{E}\right)} dA, \quad \alpha = 4.9 \tag{3}$$

---

1. Surface gradients were measured by A. Schelberg, using the BB technique.

2. W. Kilpatrick, UCRL-1573, 5, (1951).

where A_o is the area affected by E_o for sparking, and the limits for integration are governed by the extent of $E \geq E_o$. The agreement of the calculated N with measured N is shown in Fig. 1. Four of various copper geometries used for field configuration are given in Table I.

Table I

Case	Surface	Maximum Surface Curvature	Electrode Diameter	Gap	Maximum Recorded E	Maximum Recorded V	E_o
A	Elliptical		7.5"	8.75"	0.20	2.75	0.097
B	Stove-pipe	0.021"	5.5"	8.75"	0.37	2.1	0.068
C	Hemisphere	0.500"	1.0"	3.30"	0.82	2.45	0.187
D	Stove-pipe	0.031"	1.0"	3.30"	0.53	1.7	0.119

where E and E_o are in Mv/cm, and V is in Mv. It should be emphasized that E_o in all cases was made as high as possible by careful cleaning, the use of phosphoric acid deplating, and avoiding dust. To establish Eq. (1) as dependent only on the number of accumulated sparks, an overvoltage technique was used.[3] At constant gradient, the sparking rate was allowed to diminish; the gradient was increased in order to spark more rapidly; then the gradient was decreased to the original value. The subsequent sparking rate was predicted precisely by Eq. (1).

Expressing Eq. (1) in terms of time predicts that

$$\frac{dn}{dt} = \tau^{-1} \qquad (4)$$

This relation was verified experimentally, as far as the statistics of low sparking rates would allow.

Since sparking was gradient dependent, and since very high x-ray intensities (presumably electronic in origin) accompanied the sparking, it was not surprising to find that the charge transport for discharging the majority of stored energy was electronic.[4] To infer this, x-ray intensity was calibrated against an auxiliary electron current directed across the gap, and the amplitude of the x-ray bursts during a spark was measured. The data indicated that electronic transport was sufficient for discharge of the stored energy. The gap at the time of these measurements was 3.3 in.; the

3. This procedure was previously used to reduce sparking, W. Kilpatrick, UCRL-1573, 5 (1951).

4. The same conclusion was inferred for B-1. C. S. Wuman, UCRL-1573, 12, (1951).

gap voltage was 1.5 Mv; and two rf cycles were apparently the main time-component of the x-ray bursts during a spark.

X-Rays

A correlation (apparently independent of voltage or gradient) between x-ray background and initial sparking rate was previously reported.[5] In addition, it has been found that minimum measurable x-ray intensities (about 0.5 mr/hr) occur at the sparking threshold, E_0. X-ray background intensity at constant voltage seems to require the same relation as sparking at constant voltage, namely

$$\frac{dR}{dt} = R^{-a \cdot E_2}, \quad E_2 > 0, \quad a = 1 \qquad (5)$$

where E_2 is a constant, R is the accumulated roentgens, and dR/dt is the rate. E_2 for x-rays was less than E_1 for sparking (order of 1:1000). Moderate heating of the electrodes (rf heating for example) apparently affects Eq. (5) slightly. The effect was not measured, but a suggested modification is that $a = 1 + f(T)$, where T is the electrode temperature. At this stage in the experiments, it appeared that x-rays and sparking were similar phenomena — differing only in magnitude of electronic charge transport. At present, it is felt that no contradictory evidence to this statement has been obtained.

Experimental Results

Various metals were used for electrodes. Each metal indicated a finite number of inherent sparks. For comparison only, the approximate results are summarized in order in Table II for samples having the same gradient on a one inch diameter hemispherical surface.

Table II

Material	E_0	Inherent Sparks	Initial Spark Rate	Initial X-ray Intensity
Rh	0.39	400	151	0.02
Cu(OFHC)	0.27	250	30	0.5
Cu	0.18	1250	350	2.0
Au	0.28	1300	134	3.0
Cr	0.25	1600	127	0.5
Mo	0.25	2300	306	14.0
Invar	<0.20	2900	-	4.0
Cu-O	0.26	>2000	80	0.8
Al	0.20	56000	455	2.0
Sn	0.25	8000)	121	1.5
Graphite	0.08	10000*	>5000*	20.0*

5. W. Kilpatrick, UCRL-1680, 7, (1951).

The voltage for x-ray and spark data listed was 2.3 Mv across a gap of 3.3 in. for all cases except graphite. The voltage for graphite[5] was 1.0 Mv and could not be increased, apparently because of extreme "electron loading".

Rhodium seemed to be the most desirable metal for few sparks and low x-ray background. The sample listed above was a plating of about 0.1×10^{-3} inches of Rh on a plating of about 0.1×10^{-3} inches of Ni on solid copper. It is felt that if a thicker coating of Rh could have been obtained, the inherent sparking would have been less than OFHC copper. Mo had a very high initial x-ray background which decreased fairly rapidly toward the level of copper or chromium. Mo however, was easily recontaminated by air—just relieving the vacuum with air and then pumping down immediately sensibly returned every inherent spark that had been previously removed. Mo was the only metal used which was so completely recontaminated by air. When oxidized copper[6] was used, the initial sparking rate and x-ray level was low. Increasing the voltage, however, to approximately 2.1 Mv (corresponding surface gradient 0.72 Mv/cm) apparently broke away parts of the oxide coating and a large increase in sparking rate ensued. Invar became cherry-red as a result of energy dissipation. Al showed clean-up tendencies above threshold sparking, but at one particular gradient, an unusually large number of sparks occurred—similar to copper oxide, just described. After the large number of sparks had been run out from one small spot, the Al behaved normally like Cu or Cr, and cleaned up. The total number of sparks in the Al was 56,000; of this total, approximately 53,00 came from the small spot. Sn behaved like Al. Carbon in the form of graphite was a prolific emitter even when outgassed, but exhibited the same tendency to clean up as did the metals.

In order to include the sparking behavior of Sn and Al as well as to anticipate a similar behavior for copper, Eq. (1) should be modified in such a way that the constant K_1 is unaffected by the abnormal flurry of sparks at a critical gradient. An expression which seems to apply is:

$$\frac{dn}{dt} = (n - n_0(E,A))^{-K_1}, \quad K_1 \gg 0 \qquad (6)$$

where n_0 is the unusually large number of sparks (or flurry) which depend on a critical gradient and/or critical area. For all observations using copper, it should be emphasized that $n_0(E,A) = 0$ for gradients up to 0.83 Mv/cm.

A "damage" experiment was conducted using Sn-coated electrodes. (The melting point of Sn is 231° C.) The geometry of these electrodes was asymetric—a blunt point facing a nearly plane surface. It was demonstrated that the electron emitting surface was damaged during the actual spark, and that no visible damage occurred to the electron bombarded side. To clarify the geometry, the electron emission came from the point, the x-rays came from the plane, and the point was damaged.

---

6. Previously described. W. Kilpatrick, UCRL-1680, 7, (1951).

A spectrographic analysis of the "cathode" light associated with a spark was attempted. A very sharp, pointed copper electrode was observed through the bore of a stove-pipe electrode. The approximate condition for sparking was: surface curvature 0.1 mm, 0.4 Mv, 4 in. gap, surface gradient 20 Mv/cm. The results of this experiment were not considered useful in interpreting normal sparking. However, four clear observations were made: Spectral analysis of "cathode" light is possible; copper spectra was present and originated at, or very near, the point electrode; glow-discharge using air presented a molecular spectrum; the "cathode" light was probably associated with electron emission effects and not with ions crossing the entire gap. The argument for ions not crossing the entire gap is based on divergent field near the point, transit time for ions, and the fact that visible light was restricted to a very small region about the point.

Spark Mechanism

The general problem concerning rf and d.c. sparking is to obtain a minimum sparking rate. In order to accomplish this, an exact knowledge of the initiation mechanism seems required, and events which are subsequent to initiation should be relatively unimportant. Events leading up to and including the major charge transport are considered here as spark initiation. There seems to be an advantage in using rf for such an investigation because ion transit time is a small contributing factor. It is felt that there is much information, both rf and d.c., which could be used to construct an adequate initiation mechanism, but that it is not sufficient at present. The following facts are intended to clarify the important points concerning this initiation phase.

1. There is a definite threshold gradient (E_o) for sparking a given metal in a practical vacuum system.

   a. D.c. - J. W. Beams, Phys. Rev. 44, 803, (1933). Using a liquid mercury cathode and stainless steel anode, the breakdown voltage was critical and could be changed slightly with the purity of the mercury.

   b. 200 Mc - First part of this report. Using a threshold hypothesis, an analysis of the sparking could be made.

2. Higher electron emission currents are produced during spark initiation than can be accounted for by field emission alone.

   a. D.c. - W. P. Dyke, Field Emission Seminar Abstracts, Linfield College, Oregon, (1952). The theoretically derived relation of Fowler and Nordheim for field emission was confirmed experimentally over a wide range of gradient (up to about 300 Mv/cm).

b. D.c. - J. W. Beams, Phys. Rev. 44, 803, (1933). Calculations show that sparking occurs with large electronic currents when the surface gradient will allow 1 electron/cm^2/sec.

c. D.c. - J. P. Blewett, Phys. Rev. 81, 305(A), (1951). An oil-like Malter layer will allow measurable electron current at 10 - 300 Kv/cm.

d. 200 Mc - First part of this report. Sparking can occur at a surface gradient of less than 100 Kv/cm, and large electron currents accompany the spark.

3. The major charge transport is electronic.

a. D.c. - Hull and Berger, Phys. Rev. 11, 1121(A), (1928). Electrons are emitted first and secondary effects involving ions apparently depend upon low voltage after the major electron discharge.

b. D.c. - H. W. Anderson, Am. Inst. Elec. Eng. 54, 1315, (1935). A fraction of the total conduction is attributable to ions, and their principle effect as to increase electron emission at subsequent lower gradient.

c. 12 Mc - C. S. Nunan, UCRL-1573, 12, (1951). The inference from work with the 12 Mc cavity was that the major charge transport for sparking was electronic. There also seems to be supporting evidence from "crowbar" experiments.

d. 200 Mc - First part of this report. The inference is made from x-ray intensities, that the transport is electronic.

4. X-rays, sparks, and "drain" are a similar if not identical phenomena as far as initiation is concerned.

a. D.c. - W. H. Bennett, Phys. Rev. 37, 582 (1931). Observed relatively large current premature to breakdown suggesting the possibility of time distribution of "drain".

b. D.c. - H. W. Anderson, Am. Inst. Elec. Eng. 54, 1315, (1935). It was shown that pre-breakdown currents (drain) required the same "total voltage effect" for varying gap as previous investigations found for sparking.

c. 200 Mc - First part of this report. Sparks and x-rays appear identical except in the magnitude of charge transport.

5. The electron emitting surface can be damaged by sparking.

a. D.c. - R. Haefer, Z. Physik 116, 604, (1940). Observations with an electron microscope indicated that for experiments in a residual gas atmosphere of argon at a pressure of about 10^{-5} mm, the sharpness of emitting points may be increased as pre-breakdown current flows. Haefer was able to melt these points by increased field emission currents.

b. 200 Mc - First part of this report. Sn(MP. = 231° C) was used.

6. Ions are not required to cross the entire gap for spark initiation.

a. D.c. - W. H. Bennett, Phys. Rev. 37, 582, (1931). Using a magnetic field it was shown that positives from the anode have questionable influence on the initial cathode emission.

b. 12 Mc - C. S. Numan, UCRL-1573, 12, (1951). A theoretical analysis of ion trajectories showed that it is impossible for ions to migrate toward the higher field electrode of the 12 Mc cavity.

c. 200 Mc - First part of this report. Sparks occurred from small radius of curvature surfaces, and the theoretical ion trajectory argument of 12 Mc holds.

7. The sparking rate at a given voltage diminshes with time and/or the number of sparks.

a. This seems to be generally observed at all frequencies including d.c., with the provision that the vacuum system be moderately free of contamination including oil.

8. Localized gas pressure can induce sparking.

   a. D.c. - H. Heard and E. Lofgren, UCRL-1680, 22, (1952). Although an experiment was not described that specifically induced sparks, observations indicate an exponential increase in gas pressure which could be associated with "drain" and sparking.

   b. 200 Mc - W. Kilpatrick, UCRL-1774, 9, (1952). Sparks were induced when gas was admitted through a hole (diameter ≈ 0.040 in.) in one electrode. Without regard to the kind of gas used, a local pressure of about 10^{-1} mm was required.

9. Gradient and not VE is the criterion for rf sparking.

   a. D.c. - L. Cranberg, Jour. App. Physics, 23, 518 (1952). This article presents literature and evidence for VE - const., or the fact that a "total voltage effect" exists for d.c.

   b. 200 Mc - First part of this report. Gradient is of prime importance, indicating that the "total voltage effect" of d.c. is secondary to initiation.

   c. 2800 Mc - Halpern, et al., Phys. Rev. 69, 688(A), (1946). 2.0 Mv was supported across a 2.0 in. gap, resulting in a higher VE product than would be expected from d.c. experience.

10. The work function concept is inapplicable in that "drain" or x-rays have a distribution in time, and a time average of these discontinuities does not meet the conditions for the Fowler-Nordheim type of field emission.

    a. References are similar to item 4, above.

    b. H. G. Heard and E. J. Lofgren, UCRL-1680, 22, (1951). A field emission microscope indicated an emission current with a time distribution.

11. Local pin-point gradients is an inadequate argument for enough primary electron field emission current to dissipate the stored energy in a spark.

    a. References are similar to item 2.

12. Different base metals do not change the sparking threshold nor the subsequent sparking rate radically.

    I. Corollary. Cleaning before installation in the vacuum system is more noticeable than changing base metals.

    II. Corollary. Metallurgically or chemically pure metals decrease the sparking rate slightly as compared with commercially available metals.

13. Visible light is associated with the electron emitting surface during a spark.

    a. D.c. - No evidence.

    b. 200 Mc - First part of this report. The visible light is capable of spectrographic analysis.

14. An electrostatically biased gap-splitter can change the x-ray background.

    a. D.c. - No evidence.

    b. 200 Mc - W. Kilpatrick, UCRL-1680, 7, (1951). This observation is interpreted to mean that ions not crossing the gap can affect x-rays and spark initiation.

15. Spark initiation is not affected by the temperature of the electrodes up to thermionic emission.

    a. D.c. - A. J. Ahearn, Phys. Rev. 50, 238, (1936). Experiments indicate that on clean surfaces of Mo, W, and thoriated tungsten there is no field current temperature effect nor temperature effect on voltage breakdown. Also, anode heat-conditioning in a sealed tube indicated no affect on voltage breakdown.

    b. 200 Mc - W. Kilpatrick, UCRL-1573, 5, (1951). Heating copper electrodes to about 800° C for several hours did not change the x-ray intensity background markedly.

16. Ions can be produced in the immediate neighborhood of the electron emitting surface.

    a. D.c. - Trump and Van de Graaff, Jour. App. Phys. 18, 327, (1947). The evidence is not conclusive, but it may be inferred that residual gas may be ionized with about 2 Kv electron energy at the rate of 9 positive ions to one electron.

b. 200 Mc - No evidence, but strongly suspected as a phase in the construction of a local Malter layer on the cathode.

17. I^2R heating occurs in the electron emitting surface due to electron emission.

a. D.c. - W. W. Dolan, Field Emission Seminar Abstracts, Linfield College, Oregon, 1952.

b. 200 Mc - No evidence.

18. Sparks are not spontaneous, and require a finite time for the initiation phase.

a. D.c. - Many references.

b. 10 Mc - R. Birge, E. Lauer and E. Lofgren, UCRL-1680, 15 (1951). X-rays apparently built up in B-1 for at least 3 cycles as a prelude to a spark.

Acknowledgements

The author wishes to thank the following people for their assistance in this investigation: S. W. Kitchen, D. D. Cudaback, and J. V. Franck, for many helpful discussions on the interpretations which could be attached to the experiments at 200 Mc; H. A. Ahrens and K. W. Ehlers for their experimental techniques and assistance; V. McIntosh and D. Parmentier.

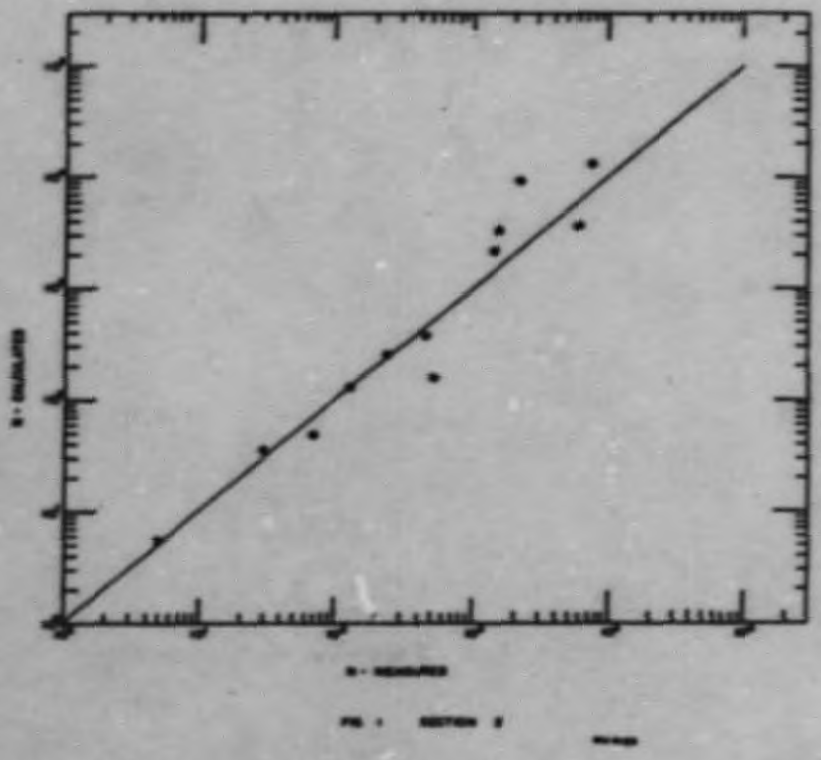

Agreement between measured and calculated number of sparks from copper. Using the relation

$$y = \left(\frac{E}{E_0}\right)^2 e^{-\alpha\left(1 - \frac{E_0}{E}\right)}, \quad \alpha = 4.9,$$

for various field configurations.

3. DRIFT TUBE CLEANING TECHNIQUE

J. E. Griffith
UCRL

General

The necessity for cleaning the surfaces of all Mark I drift tubes was established as a result of data taken from the 200 Mc cavities (B-2, B-3, B-4) and the 12 Mc cavity (B-1) during the course of an investigation of field emission.* Electrons emitted due to the radiofrequency electric field at the drift tube surface are known as field emission electrons. These stray electrons produce the following effects:

a. Electron loading which wastes oscillator power in accelerating the electrons across the gap.

b. X-rays, which are produced when the accelerated electrons strike a surface.

c. Sparks, which are initiated by the electrons.

Various cleaning techniques were tried on scale model drift tubes in the 200 Mc cavities, and one guiding principle was established: That one cannot get a sufficiently clean copper surface without removing a thin layer of copper from the surface itself. This implies that the impurities remaining on a worked copper surface cannot be wholly or satisfactorily removed by external means. Thus, it is necessary to remove a thin layer of copper from a given surface in order to remove the contaminants adhering to it. This reduces the problem to the design of a method to remove the outer (contaminated) layer of copper without introducing new contaminants to the underlying surface.

Inasmuch as present theory is inadequate to predict the results of any given surface treatment, the final authority must rest with the results of rf tests. The 200 Mc cavities were used at Berkeley for tests of most of the cleaning methods, but a 13 Mc cavity is preferable in order to eliminate possible frequency dependencies. This means that no further research on cleaning methods can take place, nor can any changes be made in the present method, until such rf testing equipment is available.

---

* cf. Previous MTA Quarterly Progress Reports.

Techniques

Several methods are available for the removal of a thin layer of copper from a surface: 1. Glow discharge and sparking. 2. Mechanical. 3. Chemical. 4. Electrochemical.

1. The Glow Discharge and/or Sparking Method. This method is not fully understood, and in any case is too slow to use as a preliminary technique prior to the initial installation of the drift tubes. At present, glow discharging and/or sparking is considered to be a desirable treatment after the vacuum is established, and the machine is ready for operation.

2. The Mechanical Method. Mechanical methods, involving the use of abrasives or scraping, leaves an amorphous copper surface which is porous. The porosity of the surface is not desirable because it serves as a potential collector of oil, dust, etc., some of which will probably outgas in vacuum and be difficult to remove in the future. Also, surface contaminants originally present may be covered by the smeared metal and hence be very difficult to remove.

3. The Chemical Method. The chemical method consists in treating the copper with a strong oxidizing solution and washing away the acid and water soluble oxidation products with clean water. The best solution for this treatment seems to be a mixture of concentrated nitric and glacial acetic acids in the ratio of 1 part nitric to 2 parts acetic by volume. This should be used on a dry surface but sometimes works better on a wet surface, depending upon the history of the surface. A 90 percent (by volume) solution of nitric acid and water works almost as well, but the resulting surface seems to have more copper oxide upon it.

After treatment with either solution, the surface is washed with an excess amount of water and then treated with absolute ether or absolute ethyl alcohol (95 percent) to dry the surface without excessive oxidation. Chemical drying is necessary because the surface will oxidize if allowed to dry in the presence of water.

The use of either solution will produce a clean copper surface in which any occlusions present will be voided of all residue. The surface produced will oxidize rapidly unless protected from the atmosphere.

This method has one disadvantage which makes its use difficult on large surfaces. Large amounts of noxious fumes (NO_2) are given off, and unless controlled, will pass over previously cleaned areas in the vicinity and produce a heavy oxide coating on such cleaned surfaces. The control of these fumes on a large scale must be very good, because they are strongly oxidizing with respect to copper, and small concentrations in the atmosphere will easily oxidize any clean surface with which they come in contact.

Copper oxide is not known to be electrically harmful, but since it is porous, it is not desirable from a vacuum viewpoint.

4. The Electrochemical Method. This method consists of placing the surface to be cleaned in an electrical circuit such that it is an anode with respect to another electrode and filling the interelectrode space with a suitable electrolyte to carry the current necessary for the cleaning action. The cleaning action consists of deplating a thin layer of copper from the surface to be cleaned. The deplated metal is deposited upon the cathode in the form of higher oxides of copper.

This method is slower than the chemical method, but it is much easier to control, and none of the parameters are critical, hence the reason for its choice in this case.

The Electrochemical Method as Used on Mark I Drift Tubes

The sequence of the different phases of the cleaning cycle was as follows: 1. Trisodiumphosphate (TSP) wash. 2. HNO_3 burn. 3. H_3PO_4 deplate. 4. H_2O wash. 5. Alcohol rinse. 6 Drying period. 7. Wrapping. Each of these phases will be described in detail.

The complete cycle of cleaning and wrapping took place in a special wash house erected in Bldg. 51. This wash house was built large enough for a drift tube to hang completely inside it. Movable scaffolding allowed access to any portion of the drift tube as it hung inside the wash house. The main purpose of the wash house was to allow the drift tube to be cleaned in a clean atmosphere. Experience has shown that the air in Bldg. 51 was contaminated by oil fumes and that a clean surface could not be produced in the presence of such air. The wash house was supplied with its own filtered air supply system such that the intake and exhaust of the system was vented to the outside of Bldg. 51. The air was changed completely twice per minute. The walls of the wash house were made of Flexboard* panels, and all seams were taped to prevent mixing of the wash house air with Bldg. 51 air.

During the entire cleaning procedure, the drift tubes were pressurized with 3 psi of filtered air to prevent possible acid seepage to the drift tube interior.

1. TSP Wash. The drift tubes were delivered with an abraded finish produced by sanding wheels. The purpose of the TSP wash was to remove excess grease and dirt from the sanded surface. The whole drift tube surface was scrubbed with cellulose sponge mops soaked with a saturated solution of TSP. The drift tube was then washed well with tap water. This phase required about 45 minutes for No. 8 drift tube. The TSP must be technical grade or better.

* Manufactured by the Johns-Manville Company.

2. HNO_3 Burn. The purpose of the HNO_3 "burn" was to remove the excess of smeared copper left by the final sanding operation. A solution of 90 percent (by volume) HNO_3 was sprayed on a wet patch of surface with an atomizer constructed for the purpose. After the HNO_3 had stood for 1 or 2 minutes, the surface was flushed with water and inspected to see if all of the amorphous copper had been removed and if all the oil spots were removed. Oil spots can be detected by the presence of water breaks while the water stands on the surface. This process was repeated until all of the surface was free of smeared copper, and there were no water breaks present.

At the finish of this operation, the surface is covered with dark brown and black copper oxide stains which will be removed during the deplating phase.

This phase required about one hour for No. 8 drift tube. The HNO_3 must be reagent or C.P. grade.

3. H_3PO_4 Deplate. The purpose of the phosphoric acid deplate is to produce the final cleaned surface. The deplating action accomplishes two things. It rounds off the sharp edges of the copper crystals which are exposed by the HNO_3 burn, and it removes a very thin layer of copper from the surface. The dark copper oxide stains are removed in process. It is safe to leave the H_3PO_4 lie on the surface since H_3PO_4 will not attack copper.

Great care must be taken to insure that no oil spots are left on the drift tube before beginning the deplating. It is impossible to deplate copper through an oil film on a surface unless it is extremely thin. This is the principal reason for treating the drift tube surface with TSP as a preliminary procedure.

The deplating is accomplished by the use of a special hollow copper probe. This probe (see Fig. 1) was constructed with many small (1/16 in.) holes drilled through the bottom face and a 3/8 in. RL fitting soldered to the top of the probe. The probe was screwed by means of the RL fitting into a probe handle made of hollow copper tubing which in turn was attached to the manifold of a liquid supply system which supplied H_3PO_4 solution to the probe in a continuous stream. Glass beads were affixed to the probe to act as insulating spacers between the probe and the drift tube surface. A welding generator was connected between each probe and the drift tube.

In operation, the H_3PO_4 supply to each probe was adjusted by means of a valve and the probe was positioned with the glass beads resting on the drift tube surface. The probe was pushed slowly across the surface while the welding generator supplied the deplating current. It was found experimentally that a current density of approximately 25 amps/in^2 of probe surface at 25-30 v d.c. was optimum.

Probes were constructed with variously curved faces to fit different drift tube curvatures.

A great excess of H_3PO_4 was supplied to each probe, and the run off from the drift tube was collected in a stainless steel basin and recirculated to the probe supply manifold. All of the pipe used in the acid recirculating system was either stainless steel, copper, or Pyrex. The pump was a stainless steel centrifugal pump with a special acid proof packing made of shredded teflon.

Although teflon was the only plastic permitted in the recirculating system, spray shields attached to the probes were made of sheet polyethylene.

H_3PO_4 will leach excess polymerizer out of all plastics except teflon, but the effect is very slow for polyethylene. Consequently, plastics were used only where absolutely necessary. The only plastics used were teflon (gaskets, packings), sheet polyethylene, and polyethylene scotch tape, or electroplaters tape.

The tape was used to bind the polyethylene spray shields onto the probes. This tape must never be used where the adhesive is exposed to the H_3PO_4; only the "back" (the normally exposed side) of the tape may be exposed to the acid.

The H_3PO_4 concentration was 21 percent by weight, but the value was not critical and could be allowed to go as high as 25 percent. The H_3PO_4 must be of N.F. (National Formulary) grade or better. At the end of a deplating phase, the H_3PO_4 was discarded and new H_3PO_4 was used for the succeeding drift tube.

The deplating phase lasted until all of the dark stains remaining from the HNO_3 burn were removed. In case any patches of smeared metal accidentally remain, these must be removed before the phase is finished.

It is important during this phase of the cleaning cycle to keep all of the drift tube surface wet with H_3PO_4 solution while the deplating is proceeding. If the H_3PO_4 solution is allowed to dry on any part of the surface, a white stain appears and is not removed by rewetting of the surface. The stain is insoluble in H_2O, H_3PO_4, and alcohol, and can be removed only by further deplating of the surface.

4. H_2O Wash. This wash is necessary to remove all traces of the H_3PO_4 solution. H_3PO_4 is not very soluble in H_2O and excess H_2O must be supplied for at least 30 to 45 minutes to insure complete removal. It is likely that the mechanical action of the H_2O is most responsible for the cleanliness obtained, since a jet of H_2O directed at the surface is better than a steady flow of H_2O over the surface. During this phase, it is imperative that no part of the drift tube surface be allowed to dry.

If the washing is not thorough, white stains of H_3PO_4 will appear when the drift tube finally dries. Distilled H_2O must be used. The smallest drift tubes (Nos. 0 and 9) were washed for 20 minutes and No. 8 drift tube was washed for 45 minutes. The time was prorated for drift tubes of intermediate size. The water flow was about 10 gpm.

5. Alcohol Rinse. The object of the alcohol rinse was to remove the water remaining after the washing was finished. If the drift tube is allowed to dry with H_2O on the surface, excessive copper oxide appears.

Absolute ether is preferable to alcohol, but the fire hazard precludes its use on a large scale, so absolute ethyl alcohol (95 percent) as substituted. Methyl alcohol and acetone are not acceptable because they leave residues. About 20 gallons of alcohol was sprayed on No. 8 drift tube and 12 gallons on No. 0 and No. 9, with prorated amounts on the intermediate sized drift tubes.

6. Drying Period. The drift tube was allowed to dry completely after the alcohol rinse. Preferably, 24 to 48 hours should be allowed for this period in order to insure complete drying. Sometimes, H_3PO_4 will ooze from fine pits in the copper surface, and this must be removed before wrapping, or the wrapping paper will stick to the surface.

7. Wrapping. After the drift tube was dry, it was wrapped with crinkled uncoated kraft paper much in the manner of wrapping an automobile tire. The paper is wrapped until it is at least two layers thick over all of the drift tube surface. It is permissible to use scotch masking tape to bind the paper to itself at the finish of the wrapping phase. During the wrapping, all handling was done with clean cotton gloves.

After the paper wrapping was secured, a special polyethylene bag was drawn over the whole drift tube and secured tight around the drift tube neck. This bag was used to protect the drift tube surface from oil and dust; the paper is not sufficiently impervious to protect the surface more than an hour or two without the polyethylene bag.

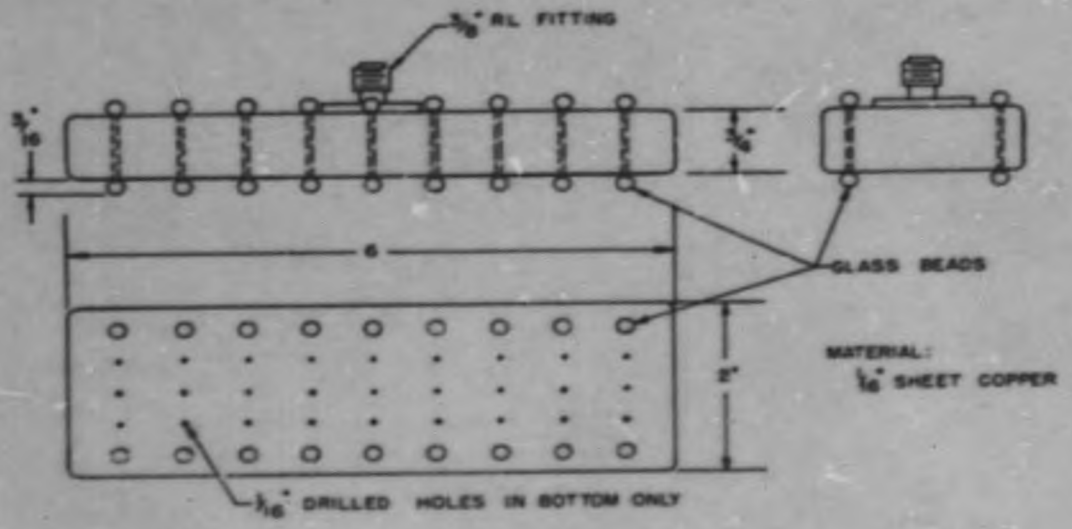

SECRET

FIG 1 SECTION 3
DEPLATING PROBE MU 4124

1903-28

4. X-RAY MONITOR VACUUM SPARKS AND RF DECAY

H. G. Heard, E. J. Lauer and R. W. Birge
UCRL

Introduction

A study has been made of the spark phenomena and rf decay of the Livermore accelerator. No control of total voltage or magnet current was exercised during operation. Photographic results show that the configuration of an x-ray burst is not changed with increasing voltage or the application of the magnetic field. The sparking rate and therefore the number of x-ray bursts increases at higher voltage.

Method

X-Ray Output. X-ray output under normal operation and during sparking has been monitored with a stilbene crystal photo-multiplier combination utilizing fast amplifiers (see Fig. 1). Time dependent phenomena were photographed from a 5XP11 cathode ray tube in either a 513D or 517 Tektronix oscilloscope. The photo-multiplier was located on the north side of the accelerator in line with the gap between drift tubes No. 7 and No. 8. The output of the terminated photo-multiplier was differentiated (approximately 5×10^{-9} sec.) at the metering area, amplified and then divided so that a signal triggered sweep was initiated with a signal delay of approximately 250×10^{-9} sec. The pulse response of the two cascaded Hewlett-Packard 100 mc. per sec. bandwidth amplifiers is less than 5×10^{-9} sec. with a total delay of $15\text{-}20 \times 10^{-9}$ sec. per amplifier.

Rf Envelope Decay. In measurements of the rf envelope decay, amplifier and cable delays were measured and matched electrically with a 5×10^{-9} sec. rise time mercury pulser (see Fig. 2). The delays for the amplifier and transmission lines were matched to within $\pm 5 \times 10^{-9}$ sec. The x-ray signal was applied to one of the vertical deflection plates while the rf signal from tank loop No. 2 was applied to the other vertical plate. Triggered sweeps were initiated by a second 1P21 phototube placed near the gap between drift tubes No. 2 and No. 3.

Phase of X-Rays. The relative phase of the background x-ray output with respect to rf was monitored by a technique which eliminated the time parameter. Continuous comparisons result from application of x-rays and rf to opposite sets deflection plates (see Fig. 3).

Discussion

X-Rays. The x-ray output for single sparks[1] has the configuration shown in Figs. 4, 5, 6 and 7. In common with the findings of Birge and Lauer[2] the x-rays are seen to occur on alternate half cycles. That is for a particular spark, all of the electrons come from the same electrode. Further, if many photographs are examined such as Fig. 8 it can be seen that two or more sparks can occur independent in time and with opposite phasing. Sparks can start from either the negative or positive reference phase.

All the observed sparks have a definite build-up time. The mechanism which operates during the spark build-up must remember from cycle to cycle which electrode is the source of electrons. It is thus possible to eliminate photons but not ions from this build-up process. This does not imply that photons and electrons are precluded from initiation of the breakdown process.

If the circuit arrangement shown in Fig. 2 is changed so that the rf imput to the bottom plate of the oscilloscope is now eliminated, this circuit becomes a coincidence circuit for sparks. With such an arrangement sparks have been seen which are of a relatively short duration. X-ray bursts occur of 1/4 to 1/2 microsecond duration which have no effect on the operation of the accelerator whereas sparks of longer duration always cause loss of tank voltage. A typical spark of short duration is shown in Fig. 9.

High intensity x-ray bursts which accompany sparks and usually last from 1/2 to 1 microsecond (5-10 cycles of the rf). Occasionally bursts have been observed which last longer than 5 microseconds (greater than 50 cycles). These results tend to indicate that the high intensity x-ray bursts are of shorter duration than the actual rf decay time accompanying a spark. That is many of the sparks in the accelerator are of self-extinguishing nature. Further comment on this will follow.

Rf Decay. Measurements of the time required for the rf envelope to change from a high constant amplitude to approximately zero amplitude show that for natural sparks approximately 5-10 microseconds is required whereas sparks triggered by the rf crowbar require from 10 to 20 microseconds (see Fig. 10). The rf crowbar trigger cannot be expected to save the tank during sparking. It will find application, however, in bringing the tank down in response to error signals from the oscillators.

---

1. A spark will be defined as the phenomenon which results in the cyclic x-ray bursts shown in Figs. 4-9. Visual checks have shown that luminisity appears on at least one electrode at large spacing and on both electrodes and frequently bridging the gap at small spacings when these cyclic bursts are observed.

2. Refer to R. Birge and E. J. Lauer, UCRL-1680 Feb. 1952.

Since many of the high intensity x-ray bursts are of short duration it is of considerable interest to establish the time relation between rf decay and x-ray bursts. In order that this correlation should be meaningful all of the delays between the rf loop and the photo-multiplier circuit were matched electrically to within 5×10^{-9} sec. The maximum error inherent in this measurement is associated with the propogation time of the x-ray photons from the spark. Utilizing the instrumentation shown in Fig. 2 both x-rays and rf were portrayed on the same sweep. These results show that the high intensity x-ray burst which accompanies the spark occur prior to the rf decay. Photographs with this coincidence arrangement show that the high intensity burst which accompanies the spark does not cause a sensible change in the amplitude of the rf train (see Fig. 11). Further by the time the amplitude does start to decay the x-ray output is below the metering level. This contradictory result is not in disagreement with data compiled by Birge and Lauer[3]. The x-ray monitored vacuum sparks in the XC-cyclotron are known to last approximately 500-700 $\times 10^{-9}$ sec. whereas the decay time of this tank has been measured as 1000-2000 $\times 10^{-9}$ sec. due to a natural spark.

Phase of X-Rays. It has now been established that the x-rays in a particular spark always occur on alternate half-cycles of the rf. It is desirable to know the configuration of the background x-rays with respect to the phase of the rf in the tank. Utilizing the instrumentation of Fig. 3 and adopting an arbitrary phase one can establish the distribution of x-ray loading with respect to particular phases of the rf in the tank. Early work of Birge and Lauer[4] suggested that x-ray loading come from unidirectional electron emission coming from that electrode with the highest gradient. This result was confirmed by x-ray pinhole camera photographs. In contrast the constant gradient design of Mark I drift tubes should show bidirectional electron loading for background x-rays. The characteristic bidirectional pattern for x-ray output has been observed, however, it was found that the relative amount of x-ray loading shifts preferentially with respect to the reference phase of the rf (see Fig. 12). This shift occurs over a period of several seconds which suggest a thermal origin. Inspection of x-ray pinhole camera photographs shows the loading to be almost equally distributed between opposite drift tube faces, though most of the loading comes, as expected, from points having a smaller radius of curvature.

Results

X-ray bursts from sparks have a finite rise time. Most of the observed bursts require 3 to 5 cycles of rf to reach full amplitude. Though the general rise of the x-ray envelope is exponential, frequently it is not a monotonic function.

---

3. loc. cit.

4. loc. cit.

Spark photographs show that several high intensity sources of electron loading can exist independently during a given rf cycle. Those sources usually do not start out in time phase together.

Background x-rays as well as spark x-rays can occur on both alternations of the rf cycle. In a measurement which eliminated the time parameter it was determined that the division of background x-rays between positive and negative alternations of the rf cycle is approximately equal. It was found, however, that this division shifts slowly with time. This shift of intensity occurs in a preferred direction and is slow enough to be of thermal origin.

Coincidence measurements between fast photo-multipliers located at widely separated portions of the tank show that x-ray bursts of 1/4 to 1/2 microsecond duration occur which have no effect on the operation of the accelerator whereas sparks of longer duration always cause loss of rf voltage.

Photographs of the rf train immediately prior to and during the spark show that the amplitude of the wave decays to zero and from 5 to 15 microseconds (5 to 50 rf cycles). Analysis of the microscope study of a particular rf train reveals that the amplitude of the wave decays in a compound exponential fashion. This finding is not in disagreement with other photographs which show several x-ray bursts developing independent of one another in time during a single sweep. The action of various safety circuits during this decay was not determined.

Careful coincidence measurements between x-rays and rf envelope indicate that the high intensity burst which accompanies the spark does not cause a sensible change in the amplitude of the rf train. By the time the amplitude does start to decay the x-ray output is below the metering level. When compared with the information from the 2C cyclotron this seems to imply that the x-ray output has decreased because of a low impedance low voltage arc between the associated drift tubes. Since this phenomenon requires an axial rather than circumferential magnetic field vector, it should be possible to confirm this hypothesis by monitoring the output of a quadrature loop during sparking.

Configuration of x-ray monitored sparks or background x-rays is not effected by the magnetic field.

Conclusions

1. The above results indicate that many sparks occur in the accelerator which are of the self-extinguishing type.

2. It has been found possible to detect within 1/2 an rf cycle when a spark occurs and to produce a low impedance high voltage trigger signal for electronic equipment. Fast photo-multipliers can detect a spark which is too small in amplitude and too short in time to necessitate loss of rf voltage. They should not be used to control the voltage level of the accelerator.

3. The decay time of the tank due to rf crowbar sparks is approximately twice that due to natural sparks. The crowbar cannot be used to protect the tank during breakdown. It can be utilized quite successfully to dissipate the tank energy in response to appropriate error signals which develop as a result of oscillator trouble.

4. Limitations can now be imposed on any theory which develops concerning the rf spark mechanism.

Acknowledgements

The authors would like to commend Howard Smith for his valuable assistance in the coordination of mechanical facilities.

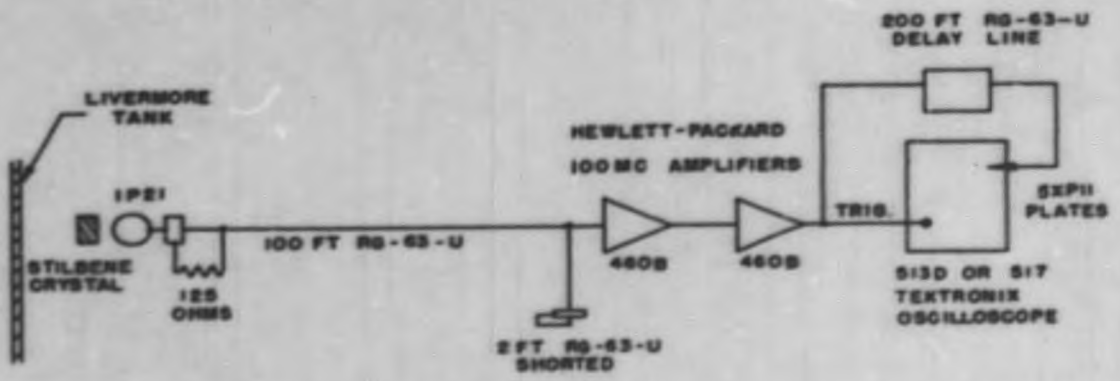

FIG. 1 SECTION 4

X-RAY OUTPUT VERSUS TIME INSTRUMENTATION

MU4125

SECRET

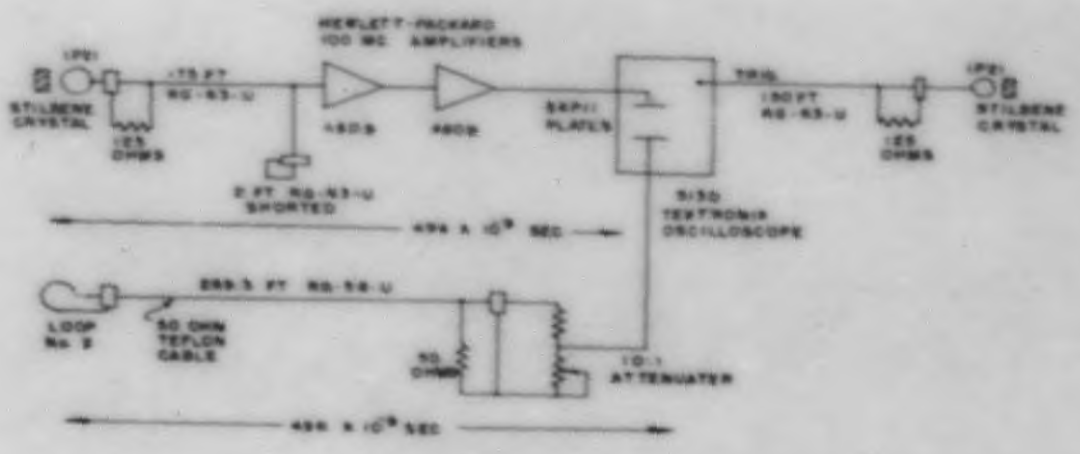

FIG 2 SECTION 4

X-RAY AND R F DECAY INSTRUMENTATION

SECRET

MU-4126

1903-35

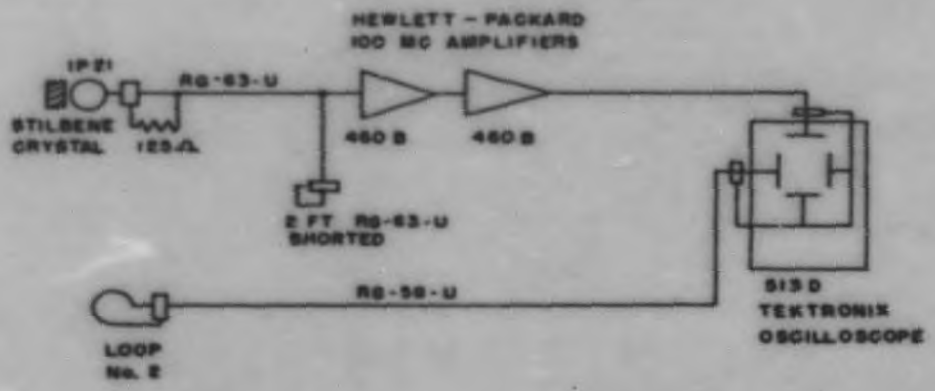

FIG. 3 SECTION 4

PHASE MEASURING INSTRUMENTATION FOR X-RAYS

SECRET

MU4127

1903.36

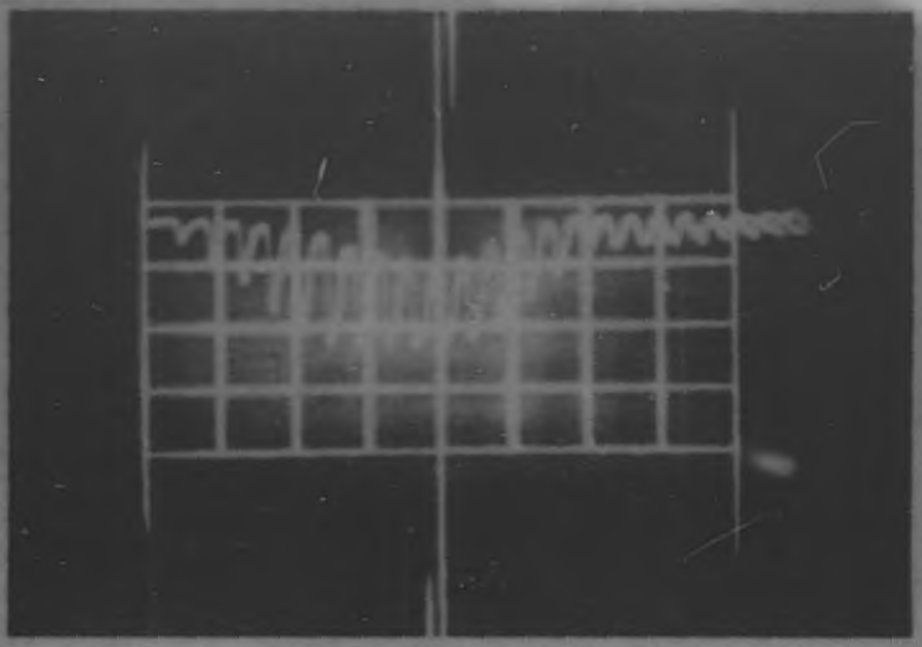

Section 4. Fig. 4 Camera 196 Frame 458 Sweep speed 200 x 10^{-9} sec/cm. typical long spark x-ray burst. Initial spark shows rectifying action.

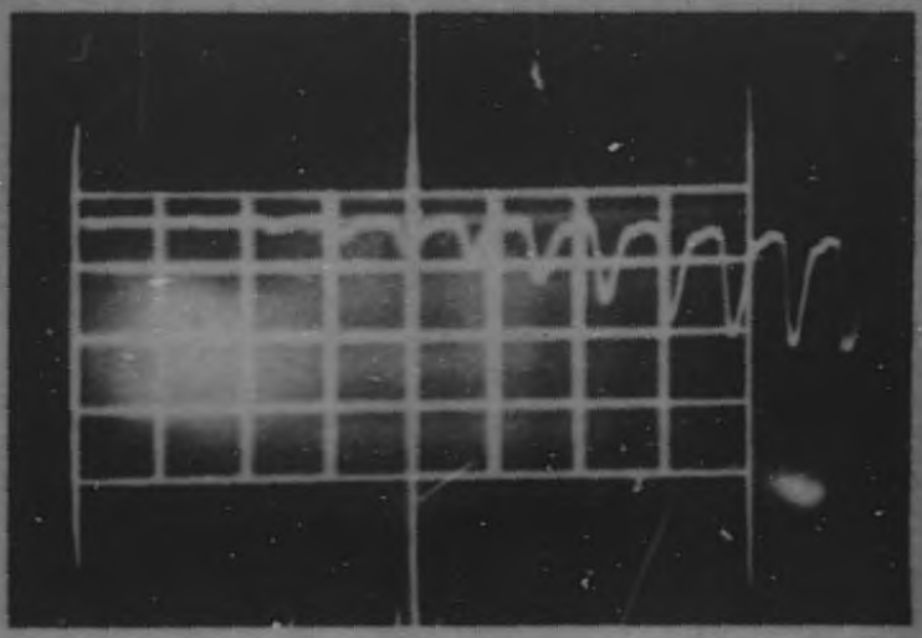

Fig. 5 Camera 196 Frame 390 Sweep speed 100 x 10^{-9} sec/cm., Note long rise of this burst.

1903-37

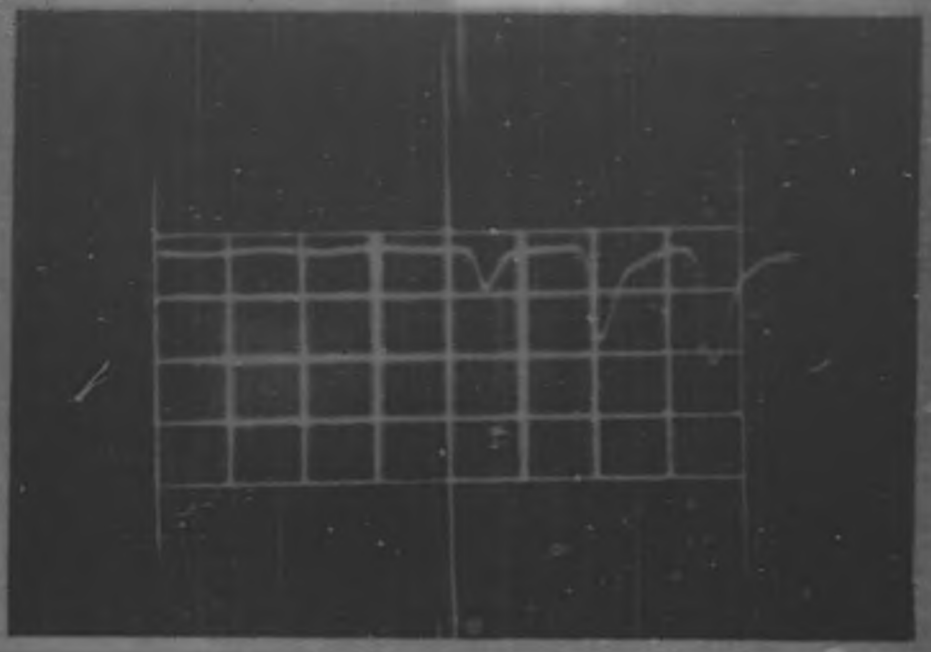

Fig. 6 Camera 196 Frame 403 Sweep speed 50 x 10^{-9} sec/cm.

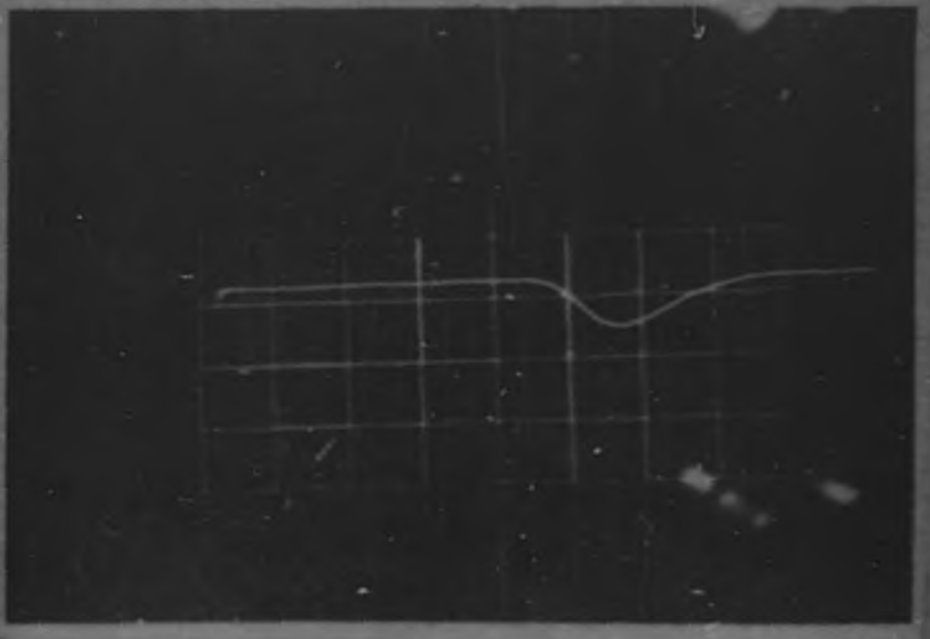

Fig. 7 Camera 196 Frame 270 Sweep speed 50 x 10^{-9} sec/cm.
Note configuration of first x-ray pulse.

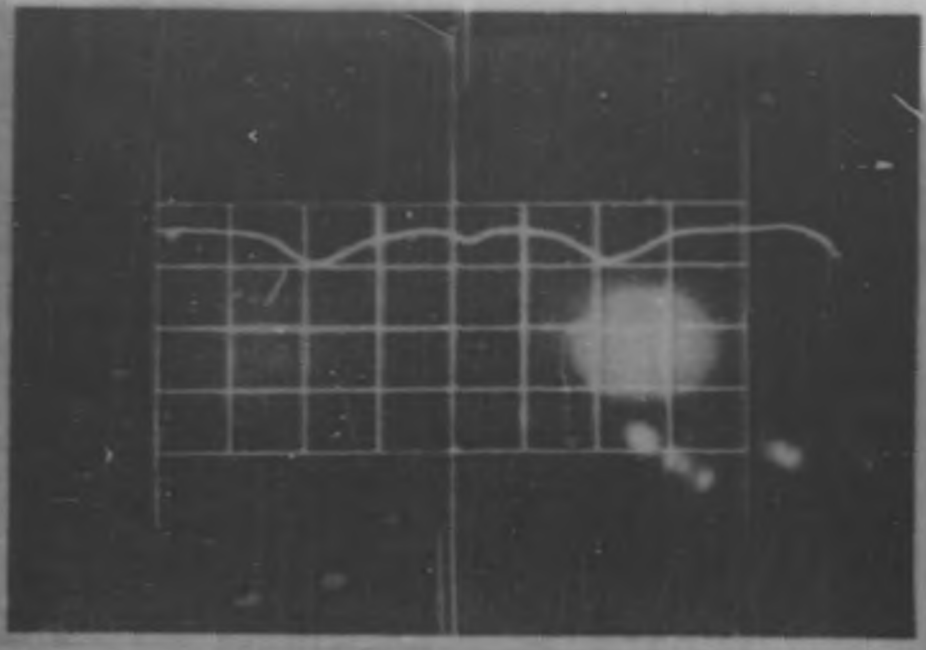

Fig. 8 Camera 190 Frame 279 Sweep speed 20 x 10^{-9} sec/cm. Note x-ray photons on both alternations of the r-f cycle.

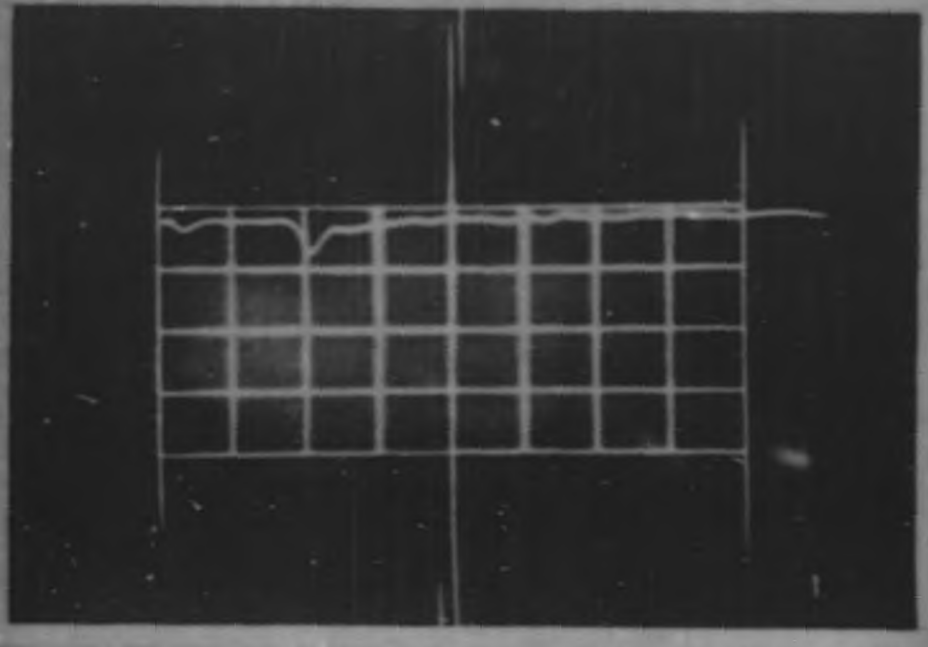

Fig. 9 Camera 190 Frame 402 Sweep speed 50 x 10^{-9} sec/cm. Short spark lasting two r-f cycles.

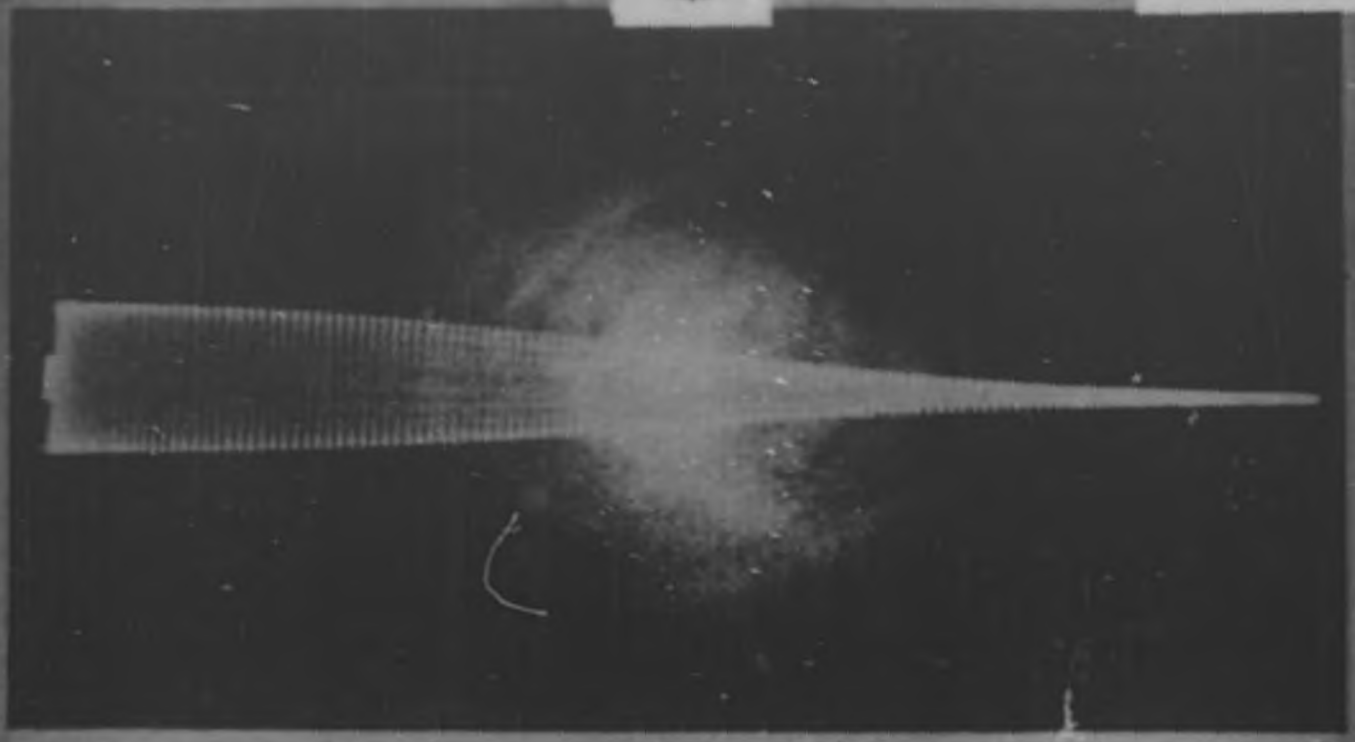

Fig. 10 Camera 121 Frame 182 Sweep speed 1000 x 10^{-9} sec/cm.

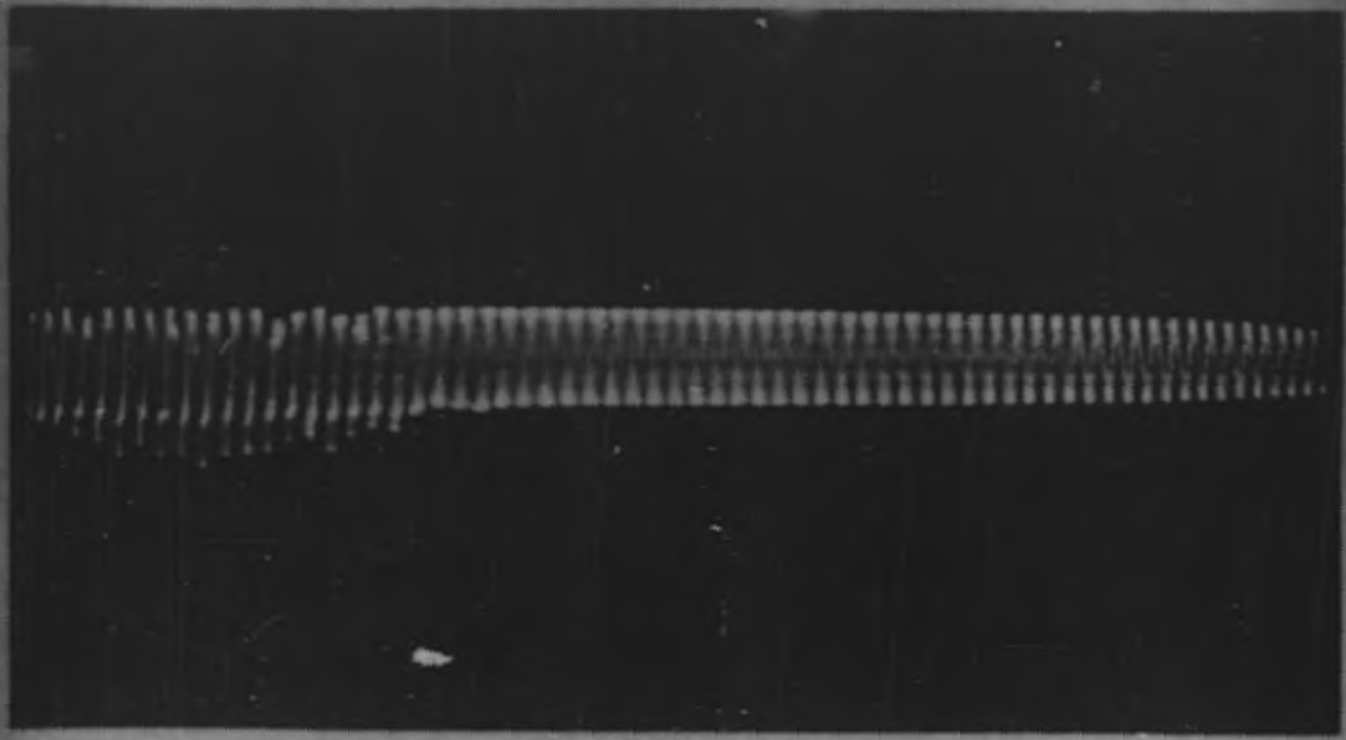

Fig. 11 Camera 174 Frame 434 Superposed r-f and x-ray decay. Sweep speed 500 x 10^{-9} sec/cm.

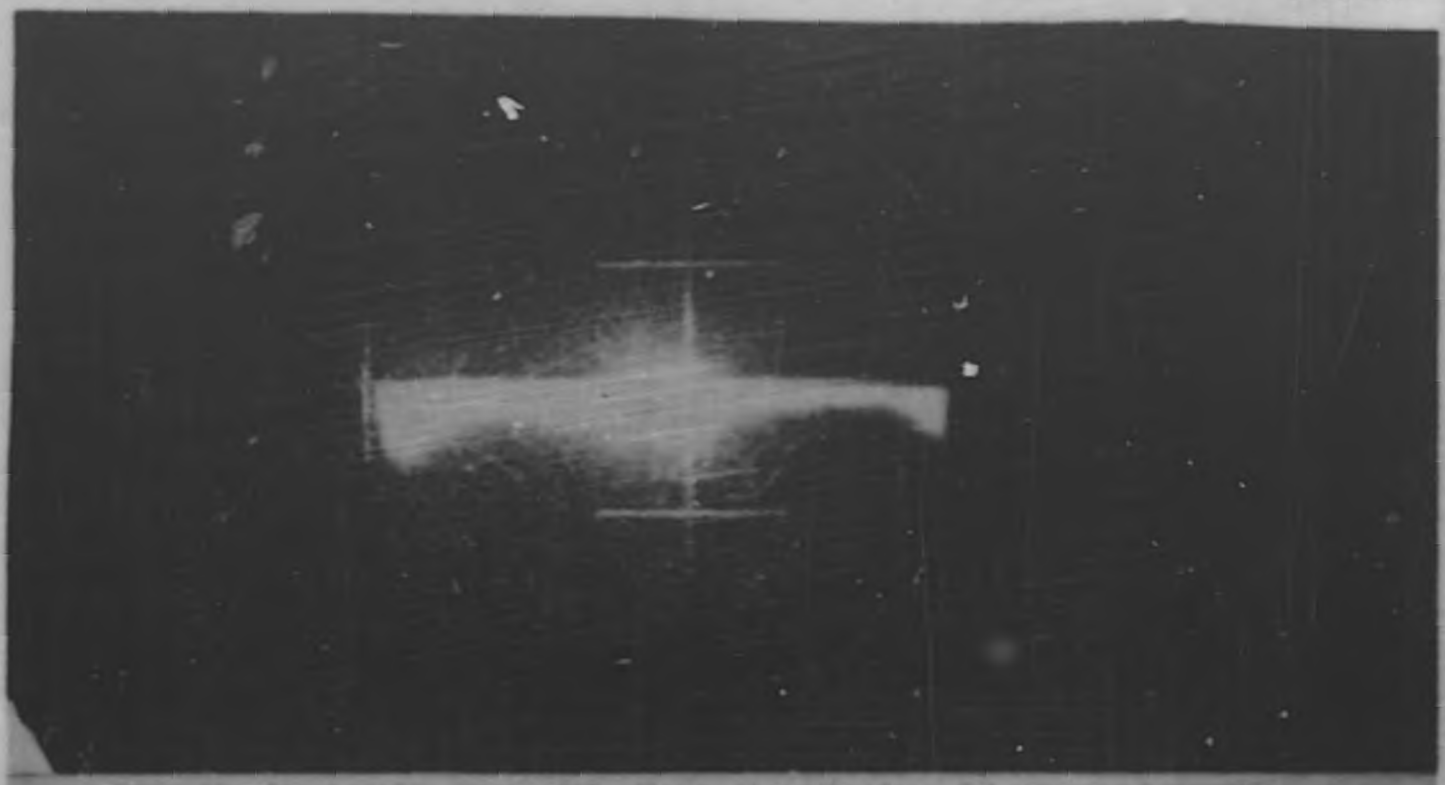

Fig. 12 Camera 171 Frame 411 Phase distribution of background x-rays near the beginning of a succession of r-f pulses.

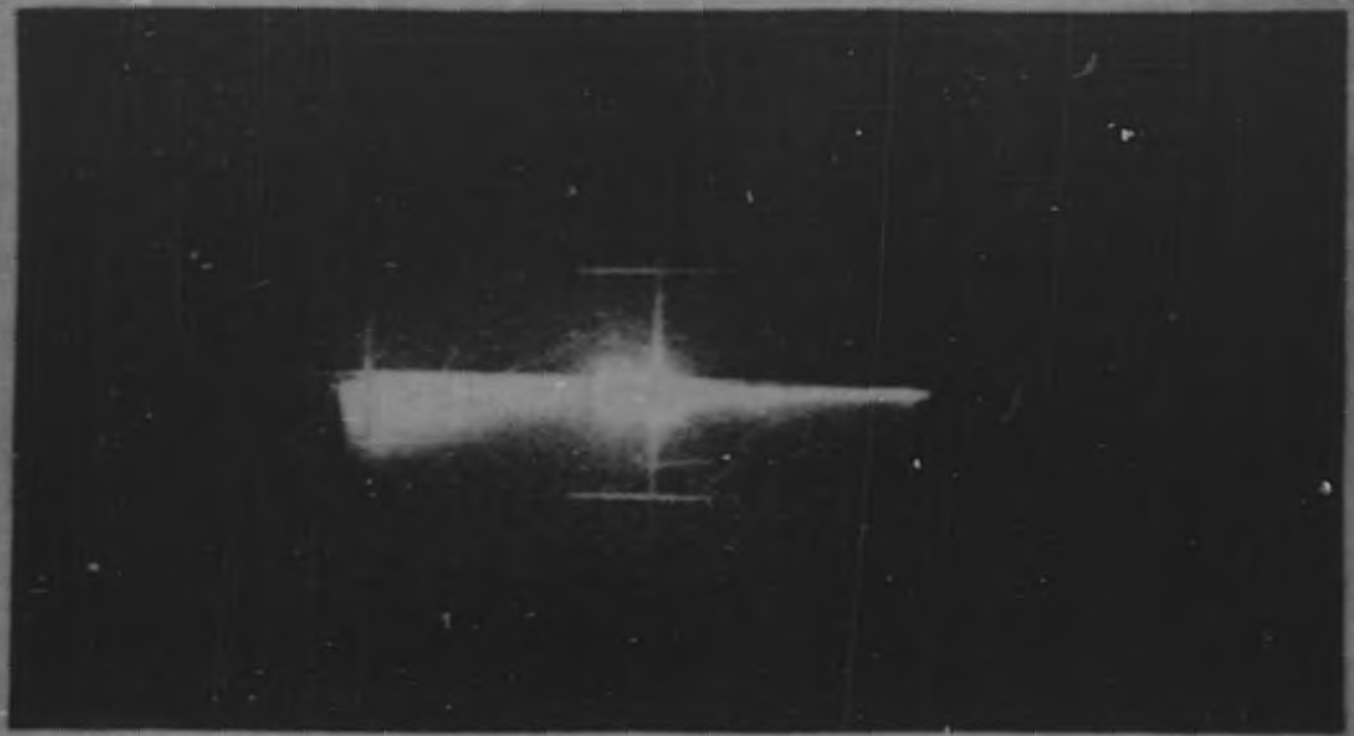

Fig. 13 Camera 172 Frame 413 Phase distribution of background x-rays just prior to a spark.

1903-41

5. THE ION PUMP PROGRAM

John S. Foster, Jr. and E. J. Lofgren
UCRL

Summary

The ion pump installed on the B-1 cavity (volume - 48,000 liters) has been set up to run automatically with only routine inspection. A cathode has been tested which will give more than two weeks of continuous operation. The time for which a pump will run is given by the cathode life.

A new base pressure of 8×10^{-7} mm. has been obtained under steady operation and the degree to which various sources limit this pressure has been investigated. Currently, experiments are being set up to measure the ion density and energy distribution.

An investigation is under way to determine the practicality of a radio frequency ion pump.

Automatic Pump Operation

The ion pump installed on the B-1 cavity has had several weeks of operation with automatic controls. As has been described previously, the arc current is regulated through automatic filament control. In addition, there is a re-cycling device which re-establishes the arc if a spark occurs in the cathode regions of the machine. Sparking has been reduced considerably by disconnecting the reflector cathode and allowing it to seek its own potential. Under these conditions, about 7 sparks occurred in 2 weeks. The unit is left unattended but is checked periodically by the Inspection Technicians on their regular rounds.

The characteristics of this particular pump have been described previously. At present it is being used to develop a cathode with longer life. For this purpose, the automatic feature of the unit is desirable. Since cathode life varies with the gas load it is important to have or simulate conditions usually encountered. Normally the unit is connected to the B-1 cavity. However, if this is not possible, an air leak of about 0.02 cc/sec. (N.T.P.) is substituted.

Pre-Exciting Difficulties

It will be recalled that trouble was encountered in pre-exciting the B-1 cavity whenever the ion pump was on. After some simple tests, the trouble was suspected to be due to photons leaving the arc and producing electrons by the photoelectric effect in the region of the cavity liner.

Simple light baffles were installed which considerably reduced this interference. Recently, baffles have been installed which reduce the speed only slightly, but which act as rather good light baffles. Fig. 1 gives the general layout of the pump, baffles, and B-1 cavity. Figs. 2, and 2a show the bias curves which indicate that some light reaches No. 2 baffle but only electrons can reach No. 3. We have not yet tested the effect of the ion pump on pre-exciting difficulty with these new baffles, or studied the effect of baffle bias.

Cathodes

Under typical operating conditions the present hot cathodes lose weight at the rate of roughly 0.8 grams per hour. The mechanism involved is mainly sputtering, although some cathode material does combine chemically with ions of the gas being pumped. In general a flat spiral filament made from 1/4 in. diameter tungsten rod seldom lasts more than 50-70 hours. Two different types of cathodes are being tried.

Radiant Cathodes. A radiant cathode consists of a thick tantalum plate radiantly heated by a tungsten filament. Construction details on this type of cathode have already been given. Fig. 3 shows two slightly different types. The first has been run for 95 hours and it is estimated that it would be good for another 25 hours. The second cathode has been operated for 336 hours (2 weeks). Initially it had a tantalum button 1/2 in. in diameter, 9/16 in. high located in the center of a 21/64 in. thick tantalum plate. The present pump operates continuously for a period determined by the cathode life.

A variation of the above cathode has been built and will be tried shortly*. This is also a radiant type, but differs in that the tantalum emitter is a cone. The notion here is that the arc, terminating inside the cone, will sputter the tantalum at the usual rate. However in this design, a large fraction of the sputtered material will be deposited inside the cone. (There is evidence from the present cathodes that material sputtered from the cathode builds up a good metal layer on the surrounding surfaces.) The tantalum cone is radiantly heated from the outside by tungsten filaments, see Fig. 4. This type of cathode is considered the most promising at present. A hollow carbon cylinder is also being made up for the reflector end.

Carbon Cathodes. Two types of carbon cathodes have been used. The first type consists of plain graphite, heated either by passing a current through it or by using radiant heating as above. Because carbon has a high emissivity and low thermal conductivity, it is very difficult to get the surface hot enough (2200° K.).

A second type is to use a carbon cathode loaded with ThO_2. (Fig. 5) This cathode runs at a reduced temperature (2000° K.) but so far no design capable of a long life has been tested. The feature of this cathode is its very low cost.

---

* Cathode is now operating continuously on a life test.

Cold Cathode with Tickler. A third type of cathode was tested and it is shown in Fig. 6 after 30 hours of operation. The cathode consists of a 1/4 in. tungsten rod "tickler" filament and a water cooled aluminum cold cathode. The wires shown in the photograph have been placed there only to cast a shadow to indicate the wear pattern. This cathode was operated with an air or oxygen exit leak and pumped well under small loads, with no forevac pumping. While this type of cathode is easier to control than straight cold cathodes it is still too erratic for reliable operation.

Factors Limiting the Base Pressure

Since the last report, measurements have been carried out to determine the sources which contribute to the base pressure. Some of the possible sources are discussed below.

Ion Drain to the Walls. Ions leaving the arc and landing on the wall in the center section of the pump will neutralize and may contribute to the local pressure. The rate of ion drain is affected by the magnetic field, the arc diameter, and the arc current. Fig. 7 shows the location of "drain plates" used for these measurements.

Normally, when these plates are at ground potential the current of particles reaching the wall consists of both positive and negative particles. Since we are concerned with the positive ion component, it is useful to vary the potential of the plate and observe the variation in current. Fig. 8 gives the general shape of the curves for the different plates. Some of these plates are very large and hence when placed at a high potential can disturb the plasma balance. It is felt however, that since it is found that plates Nos. 2, 3, 4 and 5 do not interact, a fair indication of the positive ion drain when the plates are grounded is given by linearly extrapolating the positive ion drain to zero volts. If the positive ion drain is measured in this way, the effect of magnetic field, arc current, and arc diameter can be investigated.

The effect of magnetic field is seen in Fig. 9. Since the arc follows the magnetic field lines, it was necessary to vary the magnetic field throughout the length of the pump so that the arc diameter would remain constant. Fig. 9 shows that one gains only a little with excessive fields, but that it is important to have enough magnetic field.

To measure the effect of arc diameter, it was necessary to change it and still keep the magnetic field constant in the vicinity in which the drain plates are located. To do this the end magnets, which maintain magnetic field at the filament and reflector were varied. Now, since it is difficult to decide just what the arc diameter is on any one observation, a plot was made of the observed arc diameter in the central region of the pump against the square root of the exit magnet current. This is shown in Fig. 10.

In measuring the positive ion drains then, the values for arc diameter were read from Fig. 10, at each exit magnet setting. The results in Fig. 11, show that very few positive ions drain until the diameter of the plasma reaches 1-1/2 in. (The magnetic field was about 1400 gauss).

Also on Fig. 11 is plotted as a dotted curve the gas pressure at the central region of the pump. It is seen to have a rather sharp minimum. The rise in pressure at small arc diameters is understandable in part since the mean free path of a molecule in the arc is comparable to the arc diameter, and hence smaller arcs have less speed. Also recombination may play a role at small diameters. The pressure rise for larger diameters may be attributed to the ion drains. In fact if one assumes that these drains are the sole source of center pressure, then the flow of gas into the arc could be equated to the ion drain.

(Pumping speed at each arc diameter) (Pressure) = K(Drains), Fig. 12 gives the ion drains associated with each pressure. Unfortunately the drain to the helix itself was not measured. However, subsequent data indicates that the helix drain would add about 30 percent to the total drain. This data then indicates that if all ions are singly charged atomic, then for each ion that arrives at the wall there are ~1.4 atoms created.

The effect of increasing the arc current was to increase the ion drain. The results for one collector plate are given in Fig. 13. The effect of changing the applied arc voltage was small. Also, increasing the center gas pressure had little effect on the center ion drain.

In actual operation the pump is adjusted so that the operating pressure is a minimum. To this end, the magnetic field, arc current, and arc voltage are adjusted for minimum center pressure. Under these conditions the total drain to the center section is at most 10 ma. if photoelectric current is neglected. This then corresponds to a pressure contribution of about 2.3×10^{-7} mm.

Back Diffusion. Another general source of pressure arises from back diffusion of molecules down the tube. It has been shown previously that molecules from the exit region do not survive the exit constriction tubes as molecules in sufficient numbers to contribute to the center pressure. Ions that land on the collector plates P_1 and P_6 however, can neutralize and diffuse down the tube. It is for just this reason that the pump has long side tubes. Now the total positive ion drain to both ends under base pressure conditions is about 0.8 amps or equivalent to about 0.093 cc/sec. of molecules. To test the effect of this, an additional gas leak was let in at P_6. Fig. 14 gives the result. It is of course the initial slope that is important, and if we assume that this slope is continued into the region where the source is due to neutralized ions, then this indicates that at most 3×10^{-7} mm of the base pressure is due to diffusion from the exit face.

Ion Recombination. It may be that neutral atoms leave the arc as a result of recombination of an electron and an ion. Normally this is considered as a very rare event in gaseous discharges because usually the density of neutral particles is quite comparable to the ion density or even larger. However, if there is an ion density n_+ which is then equal to the electron density, the number of neutral atoms created per cubic centimeter per second is

$$N_o = \alpha n^2$$

α, the recombination coefficient has been measured for "low pressure discharge" (10^{-2} mm) and temperature of 0.3 volts to be about 2×10^{-10} for Argon, and may vary as $(\text{Energy})^{-1}$. The ion energies and density of this arc have not yet been measured. If one uses reasonable values however, it is seen that recombination could easily be a factor. Experimentally there is an indication of its presence. For instance, recently one of the ion pumps has reached a base pressure of $\sim 8 \times 10^{-7}$ mm, using nitrogen in the exit leak. This was obtained by using very little exit pressure and a higher arc voltage and current then is usually run**. The situation here is then that there are few positive ions and the current is mainly energetic electrons. Under these conditions, the probability of recombination is reduced. One might say the pressure is reduced merely because the chance for ionization has been increased. But the ionization increase could be achieved by using a higher current at the same voltage, and usually this is found to increase the pressure, or have no effect.

Ions are neutralized all along the surface of the tubes on each side of the central region, but no measurements have been made on this particular source.

Positive Ion Analysis

Equipment is being set up to measure the state of ions landing on the reflecting cathode. A small hole in the cathode will allow a beam of ions to be accelerated and then magnetically analyzed. Also an arrangement of a probe and guard ring is to be established in the reflector cathode so that the number of positive ions and possibly their energy can be determined. Since the arc has many volts of rf on it, an energy measurement is very doubtful.

Preliminary measurements have been made on the light given out by the arc. This light consists of a line spectra and it is hoped that the line

---

** A heavier cathode reduced the tendency to "run away" and permitted operation at 400 V, 20 A instead of say 300 V, 10 A.

width can be correlated with the ion velocity. For low velocities,

$$\Delta\lambda = v_{\parallel}\,\lambda_s/c.$$

Where: $\Delta\lambda$ is the shift in wavelength.
$v_{\parallel}$ is the velocity along the direction of observation.
λ_s is the source wavelength.

The doppler shift expected is well within the limits of optical interferometers. It is seen then that the distribution of intensity with wavelength from doppler broadening gives directly the velocity distribution in the direction of observation. Now normally the doppler shift is comparable to pressure broadening. In this case we have an arc running in a region where the pressure can be $\sim 10^{-6}$ mm, and hence collision broadening is not expected to enter. Stark broadening in the normal sense does not enter since it requites gradients of ~1 Kv/cm. However within the arc there is a local field due to the individual charges themselves. If the ion density is n, and the ions are singly ionized, the average microfield is

$$\bar{E} = 1.74 \times 10^{-6}\ n^{2/3}\ \text{volts/cm.}$$

so that for $n = 10^{12}$ the local field strength is about 175 volts/cm. A field of this order of magnitude would not be expected to give broadening comparable to the doppler shift. In fact, the H_α, H_β, H_γ,----- lines have been photographed and the interference fringes are equally broad for each line, indicating the local fields do not contribute much to the line width. At present an attempt is being made to improve the gas purity and instrumentation.

Rf Ion Pump

In the ion pumps described above, gas is ionized mainly by a stream of energetic electrons which were initially emitted by the filament. The positive ions hit the cathode with energies of several hundred volts and the sputtering which takes place is sufficient to make cathode life the most serious limitation of the pump at present.

An rf ion pump might be expected to operate in much the same way as present pumps except that the ionizing electrons are created from the gas itself at the exit. It is hoped that a high enough plasma temperature can be produced so that neutral particles falling into the plasma in the central region of the pump will have some chance of being ionized. As usual the mobility of the positive ions, being so much less than electrons will force the plasma potential to be positive with respect to the end plates. In this way it may be that there will be little need for the application of any d.c. power. This program has just begun and while the initial results are encouraging a detailed description will be left until the next report.

Other Work

Work on the large ion pump (No. 101) has been held up because of a material failure in the aluminum tank.

Personnel

Work on the ion pump during this period has been carried out by the following people: William Bush, Paul Byerly, Bruce Cork, Warren Eukel, Forrest Fairbrother, John Foster, Walter Hartsough, Marion Jones (Electrical), Robert Richter and Howard Smith.

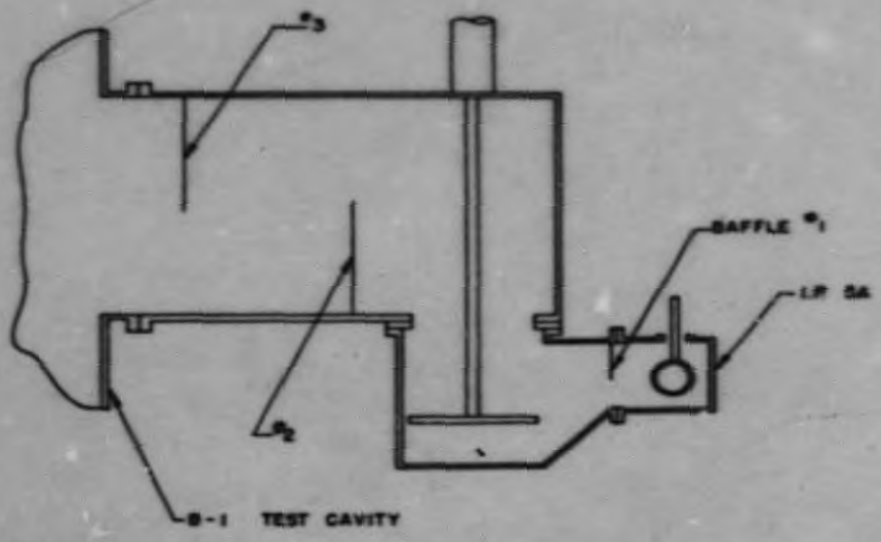

SECRET

FIG. 1 SECTION 5
ION PUMP 5A MANIFOLD BAFFLES
SCALE: $\frac{1}{16}$" = 1"

MU-4128

1903-49

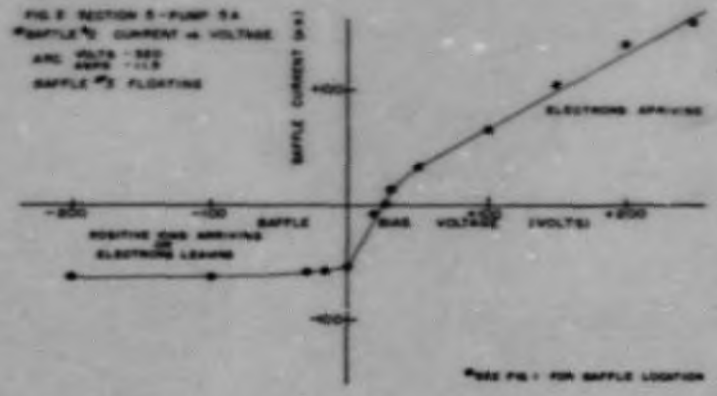
BAFFLE CURRENT
+100
-100
ELECTRONS ARRIVING
-200
-100
BAFFLE
+100
+200
(VOLTS)
ELECTRONS LEAVING

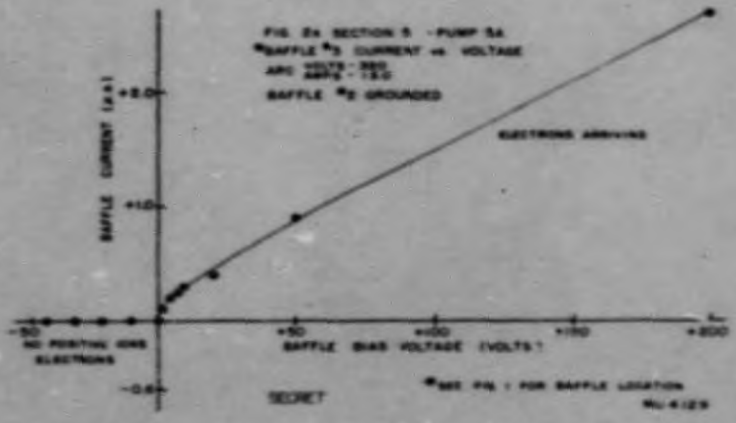
BAFFLE CURRENT
+2.0
+1.0
-0.6
ELECTRONS ARRIVING
-50
+50
+100
+150
+200
BAFFLE BIAS VOLTAGE (VOLTS)
SECRET

1903-50

Tantalum plate, radiantly heated. 95 hrs. of operation.

A slightly different design after 336 hrs. of operation.

Fig. 3

Cone cathode radiantly heated.

Fig. 4

19-3-51

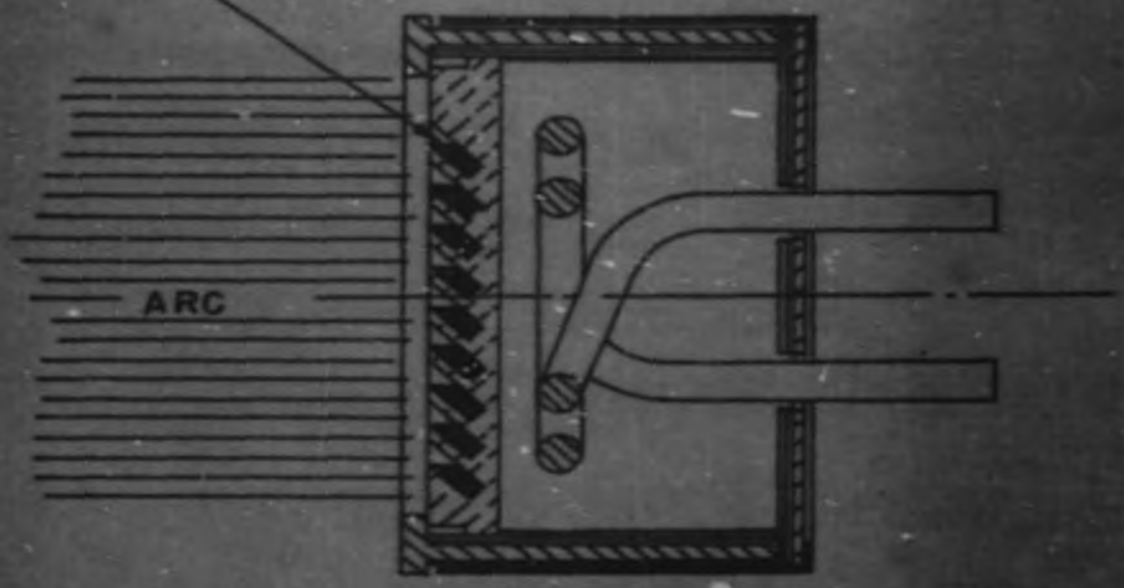

FIG. 5 SECTION 5

CARBON-THORIUM OXIDE CATHODE

FIG. 6 SECTION 5

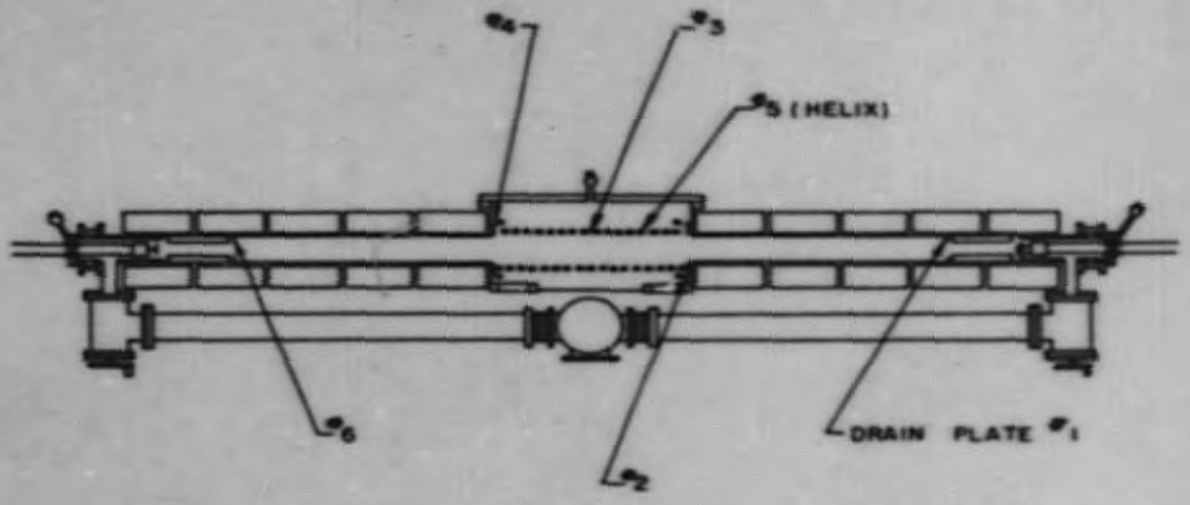

FIG. 7 SECTION 5
ION PUMP 5B
DRAIN PLATE LOCATION

SECRET

MU 4130

1903.53

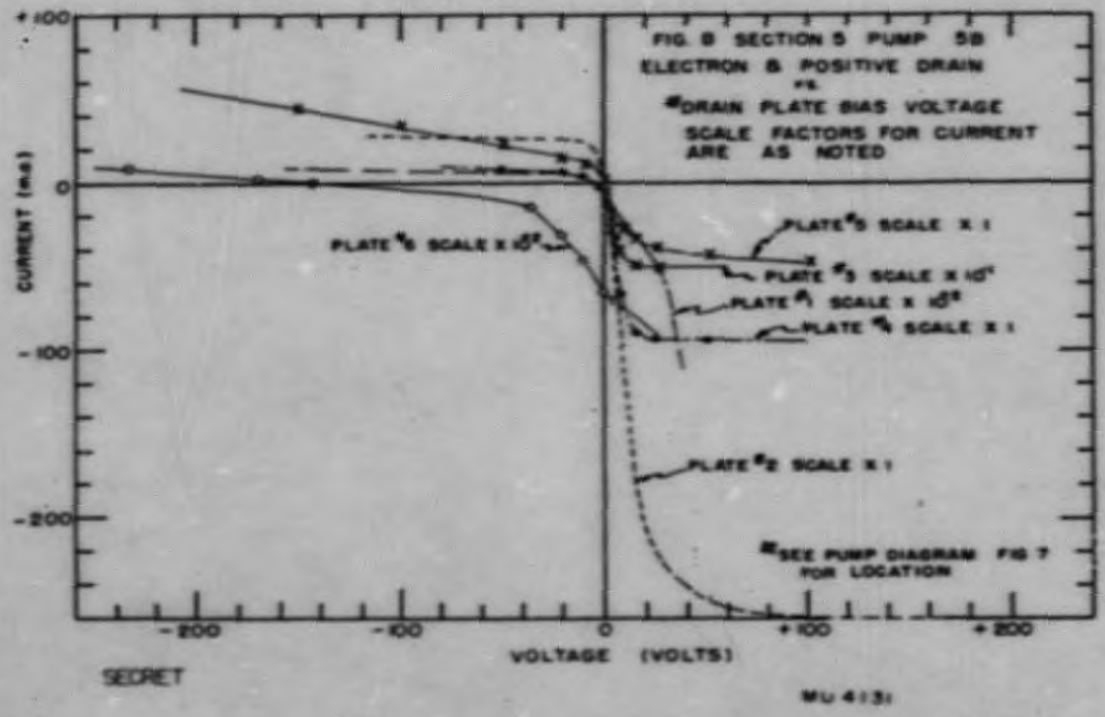

SECRET

MU 4131

1903-54

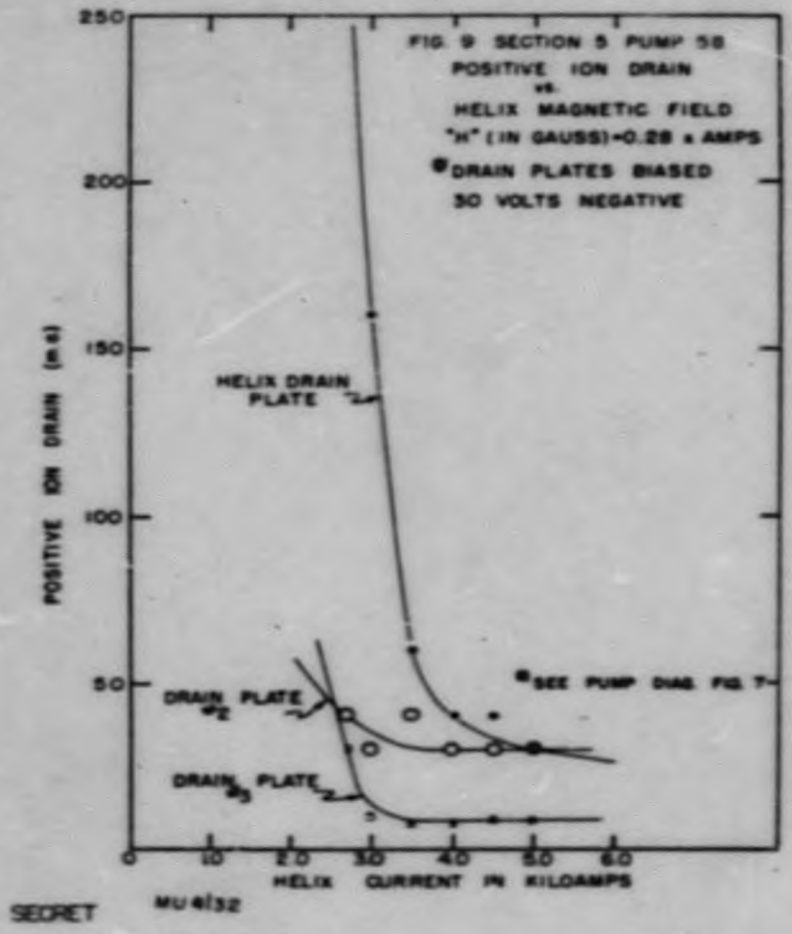
FIG. 9 SECTION 5 PUMP 58
POSITIVE ION DRAIN
vs.
HELIX MAGNETIC FIELD
"H" (IN GAUSS)=0.28 x AMPS
*DRAIN PLATES BIASED
50 VOLTS NEGATIVE
POSITIVE ION DRAIN (m.a)
250
200
150
100
50
0
HELIX DRAIN PLATE #2
DRAIN #2 PLATE #1
DRAIN #3 PLATE #2
*SEE PUMP DIAG. FIG. 7
1.0
2.0
3.0
4.0
5.0
6.0
HELIX CURRENT IN KILOAMPS
SECRET
MU 41132

1903.55

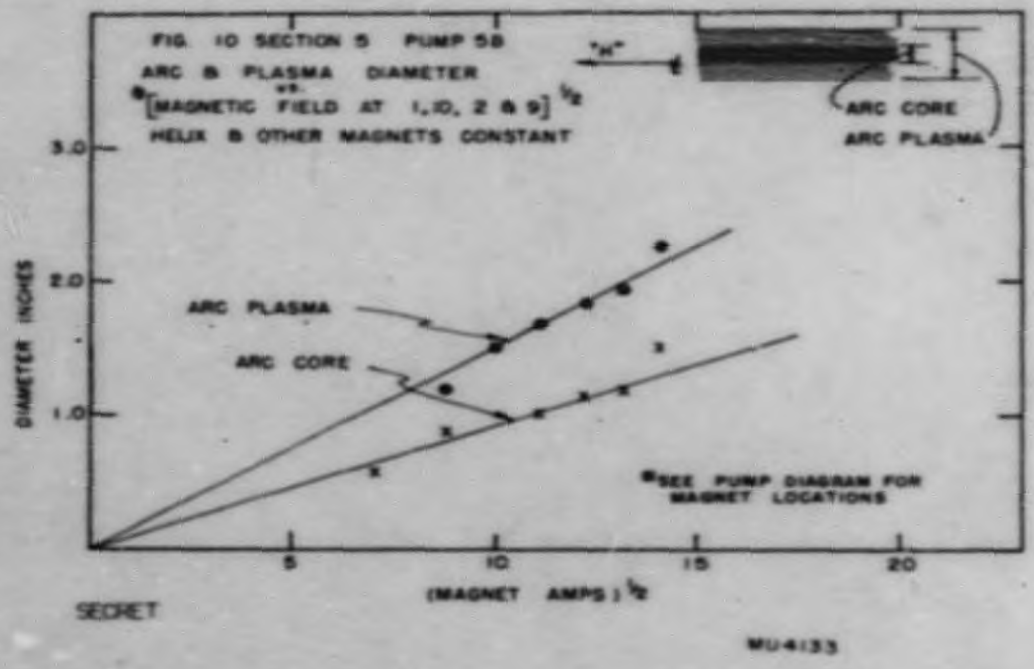
FIG. 10 SECTION 5 PUMP 58
ARC & PLASMA DIAMETER
vs.
*[MAGNETIC FIELD AT 1, 10, 2 & 9] ½
HELIX & OTHER MAGNETS CONSTANT
"H"
ARC CORE
ARC PLASMA
3.0
2.0
1.0
DIAMETER INCHES
ARC PLASMA
ARC CORE
*SEE PUMP DIAGRAM FOR MAGNET LOCATIONS
5
10
15
20
(MAGNET AMPS)½
SECRET
MU-4133

1903-56

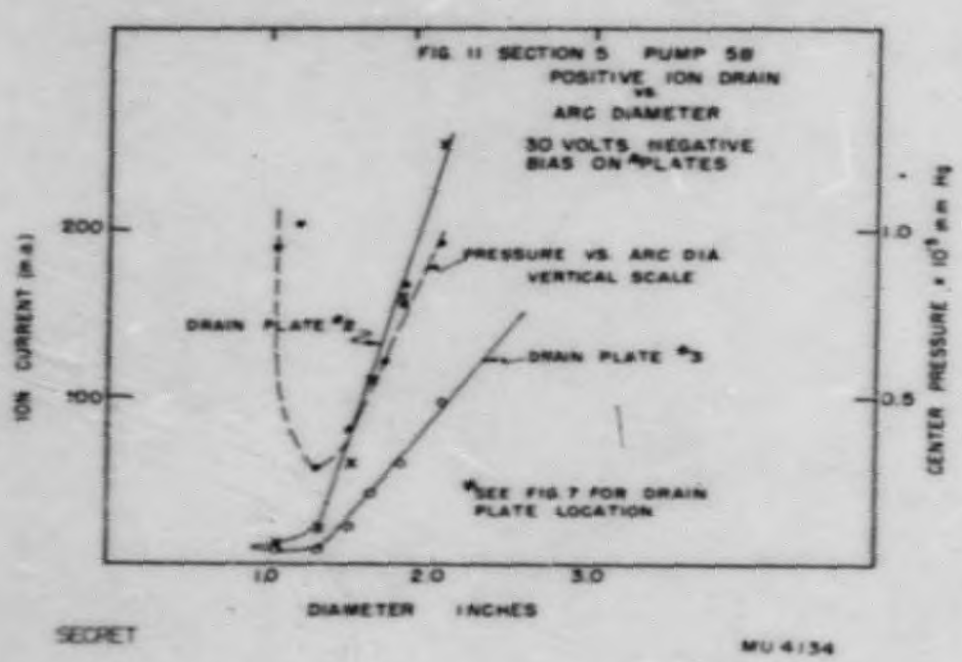

SECRET

MU 4134

1903-57

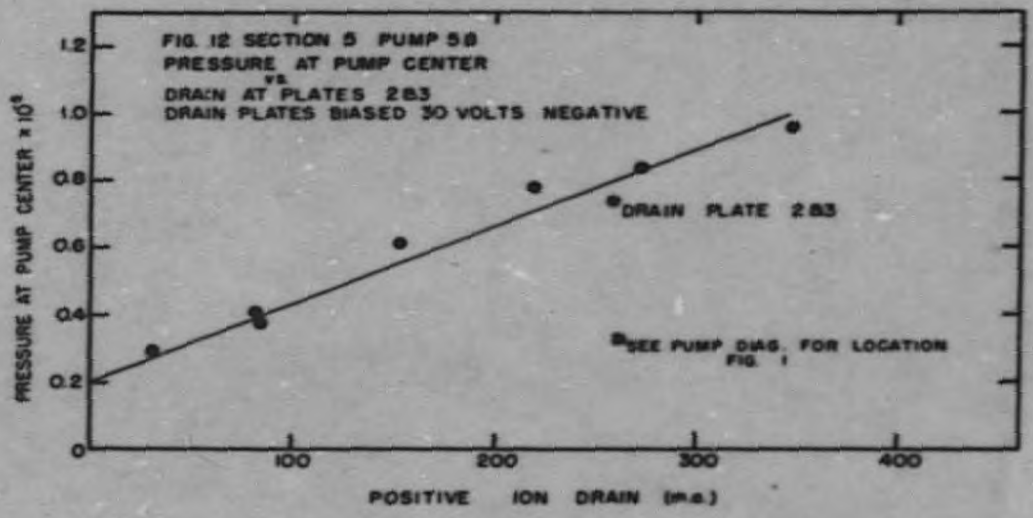

SECRET

MU 4135

1903.58

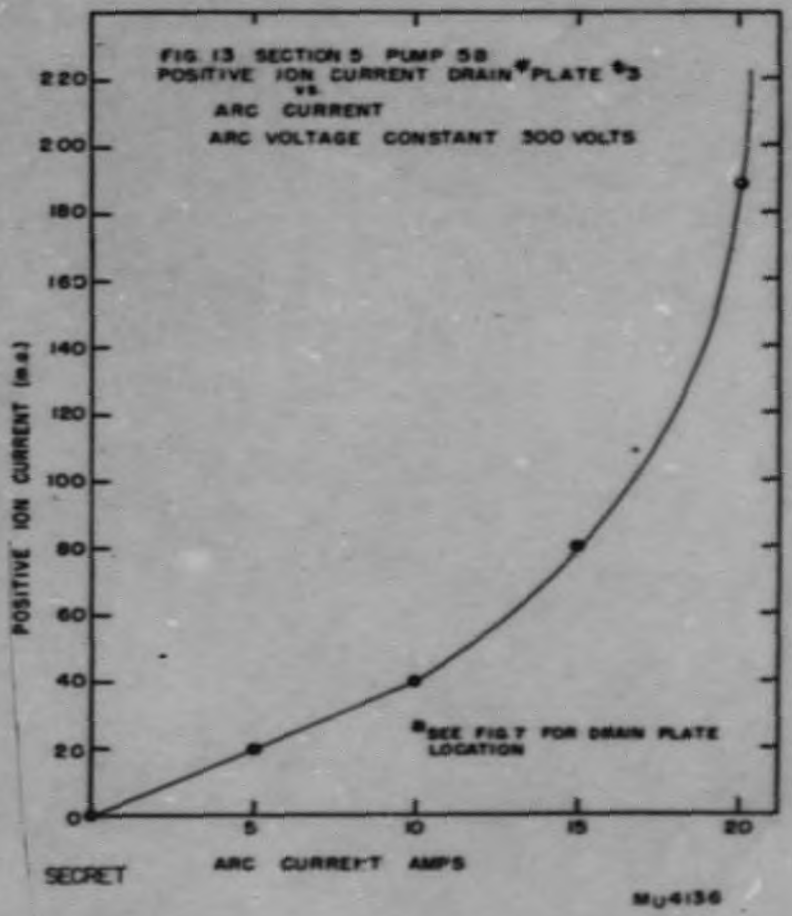
FIG 13 SECTION 5 PUMP 58
POSITIVE ION CURRENT DRAIN* PLATE #3
vs.
ARC CURRENT
ARC VOLTAGE CONSTANT 300 VOLTS
POSITIVE ION CURRENT (m.a.)
220
200
180
160
140
120
100
80
60
40
20
0
5
10
15
20
ARC CURRENT AMPS
*SEE FIG 7 FOR DRAIN PLATE LOCATION
SECRET
MU4136

1903.59

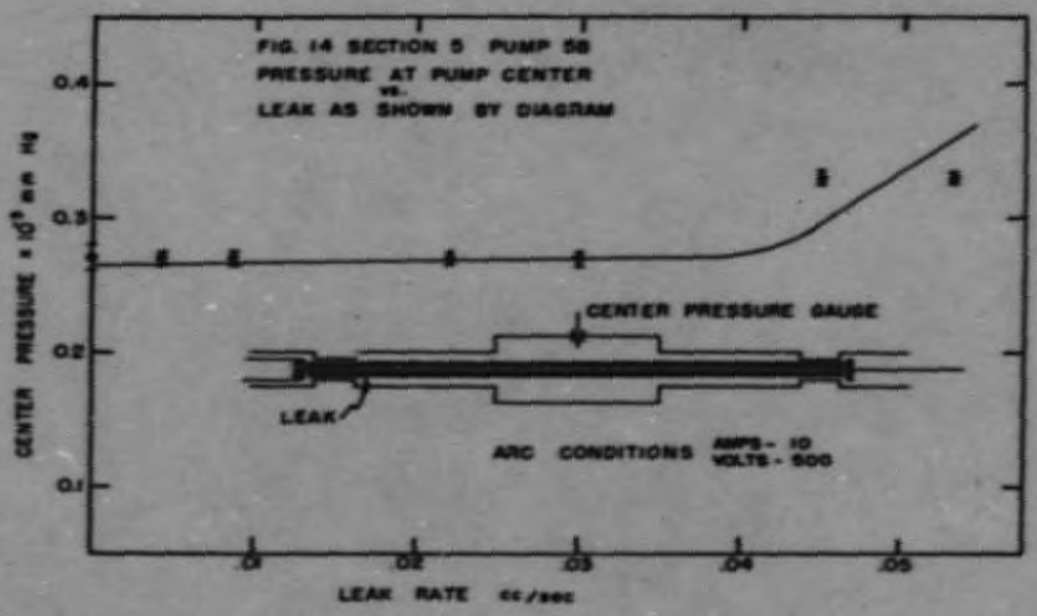

SECRET

MU 4137

6. HIGH FREQUENCY PROGRAM

W. R. Baker
UCRL

Apparently the last parasitic problem, the 70 Mc one, has been eliminated by the internal tube geometry change mentioned previously. Two tubes that had been known to give trouble have been modified, and now show no indications of either 70 Mc, 980 Mc or shorts due to mechanical grid resonance. It is reasonably safe to assume that our remaining stock of problem tubes can be recovered in this manner.

Operation of the Mark I tank under vacuum conditions has been successfully accomplished over a several weeks period, and we now know enough about the problems to be certain that rf-wise the machine is going to be practical. We know that the initial rate of rise of rf required is approximately 2 Kv per microsecond, and that it should be made about five times faster than this for reliable starting. There are many ion lock levels, from about 10 Kv tank rf to several megavolts. The higher lock levels are also sensitive to drift tube magnetic field settings, but, fortunately, at the operating field there is no bad lock problem.

Because the sparking problem has limited operation to proton gradient in the tank, and the oscillators are coupled for deuterons instead, the rf power is only about 25 percent of the designed value. Also, four oscillator positions were not in use for various reasons, such as missing transmission lines and experimental work. This all added up to a marginal power problem that resulted in relaxing various protective interlocks, so that large overloads could be forced on the remaining oscillators. The remedy is to change the coupling, either by larger loops or by oscillator adjustments and to use all oscillator stations to supply useful power. Mistakes in relative loop couplings also reduced the available power considerably.

First operation of the tank in vacuum required negative bias on the drift tubes for a clearing field to permit excitation. When magnetic field was applied the presence of such bias set up a discharge in the tank that prevented rf buildup. This was finally overcome by pulsed bias applied simultaneously with the rf pre-excitation pulse. The reasoning was that the bias discharge would require considerable time to develop, and with a properly planned pulse the rf could be built up before it occurred. Any sort of bias however, whether pulsed or not will very likely be unnecessary with a steeper rate of rise of rf voltage.

Experiments in D1 and D2 oscillator positions have shown that it is possible to eliminate the big rotating loop pre-exciters by a much simpler and more convenient shift in an inductive reactance at the normal node of the transmission line. It is now planned to make a permanent installation of this

new system in at least two positions with more to follow when additional A2332 tubes are available. The system planned will use these new type pre-exciters as rf power amplifiers after the pre-excitation cycle is completed. The original planning of the 5831 type grounded grid oscillator system was done with future conversion to an A2332 amplifier system in mind, so that the work involved is relatively minor. When tubes are available and all oscillators are converted it will then be possible to eliminate reactance switching entirely and the sub-exciter as well.

A problem that has been holding up the production of more A2332 tubes has been the presence of thermal grid emission. This seriously limited the drive power that could be applied and led to a run-away plate and grid current condition once it started. The effect is also present in the 5831 tubes, but not so noticeable at the designed power level. Steps to correct this are proving quite effective, and include keeping gun geometry accurately aligned to reduce the number of electrons bombarding the grid and coating the tungsten grids with molybdenum powder to increase their emissivity.

Some model work with coupling loops has disclosed a simple and practical means of making a very efficient and compact design for the A-12 rf system. It will reduce the original space requirement by approximately three.

An interim report on the experimental characteristics of Mark I and on phase correction stabilizing networks will be published during the next report period.

7. INJECTOR ELECTRICAL EQUIPMENT

H. M. Owren
UCRL

During this period the Mark I injector electrical equipment supplied by UCRL was delivered to Livermore and installed. The operation of this equipment was very satisfactory and no revisions were necessary.

Some shorted windings in the 100 kv isolation transformers were detected during the installation. This condition was a result of poor workmanship and the transformers were repaired by the supplier without causing any delay in the operating schedule.

All necessary information on this equipment was supplied to CR& D and spare components were delivered to Livermore.

The Dry Dock facilities of Bldg. 51 were dismantled and moved to Livermore during this period. This equipment is to be installed at Livermore with testing of installation to begin in July 1952.

As all the equipment and necessary information has been supplied to CR&D it would appear that this part of the UCRL activities is completed.

8. M.T.A. MECHANICAL DESIGN

W. M. Brobeck
UCRL

Distribution of Activities

During this period approximately 37 members, compared to 48 in the last quarter, of the Mechanical Engineering and Drafting section were employed on the MTA project. Their effort was distributed as follows: 11 persons on the Mark I program; 15 on A-12; 11 on J-16.

Mark I Accelerator Program (Livermore Linac)

All Mark I components designed by UCRL have been installed at Livermore. Approximately 98 percent of the service manuals (over 700 pages), parts lists (over 400 pages), and duplicate tracings of drawings (over 2000) are completed and have been sent to Livermore. The following improvements, found desirable during the initial Mark I start-up period, were designed during this period:

1. Pre-exciter line automatic node shorts with knife-switch contacts, and an alternative design with pneumatically operated button contacts.

2. Drift tube shorting bars to permit short circuiting the rf bypass condensers when they are not needed thereby reducing the possibility of damage to the condensers.

3. Teflon O-ring vacuum seals as alternates for the Crane teflon chevron packings in the cavity discharge probe and rf voltage pickup lines.

The design of an improved centering adjustment for the cavity discharge probe was 50 percent complete at the end of the period. Auxiliary test equipment requiring mechanical design included a portable pin-hole x-ray camera and an x-ray spark detector, using a photomultiplier, to determine the number and location of sparks between drift tubes.

Mechanical design studies are continuing on the application of refractory facings for the drift tube surfaces to minimize damage due to sparks in the 0-1 and 1-2 gaps. Graphite, chromium, and molybdenum facings have been considered, but molybdenum seems the most promising at present.

A-12 Accelerator (Full Scale Linac)

Ion Pumps. Mechanical design has been completed on (1) Ion Pump 5B which is being used to study pump performance, (2) Ion Pump 101 which will be used to study designs of large cathode structures, (3) various cathodes which have been tested in Ion Pump 5B, (4) a scanning collector for determining the intensity distribution of the ions bombarding the cold cathode of Ion Pump 5B. Mechanical design has been started on a mass spectrograph for analyzing the constituents of the arc of Ion Pump 5B.

Oscillator Transmission Line Test. Design was almost complete at the end of the period on a 1/2-wave transmission line (8-1/4 in. o.d. and 40 ft. long) to be connected to the B-1 cavity. One-half of the line, the cavity end, will be rotated to permit uncoupling the line when an oscillator is removed.

Rf Model. Design was 50 percent complete at the end of the period on the 0.03 scale rf model of the low energy end (first 20 drift tubes) of the A-12 Accelerator. The cavity will be 20 in. dia. x 44 in. long with silver plated steel walls, and the drift tubes will be adjustable in three planes.

Target. UCRL engineering personnel contributed to the "base case" preliminary design which was completed for a target producing plutonium from depleted uranium, and a small scale model of the assembly was constructed at Livermore. The joint UCRL-CRDC design group prepared additional studies of alternative target components (including a beryllium primary target and a gas-cooled secondary target) and prepared a proposal for the experimental engineering facilities required to establish final design specifications for an MTA target.

J-16 Program (Cloverleaf Cyclotron)

Electron Model No. 2. Only minor mechanical engineering efforts have been required by this machine during the last quarter. The main portion of the experimental program has involved experimentation with the magnetic channel for the removal of the beam.

Electron Model No. 3. Construction of the magnet for this machine is complete and magnetic field mapping is in progress. The automatic field mapping equipment has been completed and is now in use in the field mapping program.

20-inch Cyclotron. Operation of the machine has not called for mechanical engineering assistance of any magnitude.

RE Magnet. None of the proposals for building a cyclotron in this magnet have been followed, the facilities having been used for continuing tests of sparking and the damage to surfaces associated therewith.

J-16 Cyclotron. Engineering work on the J-16 machine has reached the point where it is believed not to be profitable to continue until authorization for construction has been obtained. Design work is therefore being stopped pending a decision of the Commission on construction of the full scale machine.

9. MARK I TARGET

G. S. Windle, G. B. Rosenblatt, Jr., G. M. Kibler,
O. J. Elgert, D. E. Lord, M. L. Bushler
CRDC

Solid Target Fabrication

As reported in the last quarterly report, satisfactory laboratory scale target sections had been prepared using an immersed casting technique. Further experiments with this immersed casting method have provided additional information leading to better design and operating details of the five foot pilot unit. Problems investigated include (1) methods for preventing bismuth leakage between cover plate and cover pressure plate with its accompanying cover plate distortion; (2) methods for correcting cover plate distortion due to unequal expansion of cover plate and pressure plate; and (3) methods for improving the quality of the Al-Bi-Al sandwich which involves improving bond quality and the quality of the crystal structure of bismuth.

It has been found that bismuth leakage between cover plate and pressure plate can be prevented by the use of a steel pressure ring to clamp the cover plate to the pressure plate during fabrication. The pressure ring, without gasketing, applies pressure sufficiently great and sufficiently uniform to prevent bismuth from entering the crevice between the two aluminum pieces.

The cover plate distortion, which occurs upon immersing the cover plate - pressure plate assembly in the molten metal (because of unequal expansion of two plates of differing thickness), can be corrected by uniform pressure from within, obtained by a 20° to 30° F temperature increase after press closure.

Investigation has also shown that quenching improves the quality of the target sandwich. The quenching operation consists in lowering the target section after removal from the fabrication tank into a quench tank filled with water at room temperature. Subsequent ultrasonic testing revealed that quenched samples were more transparent to the sonic beam and that there were fewer bond and bismuth flaws than in unquenched sections. A possible explanation of the improvement - as yet unconfirmed by metallographic examination - is that finer grain structure both of bismuth and any occlusions results from this treatment.

A study of the optimum temperature of fabrication revealed that better Al-Bi-Al sandwiches result from bonding in the 585° to 615° F temperature range. Below this lower limit poorer bonds resulted, while above the upper limit flaws in the bismuth were more numerous and more pronounced.

Measurement by ultrasonic means of the thickness of the bismuth layer in those samples prepared by laboratory immersed casting revealed that in each case the measured dimension fell within the machining tolerance set for the aluminum backing plate. It thus appears that the production target bismuth layer will be within design tolerance.

Interest has been renewed in the application of ultrasonic bonding techniques to target fabrication problems. This bonding method was briefly examined several months ago and rejected because commercial sizes of transducers were not then available. In the interim, two vendors have announced their intention to produce larger transducers. Accordingly, a Mullard ultrasonic soldering iron and power supply has been ordered for laboratory scale fabrication experiments. If this application is successful, it is expected that ultrasonic bonding will make obsolete the current mechanical bonding procedure. However, even if successful, the use of ultrasonic fabrication for pilot size target sections is six to twelve months away, and the first pilot sections (and probably the probes) will be fabricated mechanically.

The design of the five foot, pilot scale target casting unit has been completed, equipment has been requisitioned, and construction is imminent.

Initial attempts by Bohn Aluminum and Brass to extrude the order for close tolerance, special alloy, aluminum target backing sections were suspended when the die failed. Extrusion was rescheduled for mid-June.

Welding of Solid Target Cover Plate

The design of the solid target calls for cover plate restraint by edge welding of the cover plate to the lip of the back plate. This weld was obtained relatively easily using vertical casting methods. The change of fabricating procedure to immersed casting has accentuated the welding problem because of the bismuth trapped between the 20 mil cover plate and the lip of the 3/4 in. backing plate. Various joining methods have been investigated for accomplishing this weld, and it appears that several solutions to the problem are available.

Three acceptable types of welds of cover plate to backing plate have been made using the manual heliarc and 5 percent Si, aluminum filler rod. The welds made include the bead weld, lap weld, and "crimp" weld. The "crimp" weld combines the more desirable features of the bead and lap welds but also requires more elaborate weld surface preparation. The three types of weld have been made on both precleaned sections and sections from which the entrapped bismuth has not been removed. It appears that precleaned surfaces give the better weld although the difference in welds is not as great as might be expected. Cover plate and backing plate bonds at the exposed edges of the sample were not materially affected by the welding procedure.

Attempts have been made to clean the bismuth from between the cover plate and backing section by use of a 6 mil jewelers slitting saw, but these attempts were not particularly successful. A better method of cleaning is accomplished by bending open the cover plate over a template; machine grinding of the bismuth from the exposed inner surfaces of the cover plate and backing plate; and closing the cover plate to its original position. It is also possible to design a rolling and grinding sequence which will accomplish the foregoing cleaning operations mechanically.

Several semi-automatic and automatic welding processes for obtaining this closure have been attempted in the laboratories of welding machine vendors, such as Linde and Air Reduction. It appears that the results obtained depend more on the skill and technical background of the operator than on the weld design or the welding method. The experiences herein stated, do not imply any preference at this time for the products or methods of one vendor over any other vendor.

Acceptable lap welds of cover plate to backing section have been made on bismuth contaminated sections using close mounted copper "chill" bars with the "Heliweld" process (Air Reduction). The welding procedure utilized a hand torch, helium shielding, direct d.c. arc with thoriated tungsten electrode and no filler rod. Very successful results were obtained when welding uncontaminated aluminum sections with the above procedure and a radiograph mounted torch travelling 20-30 inches per minute. This semi-automatic method was not successful with contaminated sections. If inert gas welding is used for the closure, it appears that the weld may be accomplished by a skillful operator using a hand torch on contaminated sections or by a semi-automatic process on bismuth-free sections. The selection would be dictated by the economics of hand welding versus precleaning bismuth from target sections.

It may yet be possible to prevent bismuth pollution of the weld puddle by the use of water cooled copper "chill" bars, and this aspect will be investigated along with other welding processes as time permits.

A visit was made to the New Kensington Laboratories of Alcoa to discuss, among other things, possible welding procedures. Alcoa confirmed the belief that the manual inert gas welding with an experienced operator would probably produce a satisfactory closure. They felt that if the adaptation of semi-automatic or automatic equipment to this weld was desired the revision of the Linde "Sigma" process or the Air Reduction "Aircomatic" process was feasible. They suggested that because of the small diameter filler wire required neither Linde or Air Reduction would be as qualified to make these revisions as some welding speciality concern such as Schnitzer of Newark, New Jersey.

Alcoa also demonstrated a hand operated pressure welding ("cold-welding") method which may be satisfactory if a good seal is more desirable than a strength weld. (Heretofore weld strength has been considered more important than a good seal. Results of radiant heating experiments suggest that the importance of weld strength has been overemphasized.) Examination of the sample that they produced by pressure welding indicated that care must be taken to prevent undue torsional stresses to welds obtained in this manner. A more complete investigation of pressure welding procedure as applied to the welding of solid target cover plates would involve a reasonably extensive development program of approximately $20,000 for design and fabrication of a cleaning and welding roll line. Alcoa suggested that one of the foremost American companies doing development work on pressure welding is the McKay Machine Company of Youngstown, Ohio.

Ultrasonic Inspection

Inspection of recently cast thermal stress bars and one immersed casting target section has indicated cracks close to the bonds or in the center of the bismuth layer. Using the Techtronix oscilloscope the depths of these cracks have been determined. One immersed casting specimen was sectioned, and the crack was found to be readily visible to the naked eye. One section of the specimen was found to contain a small void about 0.002 in. dia. and 0.005 in. below the top bond which was readily found ultrasonically using the 20 megacycle crystal with 1/4 in. dia. collimation. Several target sections were subjected to metallographic examination to determine the nature of different types of flaws found ultrasonically. Results indicate that an ultrasonic reflection may be caused by aluminum oxide occlusions in the bismuth. One sample which ultrasonically indicated a very thin flaw (less than 1/32 inch) about an inch long was found to consist of a line of minute occlusions. Another sample, which ultrasonically indicated a lower bond flaw, was found to have a large occulsion at the lower bond.

In the inspection of target sections, it was found that better results were obtained when the crystal was positioned from 1/8 inch to 1/4 inch from the target using no collimation. At this range the beam exhibits collimating tendencies in that a 1/8 in. flaw exactly in the center of the 3/8 in. diameter beam area gives a large reflection and the same flaw gives practically no reflection when the crystal is shifted approximately 1/8 in.

The 0.020 inch aluminum cover plate has been resolved directly by the technique of using only the lower side band of the transmitted pulse envelope; that is, the crystal and the receiver are tuned to center frequencies of 17.5 megacycles, and 15 megacycles respectively. The 5 megacycle band width allows a 2.5 megacycle overlap from 15 to 17.5 megacycles. It appears that the carrier frequency, 17.5 Mc is rejected or reduced by the band pass characteristics of the receiver. This remaining lower side

band, 15 to 17.4 Mc after amplification showed two clearly separated pulses on the Techtronix oscilloscope exactly 0.1675 micro seconds apart, the time corresponding to 0.020 inches of aluminum. These results are reproducible and appear valid. This technique was used with an air-backed 0.020 inch sheet and also on a bonded target section. The air-backed sheet gave a strong back reflection and several multiple echoes while the bonded target cover gave a lesser back reflection and no multiples, as would be expected. In resolution of thin sheets the normalness of the crystal to the sheet is much more critical than when resolving thicker sections. This was found to be true in resolving the bonded target cover. Normalness readjustments had to be made at various points on the section to clearly resolve the cover. This can be attributed to a slightly uneven cover, and therefore the direct inspection of the cover bond by this method is not adapted to automatic scanner operation as presently designed. The indirect cover bond method (attenuation of rear echo) is a more reliable system when used with the automatic scanner.

Another method of resolving the 0.020 inch aluminum cover plate, which may lend itself better to automatic scan operation, has been suggested by Dr. W. W. Salisbury of CRDC. This method transmits a square pulse envelope of rf energy, and because the reflections are the same shape as the transmitted pulse, the cover bond echo would be clearly visible as a "step" on the trailing edge of the cover echo. The square pulse shape is obtained by inverse feed back to the crystal which prevents the crystal from "ringing" after the energy pulse has passed. This cuts off the pulse "tail" giving a sharply defined, nearly vertical trailing edge to the pulse. Thus, the cover bond echo is not obscured by the cover echo, and resolution is possible. A unit of this type, as a modification to the wide band converter, has been designed with the assistance of Dr. Salisbury.

The experimental "D" scan electronic unit has proved to be practical, and a larger two channel electronic scanner-recorder is in the process of construction.

Preliminary design of the automatic motor-driven mechanical scanner has been completed. This scanner equipment will need only a larger water tank and a longer length of guide rail to modify it for use with the full scale production target.

Revisions to Target Design

It has always been realized that the presently contemplated target design condition calling for a 29 foot square target with 130 foot setback and circular precession, is not optimum for a given beam size since this design is predicated on a beam diameter of 2 feet plus or minus 50 percent. Recent information indicates that the beam diameter may be more nearly 30 in.

It is also felt that the calculated peak to average beam intensity profile of 33 to 1 (Panofsky) may be improved upon.

Accordingly, preliminary calculations were made with the assistance of A-12 group members to evaluate the effect on target design of the latest thinking in beam specifications. Assuming a 30 in. beam, optimum circular precession (rho = r_{max}), and a maximum allowable peak heat flux of 416,000 BTU/hr sq. ft. (CRC report SPL-51:20, 7/6/51), the following table summarizes possible design improvements:

Peak to Ave	Set back (feet)	Target Diameter (feet)	Q/A (BTU/hr/sq. ft.)
33:1	95	21.4	390M
20:1	88	20.0	403M
10:1	78	18.2	416M

If spiral sweeping may be considered, which would entail material changes to the present magnet system, it may be possible to operate a 19 foot target at a set-back of 51 feet with a peak flux of 404,000 BTU/hr/sq. ft. If one considers that the present D-8 vessel setback is approximately 40 feet, a 51 foot set-back would be a worthwhile achievement. To summarize, it is probable that when beam characteristics are actually determined, considerable improvements in solid target design may be expected. Studies to bracket probable beam characteristics are in progress.

Probe Design and Limitations

Because of various schedule changes it now seems feasible to fabricate the probes using the five foot pilot casting unit, and plans for vertical casting of probes have been abandoned.

Further consideration of the design of the solid target probe has revealed several factors which will limit the amount of information obtainable by operation of the probe. These are:

(a) A PW deuteron beam is not equivalent to a CW proton beam of the same energy. First, to duplicate the target temperature profile, it is necessary to adjust the thickness of cover plate and bismuth. Second, pulsing causes slower cyclic temperature variations of greater amplitude than does the more rapid precessing.

(b) Because of the differences between CW protons and PW deuterons, it will be impossible to duplicate simultaneously both the temperature profile and the cyclic temperature variations expected in the target. For example, proper

cover plate and bismuth thicknesses and proper beam power (500 microamp) to reproduce the temperature profile (ΔT = 250° F) result in a cyclic T of 200° F. When irradiated (with 45 microamp beam) so as to reproduce the cyclic temperature variation, (ΔT = 17° F average), the temperature difference front to back will be only about 20° F.

(c) Failure of the probe irradiated by a low amperage beam can be due only to the stresses induced by the thermal cycling, but failure of the probe at high beam current can result either because of excessive front-to-back temperature difference or, more probably, to large temperature cycling. It will be difficult to determine the cause of failure.

Because of these factors the following are the only conclusions expected from probe operation:

(a) If the probe does not fail at high currents, (500 μa), it can be concluded that the target as designed will not fail.

(b) If the probe fails at low beam current, (45 μa) the target as designed will fail.

(c) If the probe fails at high beam current, as is most probable, the target as designed may or may not fail.

Operation of a probe, while very valuable for understanding the design, will not answer all questions pertaining to operation of the solid target.

The original design of Mark I probe support has been modified and simplified to conform to the design currently contemplated by the Radiation Damage Group for their probe supports.

Thermal Cycling by Radiant Heating

The radiant heat cycling test has been terminated with the completion of 1010 cycles - the equivalent of ten spark-downs per day during the period of irradiation planned for the production target. This test was designed as a "go-no go" test to determine (1) the ability of the production target to withstand the high front-to-back temperature differential expected and (2) the ability of the production target to withstand conditions of start-up and spark-down during proton irradiation. The data obtained are now being analyzed, but in general it may be stated - subject to later modification - that the production target probably can withstand these conditions without failure.

1903-73

In this test a specially designed target replica was exposed to radiant energy striking its face from a port in a Globar furnace at 2600° F while being cooled through water channels in the target backing. Cycling was obtained by manually opening and closing a shutter placed between the furnace port and target.

Briefly summarizing the results, visual examination after completion of the test shows that there was little change in the target. The cover plate did not crack nor separate from the bismuth. Edge welds are apparently unchanged, the one inch cold bismuth-aluminum bond at either end of the sample provided sufficient restraint, and there was no leakage of molten bismuth. An orange-peel rippling is observable on a portion of the cover. Periodic ultrasonic examination revealed that during the course of the cycling; (1) there was some growth or extension of pre-existing bismuth flaws; (2) there was some increase in size and number of "cover flaws" (so designated although the bonds themselves appear to be satisfactory by other tests); and (3) one apparent rear bond flaw has developed. The test is believed to have been particularly severe in every respect except in the number of cycles applied.

Comparisons with the production target are summarized below; note that the peak face temperature measured for the radiant heat target is above the melting point of bismuth although no leakage occurred and there was no observed evidence of melting:

	Calculated Conditions for Production Target	Measured Conditions for Radiant Heat Target
Thickness Bi layer, inches	0.065	0.116
Heat flux BTU/hr ft^2	416,000 (peak)	100,000 (approx. avg.)
Peak target-face temperature	485° F	More than 600° F
Front-to-back ΔT,	260° F	More than 400° F
Cyclic ΔT, cover bond	14° F	More than 350° F
Cyclic ΔT, back bond	38° F	More than 50° F

Cursory examination of the radiated target and the above data suggest that the present target design is conservative, but firm conclusions will await detailed analysis of experimental results.

Mechanical Stress Cycling

Three bar pairs were successfully vertical-cast and cooled by quenching in water. The quench cooling eliminated the apparent cracking of the bismuth layer as shown by ultrasonic inspection. The bar pairs were

inspected by ultrasonic equipment before vibrating and after approximately 1 x 10^8 and 2 x 10^8 cycles. The following table summarizes the data:

Bar Pair No.	Temperature Level °F	Maximum Simulated ΔT - °F	Cycles	Length of Rippling - Inch
1	390	41°	2.25x10^8	9-1/2
2	255	75°	2.05x10^8	Entire Bar
3	505	41°	2.02x10^8	None

Ultrasonic inspection of the covered bars after 1 x 10^8 cycles showed that cover bond flaws had been extended in all three bars. This may have been partially due to end effects on the unrestrained cover plates. Therefore new bars with welded cover plates will be tested as a check. Bismuth cracks and lower bond flaws did not change materially after 1 x 10^8 cycles. After 2 x 10^8 cycles, ultrasonic inspection showed an increase in both bismuth cracks and lower bond flaws for the bars of the higher temperature levels (No's. 1 and 3). Only a very small increase in bismuth cracks was observed in the low temperature bar (No. 2) even though it was under a higher stress.

The uncovered bars showed no increase in back bond flaws or bismuth cracks, after 2 x 10^8 cycles. Uncovered bar No. 2 improved incredibly after 2 x 10^8 cycles. Nearly all bismuth cracks had been healed and even the lower bond flaws had improved somewhat.

Rippling (creep) covered the entire length of uncovered bar No. 1, at 390° F and 41° F ΔT, and it was especially severe at the high stress end. Rippling on bar No. 1, at 390° F and 41° ΔT, extended to about 9-1/2 in. from the high stress end. No rippling was present on bar No. 2, at 255° F and 75° F ΔT. It can be concluded that rippling increases markedly with increasing temperature level.

Corrosion Studies in System Steel-Bismuth

Encouraging results in solid target development and limited manpower available for Mark I Target work have necessitated reduction of the emphasis placed on molten target development. A limited amount of this work is still maintained in case unforseen developments should rule the solid target impractical. As outlined previously, the feasibility of the molten target is dependent on solving the mass transfer problem, and only a minor amount of time has been spent on this project.

Modifications have been made on the auxiliary equipment for the thermal loops. A reducing furnace to remove oxygen has been placed in the helium line. A water cooling jacket to cool hydrogen gas has been placed on the outgas line from the thermal loop. Hydrogen will be used to reduce any bismuth oxide in the charge before beginning the next series of runs. The

new loop of Sicromo-5S steel has been installed and is ready for operation. All other loops are now out of service due to perforation of the reservoirs by air oxidation.

Deuteron Fate

Design and fabrication have been completed of sample holders and monitoring equipment for repetition of the deuteron fate experiment in the 60-in. cyclotron. This experiment is being repeated in an attempt to resolve the inconclusive results obtained previously. Bombardment is scheduled for mid-June.

Metallography

Up to the present time there has been a notable lack of correlation between the results of ultrasonic inspection and those obtained from metallurgical examination of Al-Bi-Al solid target sandwiches. For example in most instances it has not been possible (1) to find bond flaws by ultrasonic inspection, although metallographic examination indicated their presence; (2) to find bond flaws by metallographic examination where indicated by ultrasonic testing, and (3) to discover any changes in grain size or structure produced by quenching of immersed cast target replicas, although ultrasonic inspection has indicated that some differences must be present. In a few instances it has been possible to discover cracks within the bismuth layer where indicated by ultrasonic reflections, and to find occlusions at locations giving ultrasonic indication of flaws, but these have been exceptions to the general experience.

It is believed that this low degree of correlation is due to the lack of success in obtaining satisfactory metallurgical polishing and etching. The difference in hardness of the two metals involved, and the softness of each of them, facilitates flow or "smearing" the metals over defects which would otherwise be seen.

An investigation of various polishing media is now underway. The most satisfactory polish yet tried consisted of finely divided chrome oxide; its sharp free-cutting particles cut but did not flow the metals. This polish did, however, leave scratches on the bismuth surface, and the true picture of the metal and its flaws was distorted thereby.

An alternative approach to a solution of the difficulty - electrolytic polishing and etching - is now being studied. The investigation has consisted in searching for a satisfactory electrolyte and for optimum conditions of temperature and electrolyte concentration. Results of the investigation to date have revealed that:

1. Nitric acid is an unsatisfactory electrolyte due to rapidity and unevenness of attack.

2. Orthophosphoric acid is unsatisfactory due to the deposition of a non-conducting film on the bismuth surface.

3. Fluoroboric acid proved partially satisfactory at low temperatures (10° C) and low concentrations (0.8 percent) in spite of its untypical voltage - current density relationship. Its etch was, however, too deep and its attack somewhat uneven.

4. Nitric acid - methyl alcohol solution (1 to 4 ratio) has been the most satisfactory electrolyte yet tried. Its voltage - current density relationship was found to be characteristic of a good electrolyte. At 30° C the polish was good though somewhat deep. It is believed that variation of temperature and concentration will produce highly satisfactory results.

19.3.77

10. TARGET AND LATTICE PHYSICS PROGRAM

Introduction

C. M. Van Atta
UCRL

Activities of the NEA target physics group during the past three months have been mainly concerned with the following problems:

1. Detailed neutron physics of the primary and secondary targets;
2. Calculations on neutron exchange and loss in various target and lattice systems;
3. Theoretical and experimental determination of neutron flux distributions;
4. Angular distribution and production of neutrons in simulated water-cooled uranium targets of large cross section;
5. Energy distribution of evaporation neutrons from uranium bombarded with 190 Mev deuterons and 340 Mev protons.

Results obtained on the angular distribution and approximate total yield of neutrons about a target of large (3 ft. x 3 ft.) cross section and with polyethylene sheets interposed between uranium plates to simulate the effect of cooling water are most directly applicable to the A-12 target design. A water tank, large enough to permit measurement of the total yield from the large target by absorption of the neutrons in manganese dissolved as $MnSO_4$ as was previously reported for targets of small cross section, has been constructed and will soon be in operation. Total yields determined by this method are regarded as more valid than those obtained by integration of the long BF_3 counter angular distributions.

The use of a small-scale water lattice for the study of the neutron flux distribution about bombarded targets is proving to be most instructive. Since the slowing down distance and thermal diffusion length for the water lattice are both quite small, many features of the production lattice can be studied on quite a small scale without getting into scaling difficulties. By combining small model flux distributions with theoretical interpretations a much firmer grasp of the product distribution and neutron losses in the full scale A-12 lattice will result.

The effort of the target physics group is turning more toward the investigation of the fundamental processes involved in neutron production by high energy particles. The angle and energy distributions of high energy stripped and knock-on nucleons, the energy distribution of evaporation neutrons from excited nuclei and the process of nuclear excitation by high energy particles are under intensive experimental and theoretical study. A conservative extrapolation of neutron yields to higher energies than are at present available has been based upon a semi-empirical method. A major objective of the physics program will be to provide through a more detailed knowledge of the high energy nuclear processes a firmer basis for this extrapolation. Since the economics of the MTA depends critically upon the yield as a function of energy, such a study may well shift our attention to the 450-600 Mev range with appreciably lower cost per gram of free neutrons or per mole of product.

Helium 3 Stripping

Warren Heckrotte
UCRL

L. Alvarez suggested that the production of a high energy deuteron beam (340 Mev) might be obtained by the stripping of He^3. The production of such high energy deuterons is of interest for MTA target design since most design problems have been met by extrapolation of results obtained at 190 Mev. The $H\rho$ of the cyclotron magnet allows the production of 510 Mev He^3 nuclei, so that a deuteron stripped from He^3 would have an energy centered about (2/3)510 = 340 Mev. A calculation has been made to determine the stripping cross section and the angular and energy distributions of the deuterons. The model used by Serber to calculate deuteron stripping was extended and applied to the stripping of He^3. Without going into the detailed analysis a few remarks which pertain to the results should be made. Since it is necessary to make a choice of wave functions for the deuteron and He^3, the results will depend somewhat upon that choice.

For simplicity, a Gaussian dependence on the coordinates was chosen with the parameters picked to give the best fit to the binding energies. Because of this choice one may expect the angular and energy distributions derived from them to have a somewhat smaller width than is actually the case.

The stripping cross section obtained is

$$\sigma_t = 0.255\, A^{1/3} \times 10^{-26}\ cm^2$$

which is about 1/20 of the deuteron stripping cross section. It should be noted that one can obtain about the same result, without explicitly introducing any particular wave function, by making appropriate approximations.

The angular distribution is given by

$$P(\theta)d\Omega = \frac{1}{2\pi\theta_0^2}\, e^{-(\theta/\theta_0)^2}\, d\Omega$$

The distribution has been normalized to 1. θ_0 is the angle at which the distribution drops to 1/e of its value in the forward direction and is given by

$$\theta_0^2 = \frac{3.518}{E} \text{ (radians)}$$

The number depends on the constants in the wave function and E is the energy of the He^3. For E = 510 Mev,

$$\theta_0 = 0.8305 \text{ rad.} = 4.76^\circ$$

The total angular width is thus $2\theta_0 = 9.52^\circ$.

The intrinsic Coulomb scattering or the Coulomb scattering due to the passage of the beam through the target has been ignored here. For an atomic number Z, of less than about 40 though, the intrinsic Coulomb scattering may be neglected. The scattering due to the passage of the beam through the target has not been considered as yet but this will be quite small if the stripping target is composed of nuclei Z < 40.

The energy distribution is given by

$$P(E)dE = \sqrt{\frac{\omega}{\pi}}\, e^{-\omega\frac{(E-E_0)^2}{E_0}}\, \frac{dE}{\sqrt{E_0}}$$

This distribution is normalized to 1. E_0 is the average energy of stripped deuterons and is equal to 2/3 E_{He^3}. ω is a constant which depends on the wave function and is

$$\omega = 0.107 \text{ Mev}$$

The half width of the distribution about the mean energy E_0 is given by $\sqrt{E_0/\omega}$. The half width is here defined as that energy for which the distribution drops to 1/e of its value at $E = E_0$. For 510 Mev He^3, this gives a half width of 56.6 Mev, or a total width of 113.2 Mev. Because of this rather large energy spread the additional spread caused by the ionization loss in the target will, at least for low Z nuclei, be comparatively small.

Fig. 1 shows energy distribution of deuterons stripped from 540 Mev He^3. Fig. 2 shows angular distribution of deuterons stripped from 540 Mev He^3.

1903.80

Resonance Escape Probability, MTR Target

R. Lelevier
UCRL

The resonance escape probabilities for the MTR primary target (1/16 in. uranium plates separated by 1/10 in. of water) and secondary target (1/4 in. uranium plates separated by 1/10 in. of water) were evaluated (UCRL-1800), using the experimental data of Untermyer (ANL-4350). Untermyer had determined the effective resonance integral as a function of mass to surface ratio. The empirical fit to his data was modified to read

$$\left[\int \sigma \frac{dE}{E}\right]_{eff} = 9.23 \left(1 + C \frac{2.5}{M/S + 0.1}\right) \text{ barns},$$

where C is a correction factor introduced to account for the reduction in surface absorption due to the proximity of nearby "lumps" of metal. For the target geometry in the MTR system,

$$C = 1 - 2E_3(a) \qquad \text{(CP-2157 or UCRL-1679)}$$

where $E_3(x)$ is the exponential integral of order 3 and a is the thickness of the water layer in units of the neutron mean free path. (For $a > 1.6$, then $C > 0.9$. In the present case $a = 0.339$ and $C = 0.436$).

The results are

$p = 0.71$, primary
$p = 0.42$, secondary

If one neglects the screening of the resonance flux incident on a given plate by its neighbors one obtains a lower limit on p for the heterogeneous system. This is done by setting $C = 1$; i.e., by considering a single cell of the target, 1/16 in. or 1/4 in. of uranium plus 1/10 in. of water, with a full dE/E spectrum incident. These lower limits are

$p = 0.59$ for the primary
$p = 0.36$ for the secondary.

Mitchell (CP-1676) has measured the effective resonance integral for homogeneous systems as a function of the total scattering cross section per uranium atom. If the targets were homogeneous systems one finds, using Mitchell's data,

$p = 0.67$, primary
$p = 0.39$, secondary.

Summarizing the results then,

	Primary	Secondary
$p_{lower\ limit}$	0.59	0.36
$p_{heterogeneous}$	0.71	0.42
$p_{homogeneous}$	0.67	0.39

An approximate upper limit on p may be found from the fact that a system of natural uranium rods and water cannot be made critical. The limits found are $p < 0.8$ for the primary and $p < 0.7$ for the secondary.

The values of $p = 0.71$ and 0.42 for the primary and secondary, respectively, found by modifying Untermyer's formula, are considered to be the best estimates available.

Neutron Streaming in a Cylindrical Cavity

R. LeLevier
UCRL

The question of the leakage into the target and out the beam hole of neutrons emitted from the lattice walls was considered. Assuming the flux is emitted with a cosine θ law, one finds the fraction of the emitted flux lost out the beam hole, $F_B(x)$, from a ring element of unit width located at x is

$$F_B(x) = 1/2 \left\{ \frac{1 + 2x^2}{\sqrt{1 + x^2}} - 2x \right\}, \qquad x = \frac{L - s}{D}$$

The fraction intercepted by the target is

$$F_T(x) = F_B\left(\frac{L}{D} - x\right).$$

$F_B(x)$ has the value 1/2 at $x = 0$, that is, for a ring element located at the end of the tube, and decreases almost exponentially as x increases. $F_B(1) = 0.06$; a ring element located one diameter away from the end of the tube losses 6 percent of the emitted flux out the end. Using the experimental data of J. Ise for the flux distribution along the walls of the cavity, one finds that 7.2 percent of the neutrons emitted from the lattice walls are lost out the beam hole and 16.6 percent of the emitted flux is intercepted by the target. The fraction intercepted by the target is greater than that lost out the beam hole since the experimental flux distribution is strongly peaked near the target.

The figure of 7.2 percent is, of course, not the actual production loss, nor are all the neutrons intercepted by the target absorbed there. The flux level in the lattice per source neutron from the target and the albedo of the target must be evaluated in order to obtain estimates of overall beam hole losses and target production and heating.

Effective Source Function--Fast Group

R. LeLevier
UCRL

An effective source function for epi-resonance neutrons, i.e., the fast group, has been derived using K. Street's chemical data. The analysis makes use of the one-dimensional transport theory. The data at hand consists of an on-axis profile of the Np^{239} activity in a 2 ft. x 2 ft. uranium block, 13 in. thick, irradiated by the 190 Mev deuteron beam. The data then provides us with the flux, $\phi(z)$, and one can determine the resultant of the source functions,

$$\int_0^L \frac{1}{v} q_0(z') E_1\left[\frac{|z - z'|}{\lambda}\right] dz' = Q_0(z)$$

from the integral equation for $\phi(z)$,

$$\phi(z) = \int_0^L \left\{\frac{c}{\lambda} \phi(z') + \frac{1}{v} q_0(z')\right\} E_1\left[\frac{|z - z'|}{\lambda}\right] \frac{dz'}{2} .$$

L is the thickness of the block
λ is the total mean free path of the group (E - 0.1 Mev)
v is the velocity
λ_c is the capture mean free path
$c = 1 - \lambda/\lambda_c$
$q_0(z)$ is the source distribution
$E_1(x)$ is the exponential integral of order one.

The expression for $\phi(z)$ assumes a one-group model with an isotropic scattering law.

The resultant of the source function, $Q_0(z)$, was fit by assuming as simple a form as possible for $q_0(z)$. This form was

$$q_0(z) = e^{-7.3z} - e^{-3.0z} + 4.3\, ze^{-3.0z}$$

which is plotted in Fig. 3.

The strong exponentials in $q_0(s)$ can not reasonably be interpreted in terms of normal cross sections, but rather must reflect the inadequacy of the model used. In order to be able to extrapolate such a source function to 350 Mev deuterons, one must devise a model for which the required cross sections have sensible values. Furthermore, the model must be compatible with the extremely rapid variations of the neutron flux near the beam face of the target (see Fig. 4). It appears, therefore, that the quantities involved will not be interaction cross sections, but will instead be "cross sections" which represent probabilities for the production of a single neutron, i.e., interaction cross section multiplied by the number of neutrons per event.

Target and Lattice Calculations

F. L. Adelman
UCRL

Loss of Neutrons through $MnSO_4$ Tank Walls

Since a significant number of neutrons can escape through a 6 in. thickness of H_2O, the reliability of neutron yield measurements made in the small tank (UCRL-1480) was under discussion early in this period. Although the tank measurements are calibrated against a Ra-Be source of known strength and energy spectrum, an error remains which depends upon the energy spectrum of the MTA neutrons.

This effect was calculated (UCRL-1736) for plane geometry, with the source neutrons incident normally upon a slab of thickness equal to the actual thickness of the $MnSO_4$ solution. Since most of the neutrons must traverse a larger thickness of the solution in order to escape, the results will tend to overestimate the absolute leakage with either source and also to exaggerate the difference between the two sources. A two-group approximation was chosen, with a first-collision source and average values for the constants of the two sources. For lack of better information, the MTA spectrum was assumed to be essentially a fission spectrum. The possibility that the averaging process may be unreasonable led to an additional computation in which the fast leakage was found for a Ra-Be source consisting of 3 components. The results are given in Table 1.

Table 1

Loss of Neutrons through Plane Slab

Source	Wall Thickness	Fast Leakage	Thermal Leakage	Total Leakage
MTA	6 in.	17.3 %	4.1 %	21.4 %
Ra-Be	6	26.7	3.9	30.6
Ra-Be (3 groups)	6	27.7	---	----
MTA	12	1.82	0.48	2.3
Ra-Be	12	6.59	1.10	7.69

1903.84

In these calculations the errors due to the approximations apparently tend to cancel, for W. Crandall et al. compared the MTA 6 in. tank with the MTA 12 in. tank and found -23 percent additional loss of neutrons from a Ra-Be source in the small tank, and K. Street found -30 percent loss of neutrons from a similar source in the small tank compared to a very large tank.

From Table 1, then, one may conclude that the results obtained from the 12 in. tank will not be more than -5 percent in error, while small tank results could be off by twice as much. Furthermore, the losses from the small tank are so large that inaccuracies in the constants used in the calculations could introduce another significant source of error. Therefore, it would seem that 12 in. of $MnSO_4$ solution (or H_2O) is a minimum thickness for reasonably accurate measurements.

A-12 Moderated Target

Calculations of the leakage, production, and heating in A-12 primary and secondary targets are underway. Two-group diffusion theory, plane geometry, and the source function for 190 Mev deuterons (see above) was used. Since the physical interpretation of the exponents in the source function is not obvious, no attempt was made to extrapolate the source function to 350 Mev. For similar reasons, the normalization of the source function has also been postponed until calculations have been completed for pure uranium targets. The results per source neutron are given in Table 2 for two primary targets with no secondary.

Table 2

Neutrons per Source Neutron

Primary	Leakage				Production	Fission
	Fast		Thermal			
	Toward Beam Hole	Away from Beam Hole	Toward Beam Hole	Away from Beam Hole		
0.065" U (0.3% U^{235}) +0.1" H_2O	0.506	0.066	0.064	0.015	0.25	0.069
0.045" U (natural) +0.1" H_2O	0.557	0.101	0.069	0.018	0.30	0.185

The computation for a primary and secondary combination is much more complicated, and, in fact, the usual approach requires the solution of eight simultaneous linear equations. In an attempt to develop a scheme to reduce the probability of computer error, H. P. Kramer has solved the equations using a "Green's matrix". The method occupies too much space to be repeated here, but it may be found in UCRL-1830.

Use of Natural Uranium in the A-12 Lattice

In view of the revised basis for the evaluation of the MTR project, a brief investigation of natural U-H_2O lattices was undertaken. The optimum triangular rod configuration for 1-inch diameter uranium rods appears to be 1-5/8 in. center-to-center spacing. Since the heating will be much greater than in the base case, process tubes are included. The actual dimensions used were

Rod radius	0.500 in.	
Al cladding	0.025	
H_2O annulus	0.086	
Al process tube	0.059	
Rod spacing (triangular)	1.625	center-to-center

Using losses* as in the base case, 3.4 moles Pu^{239} per mole of neutrons incident on the lattices are produced (1.5 in the resonance region). (The base case gives 1.25 moles Pu^{239} per mole of incident neutrons, of which somewhat over half was resonance production).

Three-Group Equations for a Multiplying Lattice

The three-group equations for a one-dimensional multiplying medium are

$$\phi_1'' - K_1^2\phi_1 + \frac{k}{p}\frac{\lambda_3 K_3^2}{\lambda_1}\phi_3 + \frac{3Q_0}{\lambda_1\lambda_0}e^{-x/\lambda_0} = 0 \qquad (1)$$

$$\phi_2'' - K_2^2\phi_2 + \frac{\lambda_1 K_1^2}{\lambda_2}\phi_1 = 0 \qquad (2)$$

$$\phi_3'' - K_3^2\phi_3 + p\frac{\lambda_2 K_2^2}{\lambda_3}\phi_2 = 0 \qquad (3)$$

In the past it was felt that the easiest way to treat this system for an MTR lattice was to solve it without the term in ϕ_3 [Eq. (1)] and then to introduce the resulting ϕ_3 in Eq. (1). This iterative procedure converged rapidly for a medium with depleted uranium fuel, and a second iteration was not needed. For natural uranium, however, the multiplication is not a small perturbation, and convergence may not be as rapid. Therefore, the exact solution was examined, and found to be quite tractable; in fact, it appears to be easier in the multi-medium case than the iterative method.

* Although the production is quite sensitive to the choice of loss coefficient, it appears that the coefficients used here are not overly optimistic.

The solution is straightforward (see UCRL-1855), but requires the solution of a cubic equation. There is always one real root, negative for a pile ($k > 1$) and positive for MTR ($k < 1$). The other roots are essentially independent of k if $(1 - k) \ll 1$, and are therefore independent of the possibility of a chain reaction. They may be either real or complex. In the latter case, the spatial oscillations of the flux are rapidly damped out and do not show up in a flux plot of convenient scale. Since there is no periodicity in the homogeneous system with the same constants, these variations cannot have any physical significance, and must result from the nature of the approximation.

In two- or three-dimensional geometries, it may be easier to use the iterative procedure than the exact solution, but this will have to be examined in each case.

Interaction of Target and Lattice

When neutrons from the lattice strike the target, they may die there and give rise to production, heating, and additional neutrons. A "cookbook" scheme for evaluating this has been devised; it is quite preliminary and it is hoped that later modification will provide significant improvements.

In essence, the method consists in following each group of neutrons as they strike either the first or second row of tubes. Any fast neutrons which are incident upon the second row of tubes or which are produced by thermal fissions are treated as source neutrons. The effects of such neutrons have been treated (see above). The number of neutrons which strike the target is 17 percent of all those which leave the lattice face (see Neutron Streaming by R. LeLevier earlier in this report).

The numbers found so far from this approach and the work of LeLevier indicate that the losses assumed in previous production estimates are somewhat on the conservative side.

Effect of H_2O Blanket between Vacuum Tank Wall and Lattice

In any lattice arrangement contemplated for the A-12 machine there will be some moderator between the outside surface of the vacuum tank and the first row of fuel rods. Since all lattice computations are based upon an equivalent homogeneous system, half the thickness of moderator associated with the lattice cell is assumed to lie in this region. If, for any reason, additional moderator is placed between the wall and the beginning of the lattice, this layer must be treated as a separate medium. For the case of MTR H_2O moderated systems, a significant variation in the relative positions of the first rod and the wall may be brought about by flexing of the vacuum tank wall. Therefore, the variation of production with thickness of a H_2O blanket was calculated for a typical lattice. The results are consistent with those derived in CRD-T4A-94 (LMS-24299), and indicate that production will be reduced by about 10 percent if a 1 cm H_2O blanket is present.

Unfortunately, the dimensions of the H_2O blanket under consideration are small compared to the fast neutron mean free path and to the slowing down length. Diffusion theory, therefore, is not valid; nevertheless, diffusion theory was employed. The use of transport theory is being studied in order to obtain a better estimate of the effect. An experimental investigation is also being attempted by John Ise.

It is obvious that, if the calculations are reasonably close, the positioning of the fuel rods with respect to the vacuum tank wall will be critical. Therefore, if these calculations are confirmed by experiment or by a better calculation, the problem of placing the fuel rods accurately within a small distance (~1/8 in) of the vacuum tank wall will become important.

UCRL Water Lattice

John Ise
UCRL

During the past few months several runs have been made with the water lattice tank in the external deuteron beam of the 184-inch cyclotron. The first problem to be studied concerned the distribution of thermal and gold resonance (4.8 ev) neutron fluxes throughout the water tank, particularly back along the beam hole, for various target positions and configurations.

Procedure

A sketch of the water lattice tank is given below.

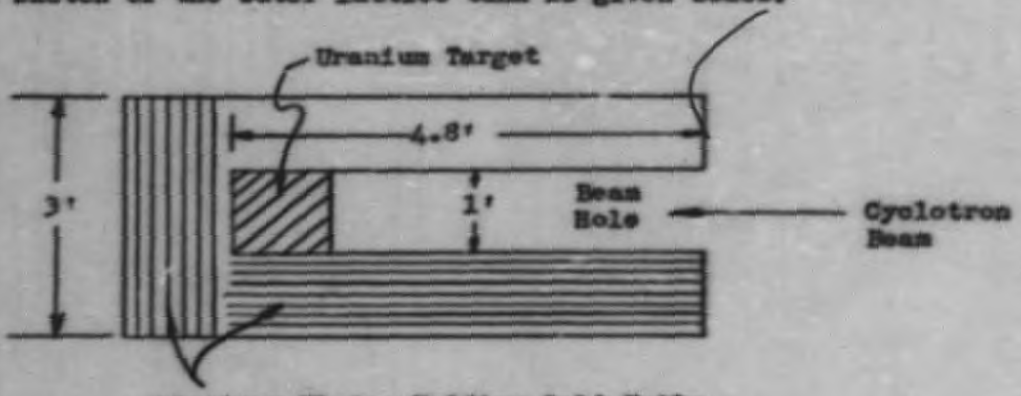

Top View

In all of the experiments to be described, the uranium target was of 12 in. x 12 in. cross section perpendicular to the beam, and was placed at various positions in the beam hole, while the gold foils were hung in thin aluminum plates in the U-shaped water tank.

The cyclotron beam was monitored by means of the activity induced in a 0.005 in. aluminum foil. This gives, of course, only the total charge passing through the foil but for runs of a few hours duration any variation in the cyclotron beam is unimportant, since the half life of the gold activity is 2.7 days.

The gold foils were counted on a revolving trafficounter, using a Tracerlab end-window Geiger counter, which was checked periodically by means of a Q-metal foil set in a polystyrene disc.

The first experiment consisted simply in using a solid block of uranium (normal isotopic content) 12 in. x 12 in. x 9 in., placed at the rear end of the beam tube, and making flux measurements throughout the water tank. Now the neutrons which make their first collisions at some point in the water behind the target, and which, therefore, become thermal near this point (since most of the distance traveled by a neutron in water is traveled in the first few collisions), are essentially of three types: those stripped directly from deuterons, direct-recoil neutrons which escape the target nucleus and the rest of the target without suffering further collisions, and particles whose energies have been degraded by further recoils. The higher energy neutrons should be better collimated around the direction of the initial deuteron beam, and since the mean free path in water goes up with neutron energy, will therefore be distributed farther out in the water blanket. This effect is seen graphically in Fig. 5. These curves show the attenuation of gold-resonance flux along lines parallel to the beam, in a horizontal plane. Curve 1 is taken along the continuation of the deuteron beam; Curve 2 is along a line displaced horizontally by 3-1/2 in.; Curve 3 along a line displaced 7 in.; and so on. It will be noticed here that all the curves except No. 1 show about the same logarithmic slope of 3.6 cm, whereas the central Curve 1 has a pronounced tail, presumably due to the well-collimated high energy neutrons which suffer their first collision well into the water.

Figure 6 shows the same curves as Fig. 5 for the case of bare gold foils (i.e., thermal flux, since the resonance capture contributes only about 10 percent to the total activity for unshielded foils). The difference between Curve 1 and the others, noticed in Fig. 5, has largely disappeared here, due to the diffusion of the neutrons in slowing down from 4.8 ev to thermal energies.

Figure 7 shows the distribution of thermal activities in the side wings of the water lattice tank, along lines parallel to the deuteron beam in the same horisontal plane and at various distances in the water. Curve 0 is taken along the water interface, Curve 1 at a "depth" of 1 in., Curve 2 at 2 in., and so on. The position of the uranium target is blocked in at the top of the page.

Since the water lattice tank should ideally approximate the actual production target as far as possible, it is important to recognize, in examining the above curves, that there are two quite major differences. First, the "L/D" ratio, where L is the length of the wings from the target face back to the front end of the tank and D is the effective diameter of the beam hole, is expected to be about 2 in the case of the A-12, whereas in this small-scale tank it has been set at more nearly 4. Secondly, the A-12 is designed to have swept-back graphite reflectors inset at the front end of the beam hole. This should raise the flux at the end of the tank and consequently throughout the wings.

With this in mind another experiment was undertaken to measure the fluxes along the beam hole with the L/D ratio set at 2 and with a graphite tunnel of 8 in. x 8 in. cross section, 2 ft. in length, and 12 in. wall thickness set up at the front end of the beam hole. This graphite is therefore inset 2 in. all around the front edge of the beam tunnel. Curves 1 and 2 of Fig. 8 show the flux distributions at the water interface along the beam hole for bare and Cd-shielded gold foils, respectively, with the uranium target position blocked in at the top of the page. Curve 3 is merely Curve 0 of Fig. 7 redrawn for comparison. The increase in flux near the graphite interface is readily noticeable in the gold-resonance case, and somewhat less so for the thermals.

From the long boron counter measurements of Roger Hildebrand it was observed that for a beryllium primary backed up by 9 or 10 in. of uranium secondary, the flux in the backward direction was greatly reduced, while the total yield as measured in the water tank was only slightly reduced, if at all. Since the secondary neutrons which produce the multiplication in the secondary are, in the case of the Be primary, of considerably higher energy than from the corresponding U primary, the collimation about the direction of the incident beam will also be better. A run was therefore made using a Be primary 8 in. x 8 in. x 4 in. separated by 22 in. from the secondary U target in the hope of both smoothing out the flux distribution along the beam hole, and, through reflection of neutrons from the U secondary by the Be primary, decreasing the loss of neutrons out the hole. The results for 4.8 ev neutrons are given in Curve 4 of Fig. 8, and the resultant smoothing is quite striking. Comparison of Curves 2 and 4 shows that, in addition to the smoothing effect, a quite considerable <u>decrease</u> of neutron flux must be attributed to the Be setup. However, the separation of 22 in. between primary and secondary was chosen quite arbitrarily and it would be expected that many neutrons from the Be primary would miss the secondary altogether. Further runs at lesser separations are in progress now to see if an optimum distance can be found which looks at all promising.

Comparison of Curves 1 and 3, Fig. 8, shows that apparently the only effect of changing the L/D ratio and introducing the graphite reflector was to shift the beam hole distribution Curve 3 to the left, the slope being left the same. To conclude from this that the graphite served no real purpose is, however, not justified, until a run is made with an L/D of 2 and without the graphite. Presumably the curve should be somewhat steeper, corresponding to lowered fluxes throughout the wings, but the experimental verification of this has not yet been made.

Effect of Water Blanket

As mentioned by F. Adelman in this report, the effect of the water blanket between the beam hole boundary and the first row of uranium bars in the tertiary target is being studied experimentally. A lattice consisting of ten rows of six 1 in. x 1 in. x 12 in. vertical uranium bars, each bar being separated from the next by 1 in. of water, and each row being staggered 1 in. from the two adjacent rows, has been suspended in the wings of the water lattice adjacent to the uranium target. The plutonium production at a given point in the lattice is measured by means of thin uranium foil between 2 halves of a 12 in. bar of uranium. After a deuteron bombardment of about 20 minutes, the foils are quickly removed and then counted, and the initial activity of the 23.5 minute $U^{239} \longrightarrow Np^{239}$ decay is taken as a measure of the production. In order to minimize the rounding of the decay curve due to the various fission product half lives, foils of Q-metal were decided upon, and the resulting decay curves (when the intrinsic background of the foils has been subtracted) are very good exponentials. Considerable question exists as to the dimensional tolerances necessary for the foils--if there are an appreciable number of uranium resonance neutrons in the lattice (7, 23, 40 ev) and if the foils protrude slightly from between the two bar ends between which they are clamped, then an abnormal surface activity around the protruding foil edge will be observed, since the uranium resonances are very high (~10000 barns). It was therefore thought desirable to mill the foils and the bars to as close tolerances as possible (± 0.0003 in.). To date only two points have been obtained on the loss of production vs. position in the lattice. It has been found that when the water blanket was increased from 1/8 in. to 1-1/8 in., the production in the first layer (counting outward from the beam hole) increased by 64 percent, while in the fifth layer the production decreased by 27 percent. The initial increase is at least qualitatively reasonable, since the flux itself increases as one goes into the water tank, for distances of the order of 1 in. (cf. Fig. 6) and then starts to decrease.

Further, more precise experiments on this effect are under way at present and will be reported in detail at a later date.

Angular Distribution and Total Yield of Neutrons from Moderated Uranium Targets Bombarded with 190 Mev Deuterons

Walter E. Crandall, George F. Millburn and Larry Schecter
UCRL

Donald A. Hicks and A. Vay Shelton, Jr.
CRDC

The angular distributions and total yields of neutrons from moderated uranium targets bombarded by 190 Mev deuterons have been determined by means of a shielded long boron trifluoride counter. The targets consisted of a primary made up of alternate layers of 1/16 in. uranium and 3/32 in. polyethylene, making a total thickness of 1 in. of uranium; and a secondary having alternate

layers of 1/2 in. uranium and 3/32 in. polyethylene, making a total thickness of 4 in. of uranium. The polyethylene was used to simulate water, 3/32 in. polyethylene being equivalent to 0.100 in. of water. The dimensions of the target normal to the beam were 3 ft. x 3 ft.[1]

The shielded long boron trifluoride counter[2] was mounted on an 11 ft. arm and was moved in the vertical plane about the target. Because of the imperfect geometry of the counter, combined with the scattering of neutrons in the experimental area, it was necessary to make a background run with every regular run. For the background run a 12 in. paraffin plug backed by 1/2 in. of boron carbide was placed in front of the counter to prevent target neutrons from being counted. The only neutrons counted during this run entered either the sides or back of the counter, or were of a very high energy. Removal of the target for a background was not appropriate as the back of the experimental area then became a source of neutrons.

Figure 9 gives counts vs. angle for a radium-beryllium source moved around the counter with the plug on and plug off. The difference of these two curves gives an effective angular resolution of the counter. Fig. 10 gives the result of intensity vs. plug thickness when the counter was directed at the Ra-Be source. It was upon this test that the plug thickness was based. The basic assumption in the above tests was that the energy spectrum of the Ra-Be source is comparable to that of the target. This is also true of the absolute measurements reported below. Because of the fairly flat energy response of the counter in the region below 10 Mev, the assumption is a good one.

In addition to the regular and background runs, measurements were also made using 1/2 gram Ra-Be source to correct for back scattering and the absolute counting efficiency and the solid angle subtended by the counter. Fig. 11 gives the results of these runs. The lack of agreement at 90° is caused by the change of target position in the experimental area with the resulting change in back scattering. The change of position was necessary in order to obtain all angles with the long counter arm.

The deuteron beam was passed through an ionization chamber before striking the target, and the charge collected. The number of deuterons striking the target is

$$I_D = \frac{q}{M \times 1.602 \times 10^{-13}} \qquad (1)$$

where M is the multiplication factor of the ionization chamber (1520 ion pairs/deuteron in the particular chamber used) and q is the charge collected in microcoulombs (used as unit charge).

---

1. For previous experiments on unmoderated targets see Engineering Notes UCRL-1415 and MTA Quarterly Progress Report UCRL-1573.

2. A. O. Hanson and J. L. McKibben, Phys. Rev. 72, 673 (1947).

If $\Delta(C_s/t)$ is the actual recorded counts per unit time of the plug on minus plug off difference using the Ra-Be source, then

$$\Delta\frac{C_s}{t} = \frac{I_n}{4\pi}\ \frac{A}{r^2}\ \epsilon_c \qquad (2)$$

where I_n is the number of neutrons given off by the Ra-Be source in unit time [$(2.62 \pm 0.13) \times 10^8$ neutrons/minute in the particular source used]; A is the area of the counter face; r is the distance from the counter to the target or source; and ϵ_c is the absolute efficiency of the counter.

If $(dN/d\Omega)$ is the number of neutrons per steridian per unit charge, then

$$\frac{dN}{d\Omega} = \Delta\frac{C_t}{q}\ \frac{r^2}{A}\ \frac{1}{\epsilon_c} \qquad (3)$$

where $\Delta(C_t/q)$ is the actual recorded counts per unit charge of the plug on minus plug off difference using the target.

Therefore, combining (1), (2), and (3)

$$\frac{1}{I_D}\ \frac{dN}{d\Omega} = \frac{I_n}{4\pi I_D}\ \frac{\Delta(C_t/q)}{\Delta(C_n/t)} \qquad (4)$$

Plots of $(1/I_D)(dN/d\Omega)$ [number of neutrons per steridian per incident deuteron] vs. angle for the primary and primary plus secondary targets are given in Figs. 12 and 13.

To find the total neutron yield, the above function can be numerically integrated over the whole sphere.

$$\therefore\ \frac{\text{Total Neutrons}}{\text{Deuteron}} = \frac{I_n}{2I_D}\int_0^{\pi}\frac{\Delta(C_t/q)}{\Delta(C_s/t)}\ \sin\Theta\ d\Theta$$

Plots of $(2\pi/I_D)(dN/d\Omega)\sin\Theta$ vs. angle for primary and primary plus secondary targets are given in Figs. 14 and 15. The area under the curves gives total neutron per deuteron yield.

Low Energy Neutron Spectra

Marian N. Whitehead
UCRL

The statistics have been improved on the energy distributions of low energy, 1-12 Mev, neutrons from thin U targets bombarded with 340 Mev protons and 190 Mev deuterons. The spectra from 1/8 in. targets are obtained by measurements on the recoil protons produced by the neutrons in nuclear emulsions placed at 45°, 90°, and 135° to the direction of the incident beam. Preliminary results and the details of the experimental method have been discussed by Frank Adelman in the previous quarterly report.

The statistics of the individual points have been improved by further scanning of the plates and by combining the data obtained at different angles. The combination is justified by the lack of any experimental or theoretical evidence that the distributions are other than isotropic. The two distributions have been normalized to the same total number of neutrons in the energy region covered. The resulting distributions are shown in Fig. 16. Within the statistical errors of the experimental points the curves for protons and deuterons appear to be identical. The most striking characteristic is the definite peak of about 2 Mev. For comparison the slow neutron fission spectrum and a Maxwellian distribution, normalized to the height of the peak, are shown. Neither curve makes even an approximate fit to the experimental distribution.

The study of the spectra is being continued and extended to lower neutron energies by the use of proton recoils in a hydrogen filled cloud chamber and the $Li^6(n,T)He^4$ reaction in nuclear emulsions.

1903-9K

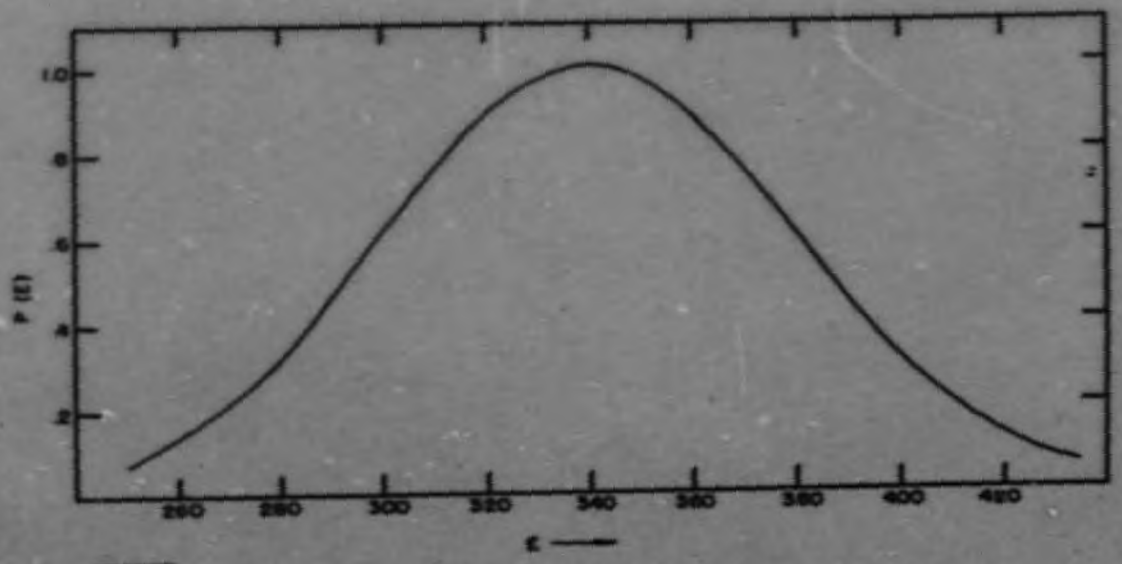

SECRET

FIG. 1 SECTION 10

MU4138

Energy distribution of deuterons stripped from 340 Mev He^3. The curve is normalized to unit area.

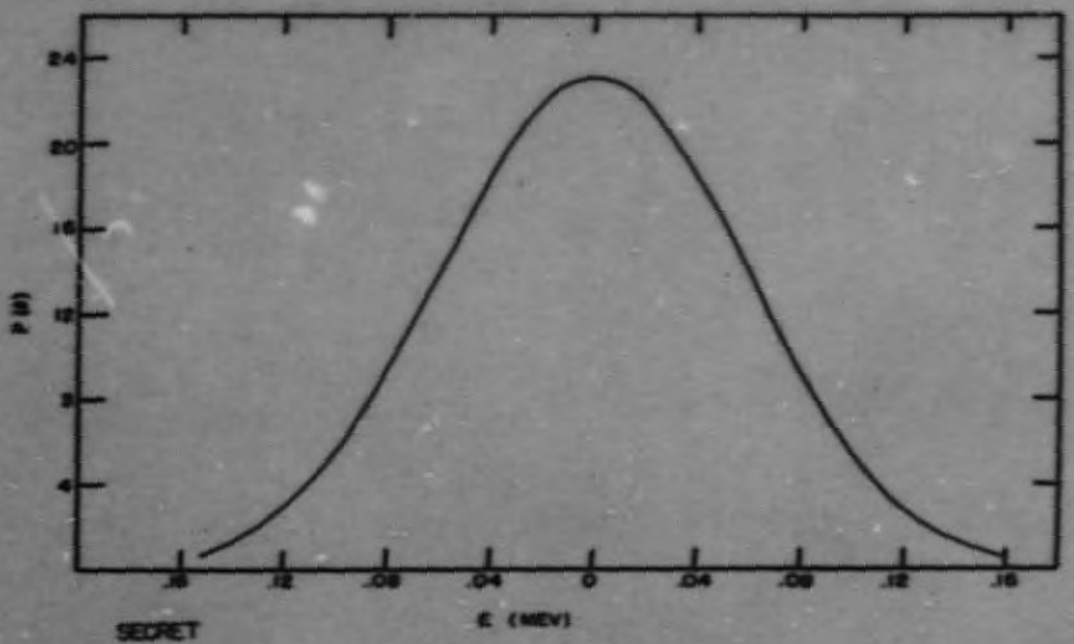

SECRET

FIG. 2 SECTION IO

MU-4139

Angular distribution of deuterons stripped from 540 Mev He^3. The curve is normalized to unit area.

1503-96

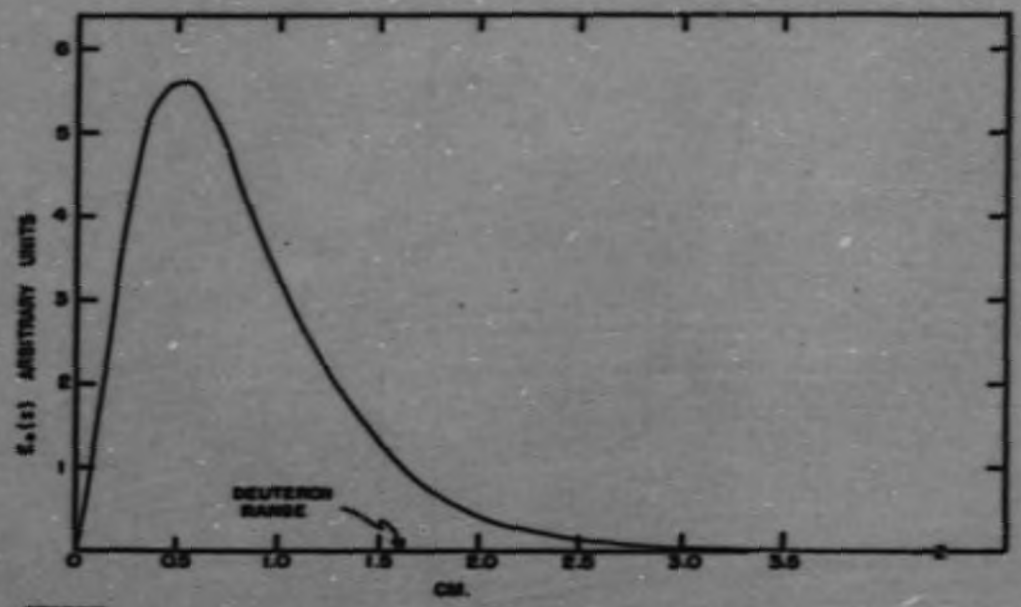

SECRET

FIG. 3 SECTION 10 MU4 140

1 Fig 3-7

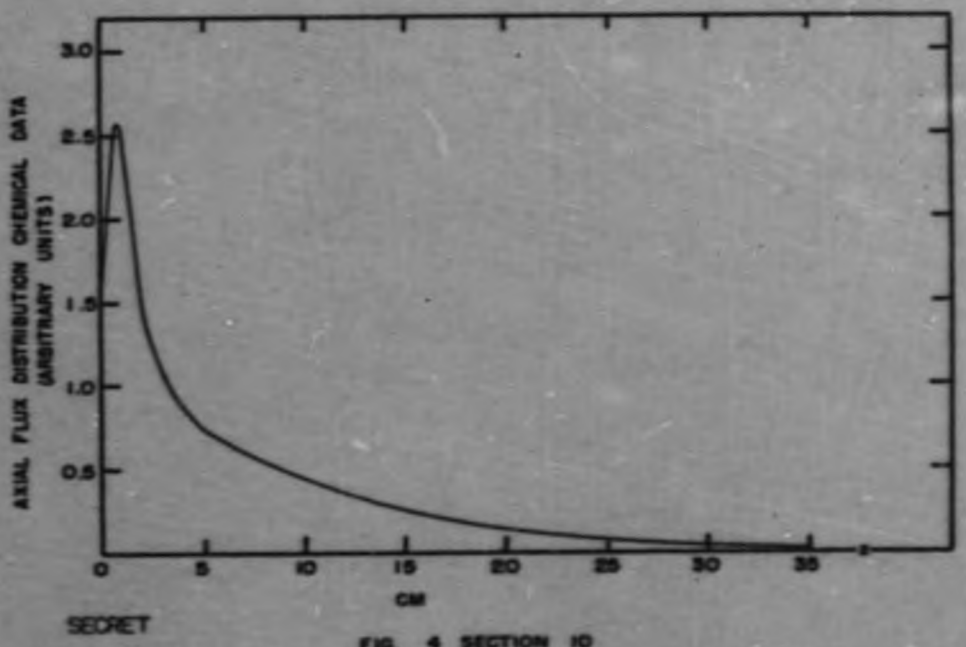

SECRET

FIG. 4 SECTION 10

MU4141

1903-98

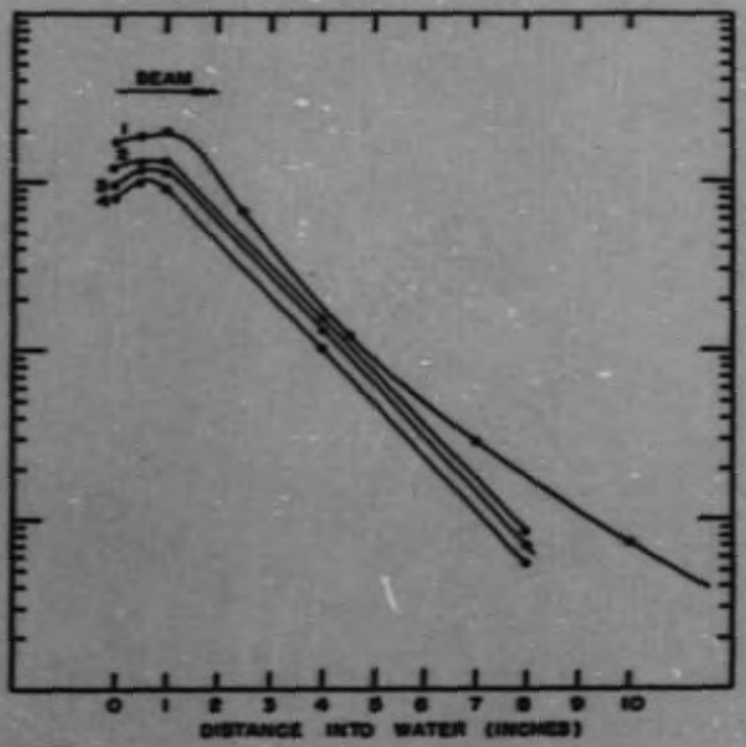

SECRET

FIG. 5 SECTION IO

MU 4142

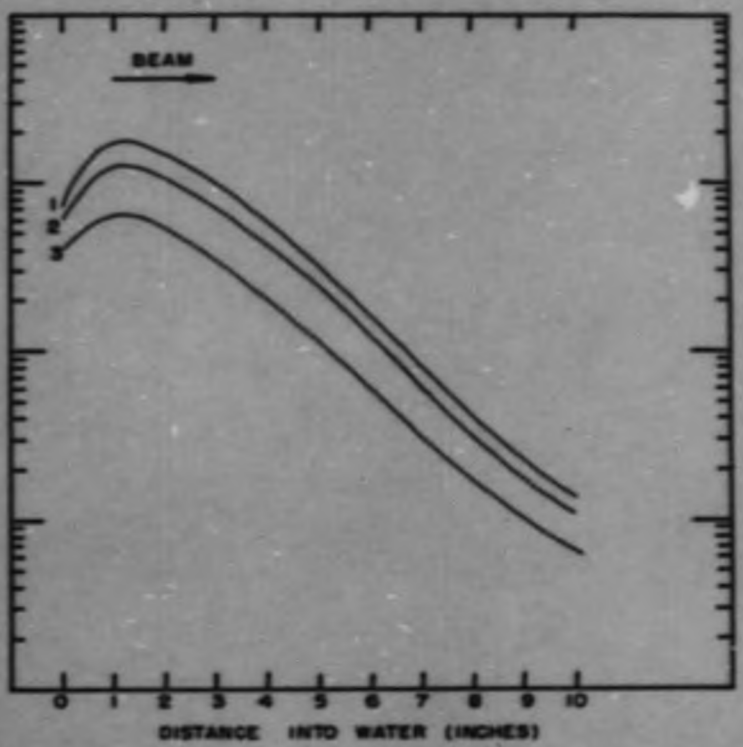

FIG. 6 SECTION 10

SECRET

MU 4143

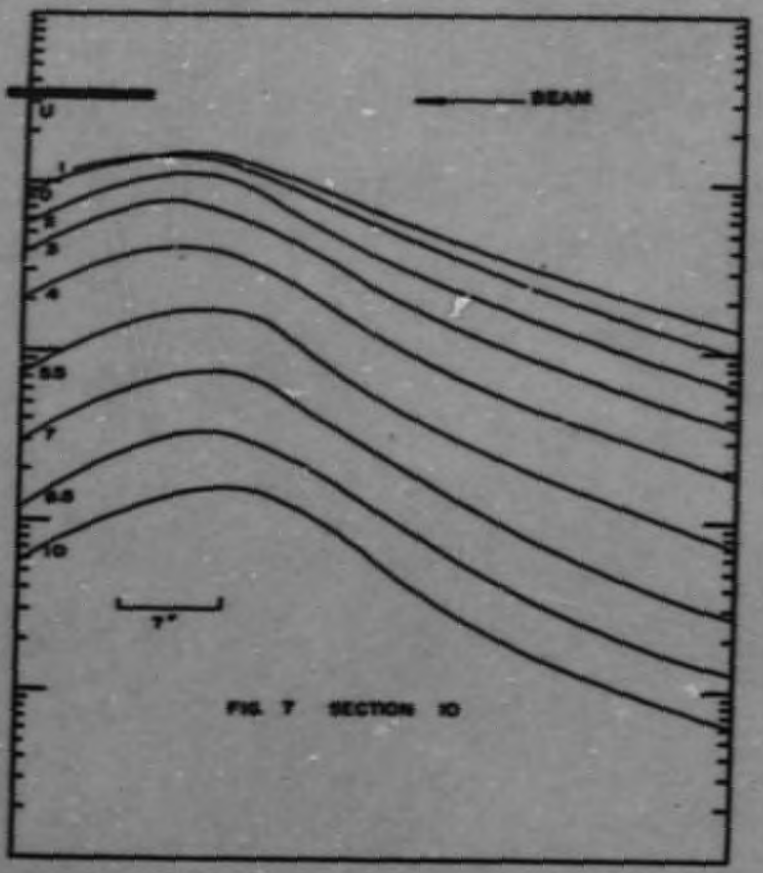

FIG. 7 SECTION XO

SECRET

MU-4144

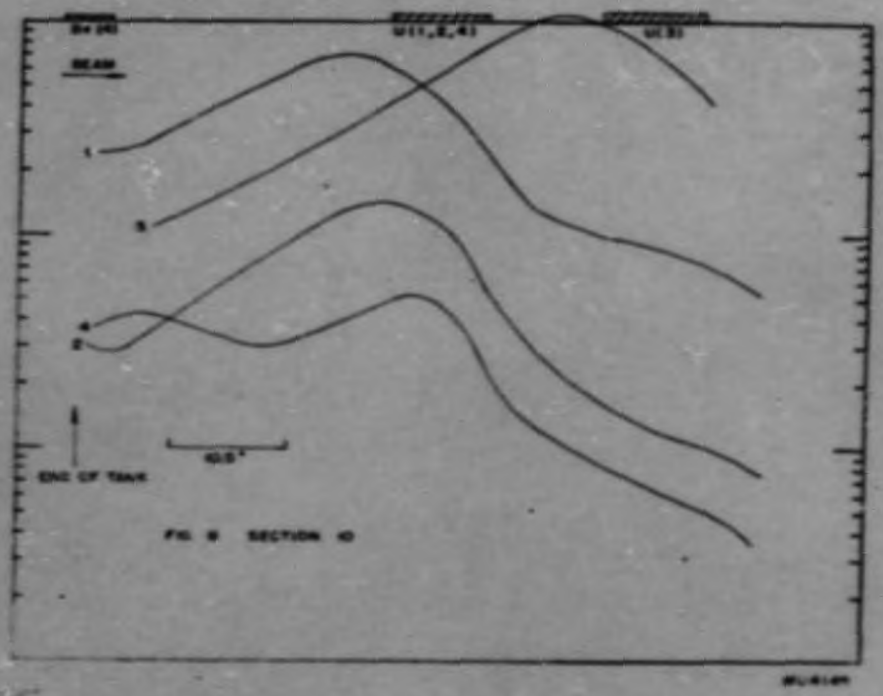

FIG. 9 SECTION 40

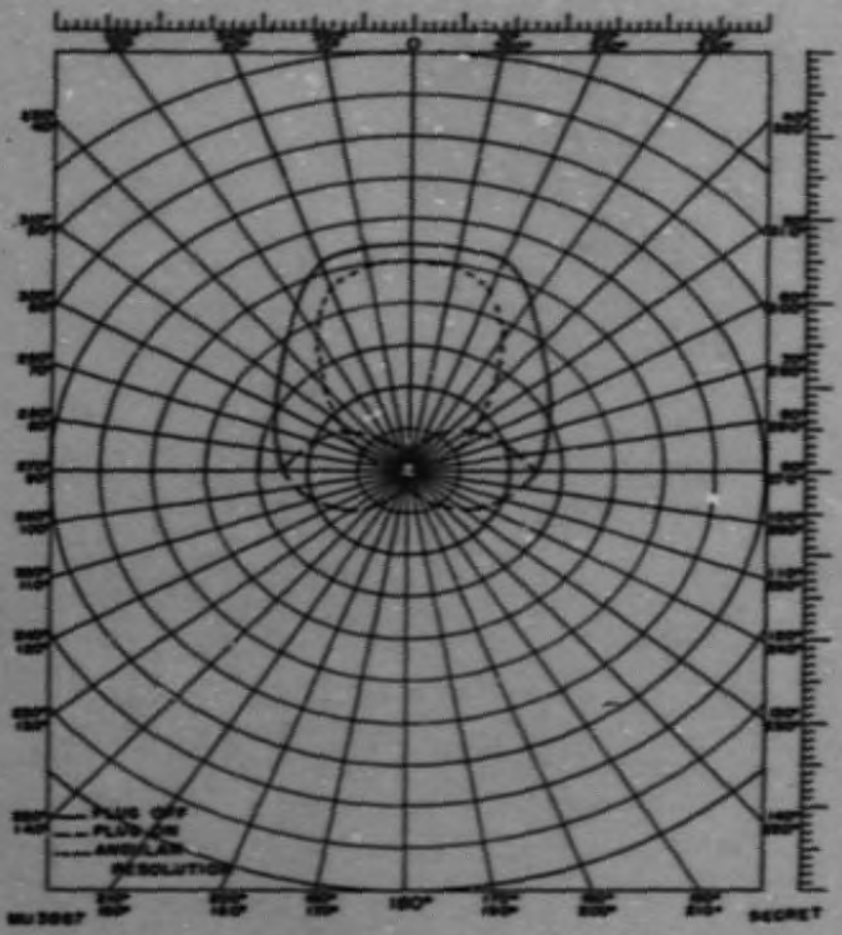

Fig. 9 Sec. 10 Angular Resolution of BF_3 Counter.

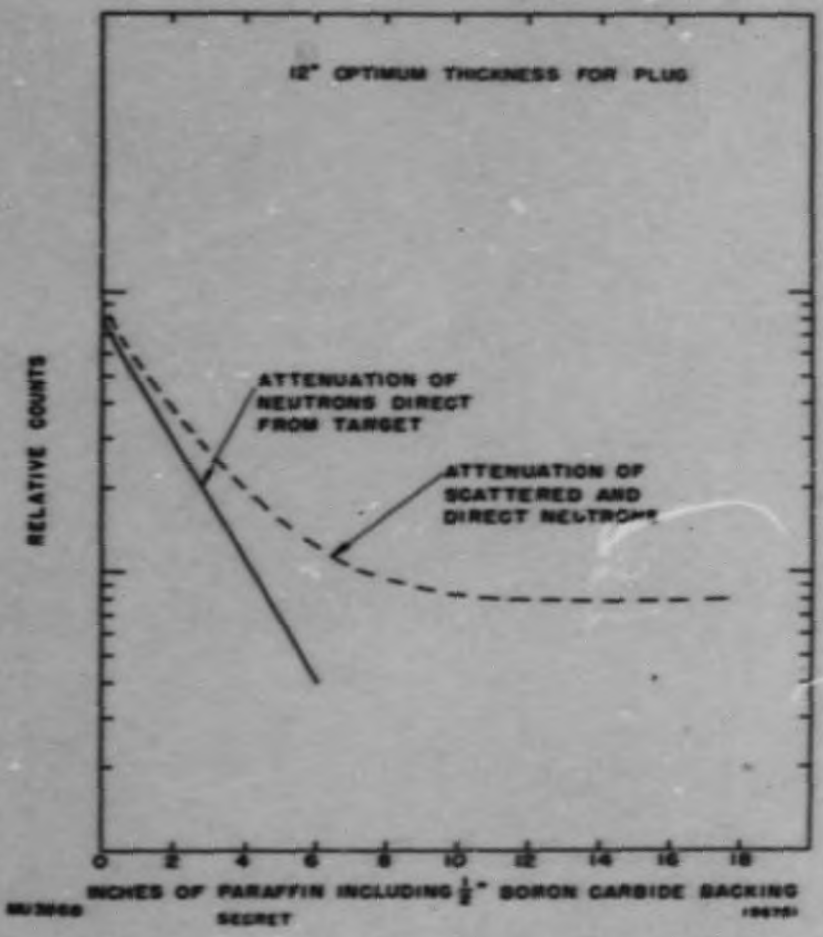

Fig. 10 Sec. 10 Attenuation of Neutrons from Radium-Beryllium Source by Paraffin in Front of BF_3 Counter.

1903.104

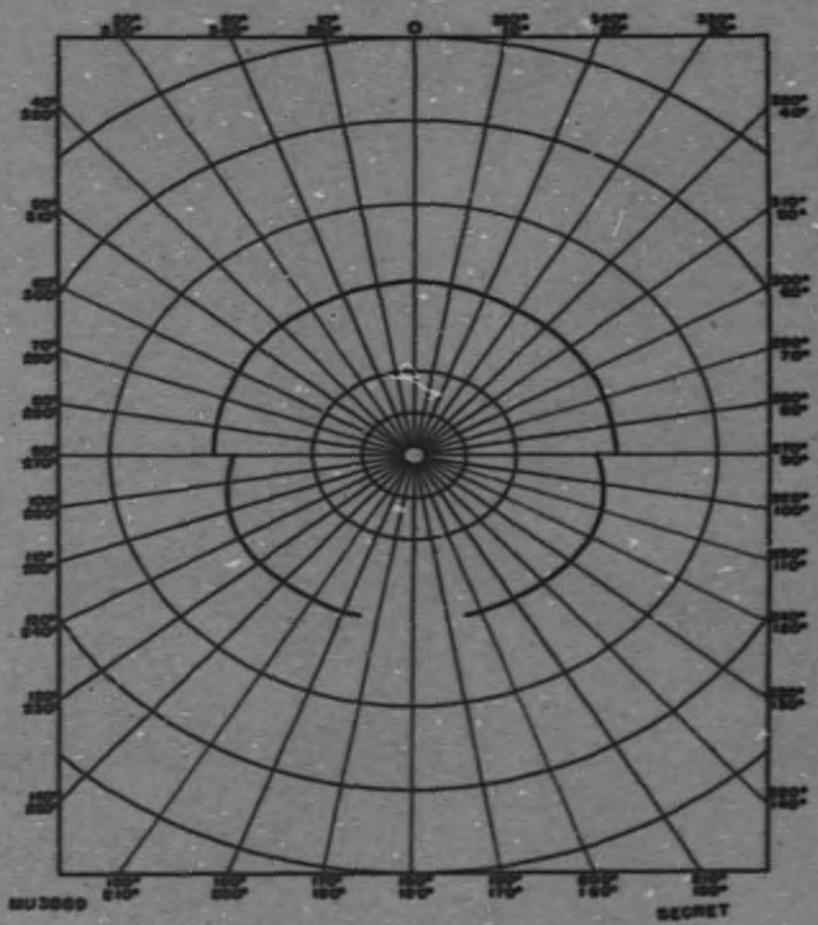

Fig. 11 Sec. 10 Angular Distribution of Neutrons from Rn-Be Source in Cave.

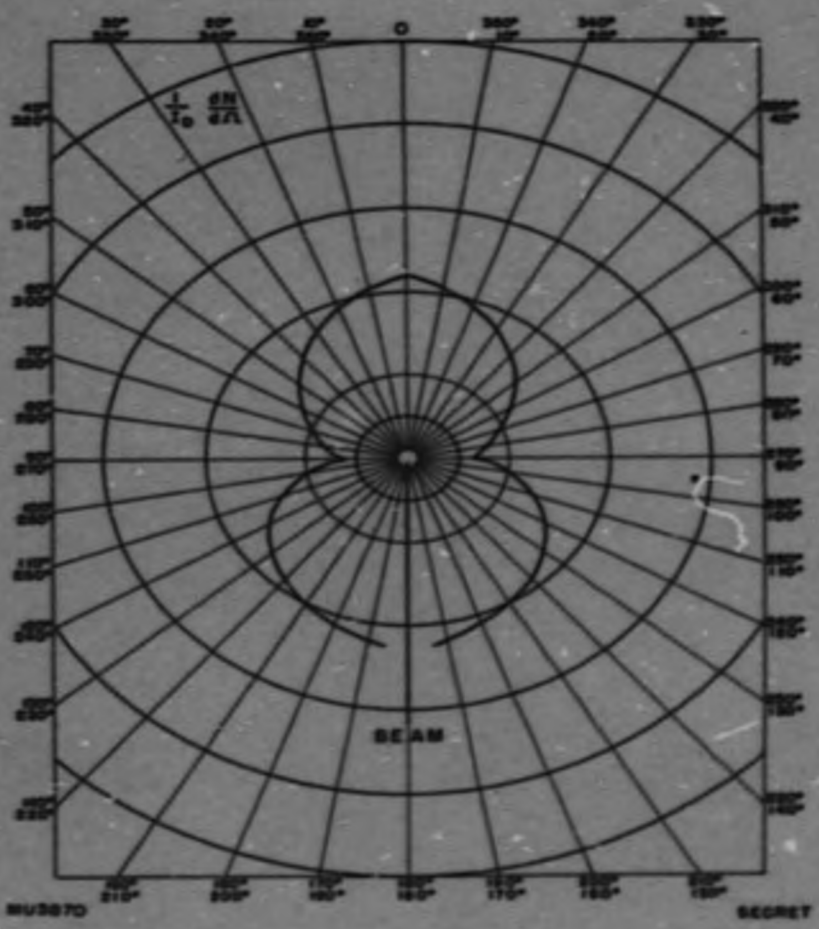

Fig. 12 Sec. 10 Angular Distribution of Neutrons from the Primary Target.

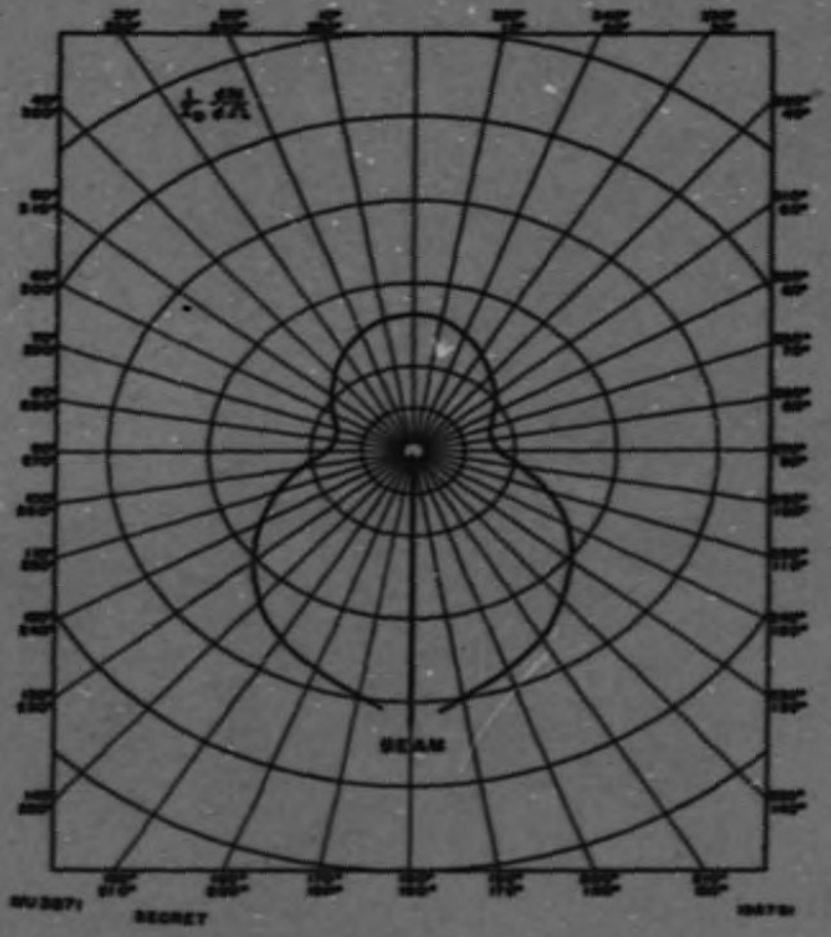

Fig. 13 Sec. 10 Angular Distribution of Neutrons from the Primary and Secondary Targets.

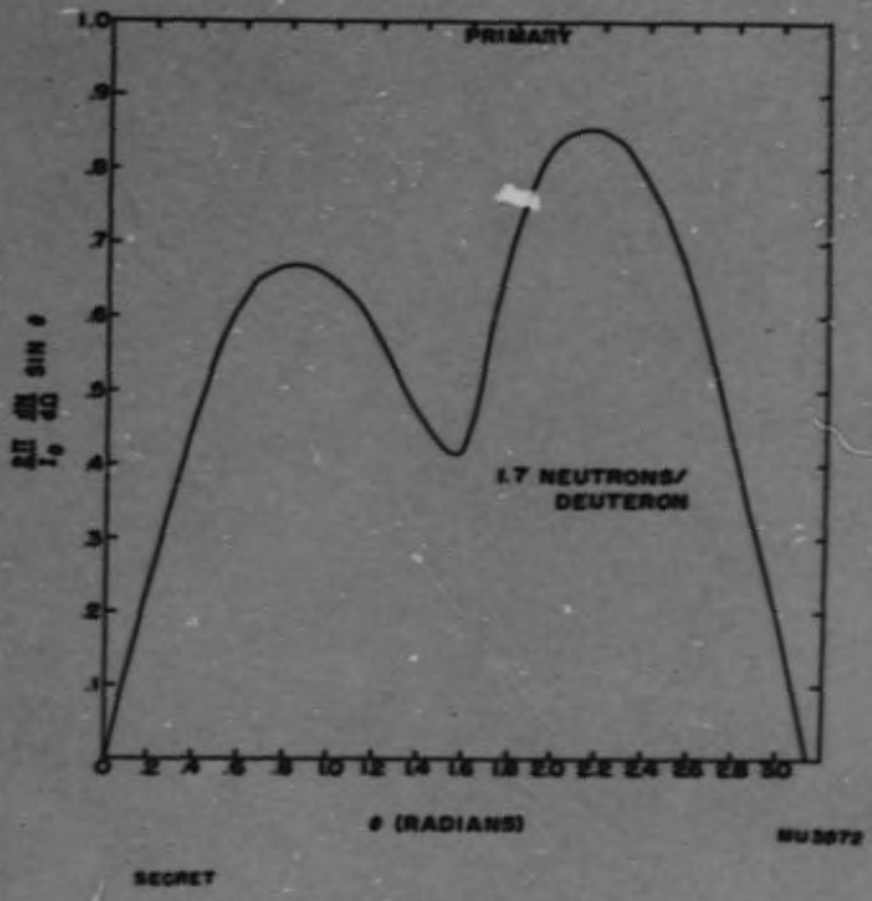

SECRET

Fig. 14 Sec. 10

1903-10f

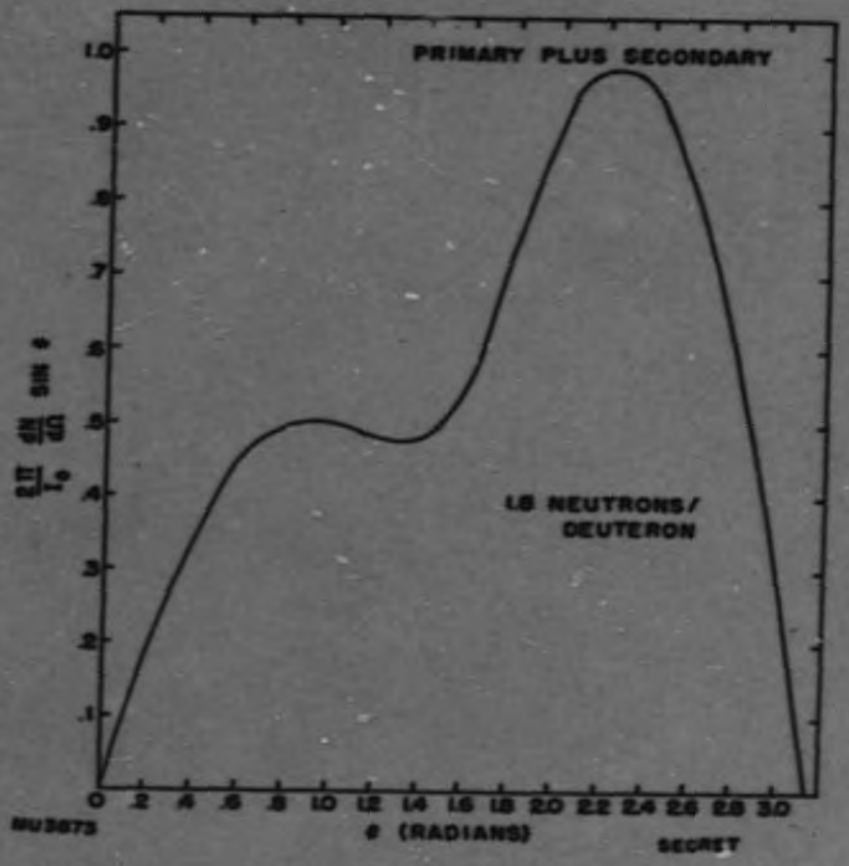
PRIMARY PLUS SECONDARY
1.8 NEUTRONS/
DEUTERON
1.0
.9
.8
.7
.6
.5
.4
.3
.2
.1
0 .2 .4 .6 .8 1.0 1.2 1.4 1.6 1.8 2.0 2.2 2.4 2.6 2.8 3.0
φ (RADIANS)
RU3873
SECRET

Fig. 15 Sec. 10

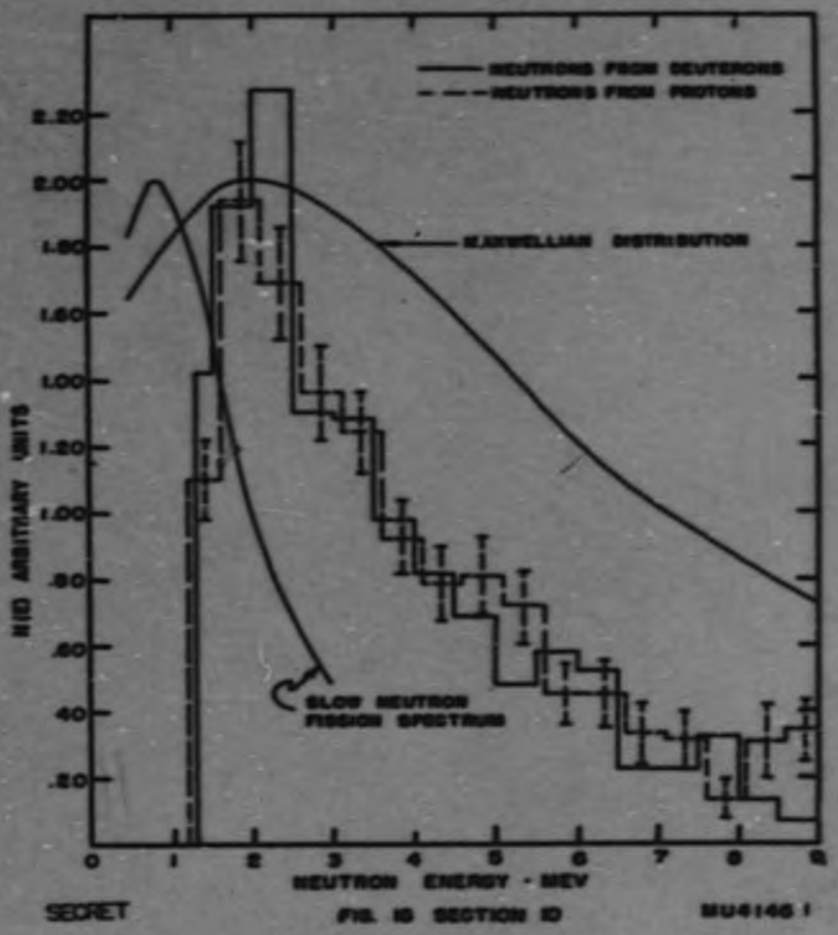

FIG. 10 SECTION D

1903-110

11. A-12 TARGET THEORETICAL AND ENGINEERING PHYSICS

D. H. Imhoff, W. H. Harker, C. C. Old, J. R. Donaldson,
R. E. Nather, J. W. Flora, R. H. Graham,
K. Bernstein, S. H. Fitch and A. E. Farnham
CRDC

Pu^{240} Content in A-12 Product

One of the most important factors limiting the processing level of the A-12 fuel is the percentage of Pu^{240} in the final product, the upper limit set by Los Alamos being the order of 5 percent. A study of the A-12 lattice and targets indicates that they may be processed to higher plutonium content levels than is feasible in a thermal reactor. Table 1 below summarizes the results of these calculations, while Fig. 1 graphically shows the relationship of Pu^{240} percentage to total plutonium concentration in the uranium.

Table 1

Unit	Characteristics	% Pu^{240} at 520 g/t	g/t at 4.5 % Pu^{240}
Hanford Reactor	Thermal Reactor	4.5	520
A-12 Lattice	52 Vol. % U-H_2O	3.1	760
A-12 Lattice	65 Vol. % U-H_2O	2.2	1000
A-12 Primary	Slab U-H_2O	- 3.5	- 700
A-12 Secondary	Slab U-H_2O	- 2.5	- 900

The analysis was based on the following information and assumptions:

Information:

1. Hanford product at 520 g/t contains about 4.5 percent Pu^{240}.

2. Two rods, one bare and one cadmium covered, were irradiated to the same g/t level in a Hanford reactor. The ratio of the percentage of Pu^{240} in the bare rod to that in the cadmium covered rod was 30:1, indicating that thermal energy neutrons are captured by Pu^{239} 29 times as effectively as are resonance energy neutrons.

3. The ratio of resonance Pu^{239} formation to thermal Pu^{239} formation in a bare rod in a Hanford reactor is 1:2.9.

Assumptions:

1. The thermal to epicadmium absorption ratio in Pu^{239} is not a function of plutonium content.

2. Pu^{240} concentration in the lattice is proportional to the square of the grams per ton level of the lattice, both in the thermal and resonance energy regions. This assumption has been observed to introduce a 14 percent error at Pu^{240} concentrations of 7 percent (corresponding to 900 g/t in the Hanford reactor), the calculated Pu^{240} level being too high.

The above considerations lead to the relation:

$$\frac{Pu^{240}}{\text{Total Pu}} \approx 1.13 \times 10^{-5} \left(\frac{R + 107}{R + T}\right) \left(\begin{array}{c}\text{Total Pu} \\ \text{concentration}\end{array}\right)$$

(where R and T are the relative Pu^{239} productions in the resonance and thermal energy regions, respectively, and the total plutonium concentration is expressed as grams of plutonium per ton of uranium.)

For the A-12 base case lattice (1 in. diameter 0.3 percent 25 uranium rods on 1-1/4 in. centers in H_2O),

$$R:T = 1:0.89 \text{ and at } 520 \text{ g/t}$$

$$\frac{Pu^{240}}{\text{Total Pu}} = 5.89 \times 10^{-5} \ (520 \text{ g/t}) = 0.031$$

The same Pu^{240} fraction as Hanford (4.5 percent) is reached at 760 g/t.

A more closely packed A-12 lattice (1 in. U rods on 1-1/8 in. centers in H_2O), due to a lower resonance escape probability, has an R to T ratio of 1:0.432.

At 520 g/t, $\frac{Pu^{240}}{\text{Total Pu}} = 4.18 \times 10^{-5} \ (520) = 0.022$

The same fraction as Hanford is reached at 1080 grams/ton.

The base case primary target is expected to correspond roughly to the base case lattice while the secondary target is expected to simulate the close packed lattice.

In summary, these calculations indicate that the components of the A-12 may be processed to higher plutonium concentrations than may be done in present thermal reactors. The figures for maximum g/t given above are to be taken as an upper limit, since isotopes Pu^{236} and Pu^{238} formed mainly in the primary and secondary targets will influence the maximum allowable plutonium concentrations.

Replacement of Lattice Material with Reflectors

Since certain portions of the base case A-12 lattice present mechanical design and handling difficulties, the effect on the lattice production of replacing a portion of the lattice with reflector material has been studied. The analysis used was that presented in the previous quarterly progress report. The performance of the [redacted] uranium-light water lattice was evaluated with its normal configuration, then with the lattice material at the beam hole end of the lattice replaced successively with aluminum, heavy water, graphite, beryllium, beryllium oxide, iron, and light water, and finally with neither reflector nor lattice material present at the beam hole end of the lattice. The results are presented in Table 2 below for the base case lattice with 7.4 percent of the material replaced.

Table 2

Effect of Replacement with Various Reflectors

End Material	Relative Lattice Production	Rel. Lattice Production Loss	Specific Loss = Fractional Loss / Fract. Replacement
Lattice	1.0000	0	0
Aluminum	0.9643	0.0357	0.48
Heavy Water	0.9624	0.0376	0.51
Graphite	0.9598	0.0402	0.54
Beryllium	0.9570	0.0430	0.58
Beryllium Oxide	0.9560	0.0440	0.60
Iron	0.9481	0.0519	0.70
Light Water	0.9009	0.0991	1.35
Nothing	0.8545	0.1455	2.00

It can be seen that the removal of /x percent of the base case lattice material at the beam hole end results in 2 /x percent lattice production loss. Replacement of the material with light water results in 1.35 /x percent loss, while replacement with the other reflectors considered results in losses from 0.5 /x to 0.7 /x percent.

Since the direction and magnitude of the effect of sidewise diffusion between the reflector and the lattice are not known, the results presented here should only be considered valid for cases where the internal lattice area replaced is of the same order as, or larger than, the contact area between the lattice and the new reflector material.

Although the exact numerical values are dependent on the position of the replaced section, the general trend of the specific loss coefficients and their approximate magnitude should remain about the same for replacement anywhere in the base case lattice.

Natural Uranium Light Water Lattice

A lattice fueled with natural uranium slugs has been compared with depleted uranium lattices. A water moderated, water cooled process tube lattice containing 1 in. diameter aluminum clad uranium slugs was studied in an attempt to optimize production by varying tube spacing. Two energy group diffusion theory was used. Preliminary results indicate that the maximum production achievable for the 1 in. natural uranium rods is about 2.3 times the production of the optimized [redacted] uranium- light water lattice, while the heat load in the natural lattice may be 4 times as great as that of the depleted lattice.

Expected Heat Loads in Bare Uranium Targets

The magnitude and distribution of heat loads is an important criterion in the design of A-12 primary and secondary targets. This heat is generated in the targets by:

1. Energy loss of beam particles by ionization in traversing the primary target.

2. Reactions induced in target materials by the particles incident on or produced in the target.

A method of calculating heat loads produced in "bare" targets, i.e. solid blocks of metal, has been developed. This method is basically a mass-energy balance for the target and may be described by:

$$qt = E_{beam} + \Delta M_0 - E_p$$

where

qt = The target heat load

E_{beam} = Beam energy incident on target, (current x voltage)

ΔM_0 = Mass change in the fission reaction; i.e. the mass that is converted into energy.

E_p = The energy carried away from the targets by neutrons, gammas, and neutrinos.

The beam energy may be simply calculated as the number of particles in the beam times the average energy per particle.

In calculating ΔM_0, the quantity is dependent to some extent on fission mode, i.e. ratio of masses of the two fission fragments, and on the number of particles released. Hence, it was considered more convenient to calculate the quantity ($\Delta M_0 - E_n$) rather than the separate components. In this calculation, it was assumed that only neutrons are released in high energy fission reactions, and that all these neutrons are released with an average energy of 2 Mev. This will overestimate the neutron energy, but is believed to compensate at least partially for the energy carried off as γ-rays.

Figure 2 shows the quantity ($\Delta M_0 - E_n$) as a function of fission mode and number of neutrons released. Figure 3 is a comparison of the symmetric lunary mode of fission, most probable mode for fission by high energy particles, with fission in the 1:1.5 mode, the most probable mode for fission by thermal neutrons. This comparison indicates that in the range of fission modes encountered in practice, the dependence of energy release on fission mode is negligible. Spallation reactions, i.e. those resulting in only one residual nucleus, may absorb energy according to Figure 2. However, recent experiments indicate that this reaction will release an average of three or four neutrons, and result in negligible energy change.

Sample calculations are based on data from the Nuclear Chemistry and Experimental Physics Groups and are used directly in the case of 190 Mev deuterons, and extrapolated to the higher energy in the case of 350 Mev deuterons. These values are given in Table 3.

Table 3

	190 Mev Deuterons	350 Mev Deuterons
Fissions in Primary Target	0.4 per deuteron	1.1 per deuteron
Neutrons Produced in Primary Target	6.5 per fission	9.7 per fission
Fissions in Secondary Target	0.6 per deuteron	1.3 per deuteron
Neutrons Produced in Secondary Target	2.0 per fission	3.1 per fission
These data lead to the following heat loads:		
Primary Target	190 Mev deuterons	350 Mev deuterons
Beam Energy	190 Mev/deuterons	350 Mev/deuterons
Spallation Reactions	0	0
Fission Energy	56 Mev/deuterons	121 Mev/deuterons
Total	246 Mev/deuterons	471 Mev/deuterons
Secondary Target Fission	111 Mev/deuterons	226 Mev/deuterons

This method indicates a heat load approximately 30 percent higher than that of previous calculation methods. Any additional heat load induced by the effects of coolant, cladding, etc. must be added to this to obtain the operating heat loads.

1903.115

LRL Experimental Physics Program

Neutron Sources. Eleven polonium-beryllium neutron sources were received from Oak Ridge during the quarter. One source with an activity of 1.25×10^7 neutrons per second on April 14, 1952 will serve as a calibration source for determining foil constants. The other ten sources are contained in double walled nickel capsules. They possessed a total emissivity of 6.46×10^8 neutrons per second on May 8, 1952.

Calibration. Most of the quarter has been devoted to calibration of counting equipment, measurement of necessary correction factors, and development of experimental techniques. Counting room procedure is now quite routine and seems satisfactory at the present. The routine calibrations, such as foil calibrations, shelf and scaler factors, coincidence corrections, and the effect of one foil on another are well in hand. Lucite was chosen as the chief material of construction after an experiment showed that it was nearly indistinguishable from water to the neutrons. Indium foils were activated in the water tank, and compared with others exposed identically except that they were placed between and against two 1 in. lucite cylinders, 1 in. in diameter, end to end. No difference in saturated counting rate was observable within the statistics of 0.3 percent.

Since no drawings were available for the Ra-Be source, the exact center of the active volume was not known. In an attempt to determine this, the source was radiographed, and the resulting films examined with a densitometer. The active center, at least of the gamma rays, was determined within about 0.03 in. by this method. This is important because comparison of data with existing data of other investigators depends on the position of the center and almost all our work thus far has been done with the Ra-Be source. As the Po-Be sources are now available, they are being substituted for the Ra-Be source.

Prototype Experiments. The Ra-Be source was used in a prototype experiment to measure neutron flux distributions in small cavities of varying length to diameter ratios. Thus far the experiments have been of an approximate nature, mostly to show how the experiments should be performed and indicate roughly what effects can be expected.

The source was mounted in a 1-3/8 in. i.d. lucite re-entrant tube in a 40 in. by 40 in. water tank. The source rested on a lucite pedestal and the annulus between the pedestal and the tube was filled with water. The length to diameter ratio was varied by adjusting the lucit pedestal. Thus the source rested at the base of an air filled cavity surrounded by water. For each length to diameter ratio, a single foil was exposed at the center of the 'open' end of the cavity. Indium foils, on aluminum backings, were used so that all neutrons capable of activating indium foils might be measured. The variation in saturated counting rate as a function of L/D of the cavity is shown in Fig. 4. A foil traverse down the center of the cavity was run for an L/D of 4.0, and another for an L/D of 14.9. The results are plotted in Fig. 5. The experiment had not previously been performed and the analysis of this data is quite difficult. Therefore, conclusions are not yet available.

In the process of doing this experiment, it became necessary to know the activation of indium foils by the unmoderated source in air. Data were procured, with some precautions to avoid reflections, and the saturated counting rate with the foil at 5.05 centimeters from the source proved to be 94 counts per minute. For the beam hole experiments thus far, with greater distances from source to foil and large counting rates, this correction has been negligible.

Series of horizontal traverses at various altitudes above the source in the small tank have been obtained, and profiles determined with the re-entrant tube filled with water, filled with air, and filled with water to the level of the source and air above. Analysis is in progress.

Current Studies. Several studies are under way, but the results obtained thus far are not sufficiently conclusive to justify detailed discussion.

Uranium plate lattices appear to compete with uranium rod lattices on a production basis. Further work will be done in an effort to achieve optimization. Lattices of close packed spheres will also be investigated.

Lattices consisting of U_3O_8 rods in light water are also under study. Preliminary results show a production of about 65 percent of that of the optimized uranium lattices. However, the oxide lattice is believed to be too far from optimization to justify any conclusions at this time.

Preliminary work on homogeneous lattices indicates that heavy water should be the most promising moderator. UO_2 - D_2O slurry and UO_2F_2 - D_2O solution both have their maximum production well within practical concentration regions. Further studies will be carried out on these materials and also on $UO_2(NO_3)_2$ - D_2O systems.

An analytical study has been initiated to reveal the depthwise distribution of plutonium production, thermal fissions, and heat generation in the primary and secondary targets, as well as the number of neutrons escaping from the target and impinging on the lattice.

The results of these studies will be reported in detail at a later date.

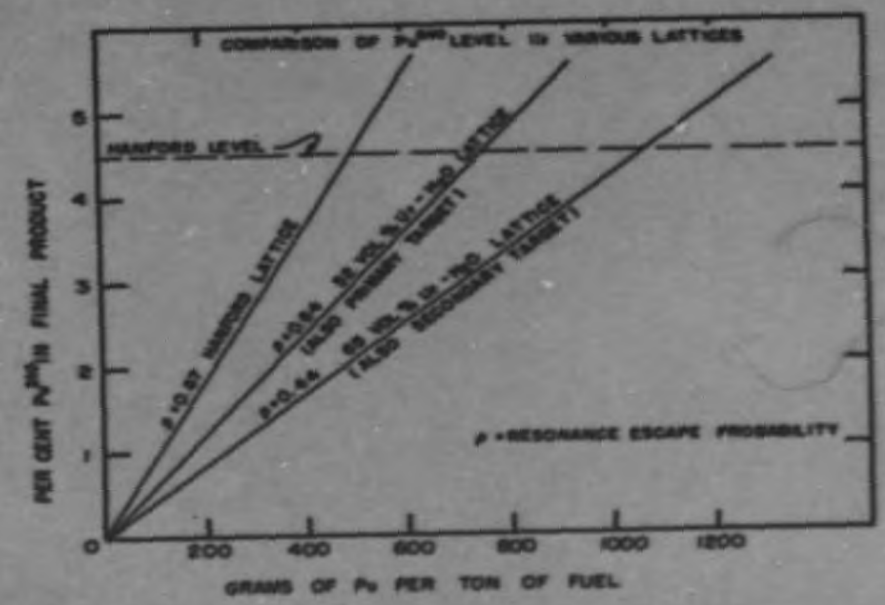

SECRET

FIG. 1 SECTION II

MU 4147

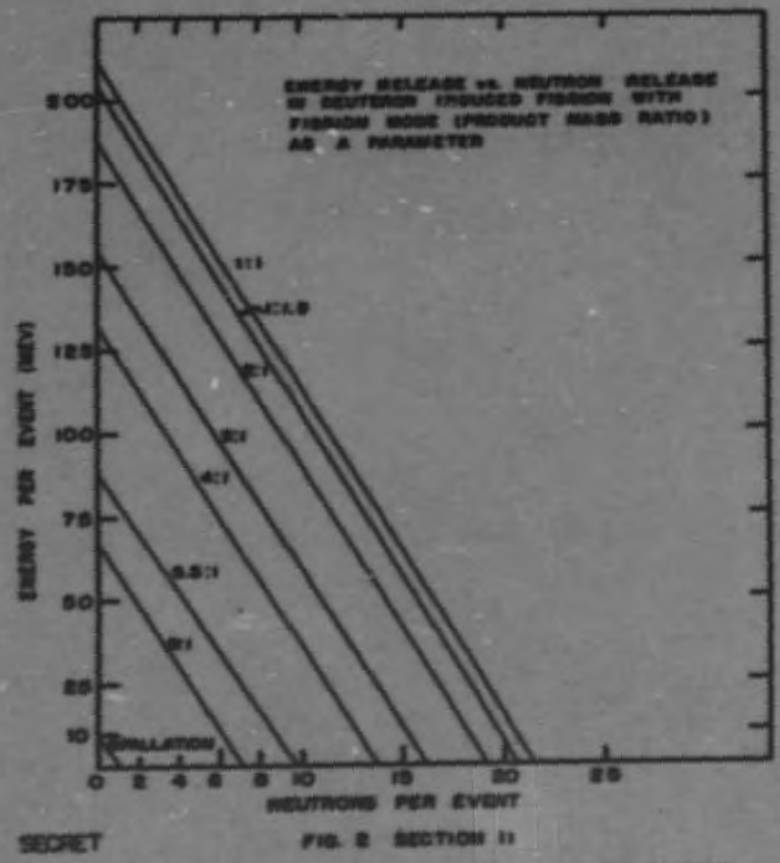

SECRET

FIG. 2 SECTION II

MU6148

1903-119

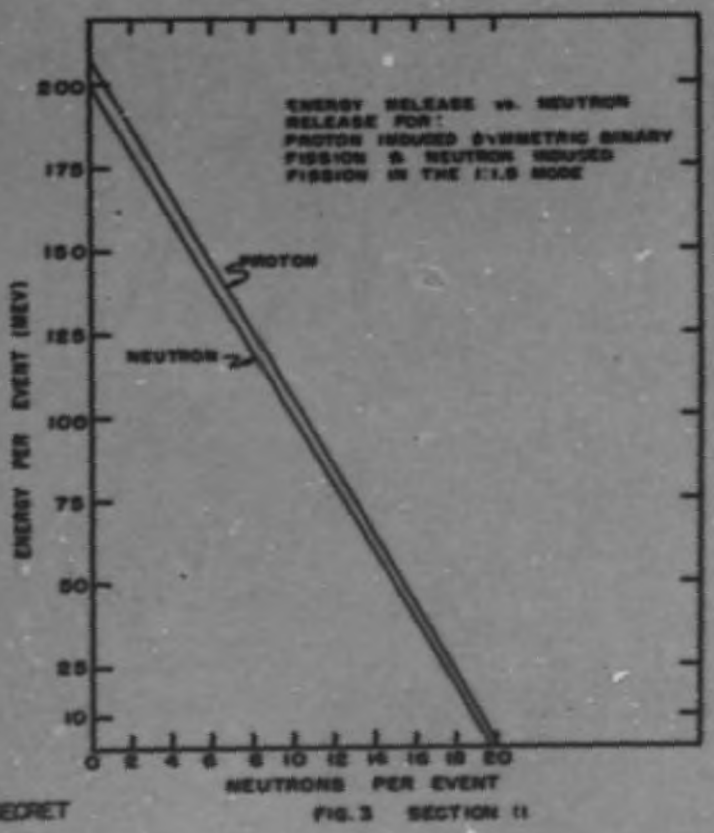

SECRET

FIG. 3 SECTION II

MU-4149

190 B-120

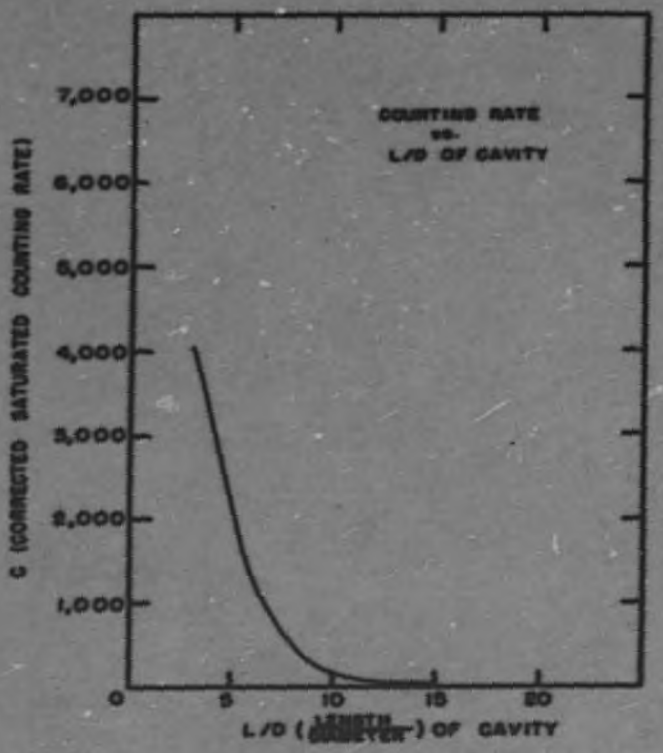

SECRET

FIG. 4 SECTION II

MU-4150

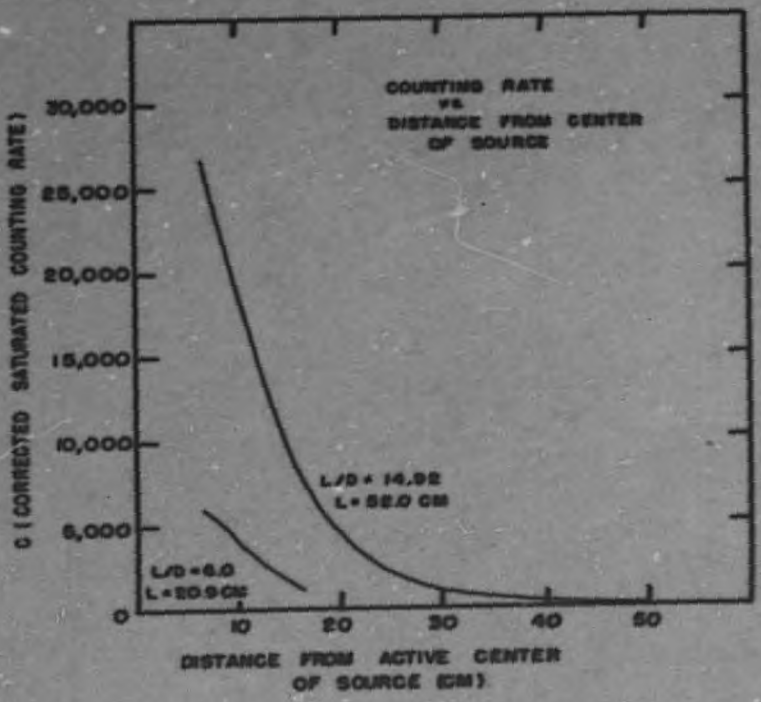

FIG. 5 SECTION II MU416

SECRET

12. NUCLEAR CHEMISTRY

K. Street
CRDC

Fission and Capture in A-12 Targets

R. E. Batzel, G. H. Coleman, W. W. Crane, R. S. Gilbert,
H. G. Hicks, W. H. Hutchin and G. M. Iddings
CRDC

P. C. Stevenson
UCRL

Studies on the fission and capture events produced by 190 Mev deuteron irradiation of uranium blocks with beryllium and uranium primaries were largely suspended during the last quarter. This was due both to a shortage of uranium foil and to allow concentration on the isotopic composition measurements reported below.

Neutron Yields

In order to supplement the information already available on the capture and fission events occurring in the uranium targets, the yields of neutrons external to the blocks were measured with the same target configurations used in measuring the internal events. Two series of runs were made; one in the "small" water tank with 6 in. of solution around the block, and a second in the "large" water tank with 18 in. of solution around the block. The uranium blocks were 12 in. x 11 in. in the direction perpendicular to the beam, and the uranium primary targets were in all cases 12 in. x 11 in. x 5/8 in. The results of the measurements are given in Table 1.

Table 1

Neutron Yields for Various Target Configurations

Target Configuration	Neutrons/Deuteron Small Water Tank	Neutrons/Deuteron Large Water Tank
Uranium Primary + 5 in. Uranium	3.3	3.2
Uranium Primary + 10 in. Uranium	3.6	3.2
Uranium Primary + 10 in. Uranium Cadmium Wrapped	3.3	2.8
Uranium Primary + 16 in. Uranium	3.6	
Beryllium Primary + 5-5/8 in. Uranium	3.0	2.6
Beryllium Primary + 10 in. Uranium	3.3	2.9
Beryllium Primary + 16 in. Uranium	3.4	

The data in the table show that the measurements in the small water tank give larger numbers of neutrons per incident deuteron than do comparable measurements in the large water tank. This discrepancy arises because all of the neutrons from the Ra-Be source used to calibrate the water tanks are not captured in the small water tank and a substantial number escape through the sides. The calibration runs are thus too low and lead to high figures for measurements in the small water tank. Thus, measurements in the small water tank are valid only if the percentage of neutrons lost from the Ra-Be source is equal to the percentage lost from the target configurations. This is very nearly the case in unmoderated target configurations.

The cadmium wrapped blocks were run to place an upper limit on any effect of thermal neutron feed back from the water tank to the block which would cause fission in the U^{235} present in natural uranium. The results show an effect of about 10 percent, and as discussed in the last quarterly report, this should be an upper limit.

Loss of Neutrons from Small Water Tank

In order to get an estimate of the number of neutrons from the Ra-Be source escaping through the walls of the small water tank, a series of measurements were made to determine the effect of increasing the thickness of solution around the source. The runs were made with the calibrated Ra-Be source and a calibrated Po-Be source. The measurements were carried out in cylindrical tanks with the exception of the 30 in. x 30 in. x 36 in. tank. Except for the small and large water tanks, the neutron sources were suspended within a 1-1/2 inch aluminum cylinder. The results were normalized with the 30 in. x 30 in. x 36 in. tank given a value of 1.00 and were corrected for volume differences. The results are shown in Figs. 1 and 2.

As can be seen from the data in Fig. 1, only 0.7 of the incident neutrons from the Ra-Be source are captured in the small water tank, and the large water tank captures essentially all of the neutrons.

The values for the "small" and "large" water tanks are plotted at their nominal thickness but because of the rectangular geometry their effective thickness is somewhat larger. The point for the large water tank falls below the 1.00 and the discrepancy can be explained, at least in part, by capture of the neutrons in the 1/4 in. 2S aluminum of which the tank is constructed.

In the course of the measurements, the calibrations of the Ra-Be and Po-Be sources were cross-checked, and it was found that the two calibrations check to within 3 percent.

Fission and Capture

An uranium block 24 in. high, 24 in. wide, and 13 in. deep was bombarded in the center of the 24 in. x 24 in. face with a beam of 350 Mev protons, 2 in. in diameter. This bombardment with protons was designed to approximate the qualitative behavior of an extended primary source function, i.e., 340 Mev deuterons.

Thin uranium foils were placed at various radial distances from the center line of the proton beam. Two sets of foils were used, one for the primary target (2-3/4 in.) and one for the secondary target (10-1/4 in.). After bombardment, these foils were dissolved separately. Np^{239} was chemically separated as a measure of the capture events and Zr^{97} chemically separated as a measure of the fission events. Figures 3-6 show the results of the bombardment, and values are tabulated in Table 2.

Table 2

Fission and Capture in an Uranium Cylinder 26 in. in Diameter and 13 in. Deep Bombarded with 350 Mev Protons

Target	Captures/Proton	Fission/Proton
Primary - 2-3/4 in.	1.0	1.45
Secondary - 10-1/4 in.	2.8	1.45
TOTAL - 13 in.	3.8	2.9

Values for fission events in large uranium blocks (24 in. x 24 in. x 5-3/4 in. or 13 in. deep) reported in the last quarterly report have been revised in view of the work done on absolute beta counting. The revised values, which are lower than those reported previously, are tabulated in Table 3. Capture values are unchanged but are reported for completeness.

Table 3

Revised Values of Fission and Capture Events in 26 in. Diameter Uranium Cylinders Bombarded with 190 Mev Deuterons

Target and Depth	Fissions per Deuteron		Captures per Deuteron	
	26 in. Diam.	Infinite Diam.	26 in. Diam.	Infinite Diam.
5-3/4 in. Uranium	0.65	0.85	0.5	0.5
13. in. Uranium				
First 5-3/4 in.	0.7	0.85	0.6	0.7
Last 7-1/4 in.	0.25	0.45	0.35	0.4
Total Target	0.95	1.3	0.95	1.1
13 in. Uranium Beryllium Primary	0.85	0.90	1.25	1.45

Isotopic Composition of Product in Primary and Secondary Targets

W. W. Crane, G. M. Iddings, and R. L. Tollefsen
CRDC

The study of the isotopic composition of the product in A-12 target configurations has been extended to the following sequence of reactions which produce Pu^{238} in primary and secondary A-12 targets:

Primary U^{238} $\begin{matrix}(d, 2pn)\\(d, 2np)\\(n, 2n)\end{matrix}$ U^{237} $\xrightarrow{\beta^-}$ Np^{237} (n, γ) Np^{238} $\xrightarrow{\beta^-}$ Pu^{238}

Secondary U^{238} $(n,2n)$ U^{237} $\xrightarrow{\beta^-}$ Np^{237} (n, γ) Np^{238} $\xrightarrow{\beta^-}$ Pu^{238}

The Pu^{238} is objectionable because of its high spontaneous fission rate.

The ratio Pu^{238} atoms formed by the above path to Pu^{239} atoms (N_{48}/N_{49}) can be calculated by the following expression:

$$\underline{\text{Primary}} \quad \frac{N_{48}}{N_{49}} = \frac{\left[\sigma(n, 2n) + \sigma\begin{pmatrix}d, 2pn\\d, 2np\end{pmatrix}\right]\sigma_{37}}{2\,\sigma_{28}^2} \frac{N_{49}}{N_{28}}$$

$$\underline{\text{Secondary}} \quad \frac{N_{48}}{N_{49}} = \frac{\sigma(n, 2n)\,\sigma_{37}}{2\sigma_{28}^2} \frac{N_{49}}{N_{28}}$$

The ratio of N_{48}/N_{49} then depends on the g.t. level N_{49}/N_{28} and the cross section ratios:

$$\text{Primary} \quad \frac{\left[\sigma(n, 2n) + \sigma\begin{pmatrix}d, 2pn\\d, 2np\end{pmatrix}\right]}{\sigma_{28}} \quad \text{and} \quad \frac{\sigma_{37}}{\sigma_{28}}$$

$$\text{Secondary} \quad \frac{\sigma(n, 2n)}{\sigma_{28}} \quad \text{and} \quad \frac{\sigma_{37}}{\sigma_{28}}$$

Measurements of the ratios for the primary of an unmoderated uranium target configuration and for the primary and secondary portions of a mock up of a moderated A-12 target bombarded with 190 Mev deuterons have been made.

The results for the ratios in the center of an unmoderated uranium primary are:

$$\frac{\left[\sigma(n, 2n) + \sigma\left(\begin{matrix} d, 2\,pn \\ d, 2\,np \end{matrix}\right)\right]}{\sigma^{28}} < 3 \text{ and } \frac{\sigma^{37}}{\sigma^{28}} < 10$$

The ratios in the primary and secondary of the moderated configuration are:

Primary

$$\frac{\left[\sigma(n, 2n) + \sigma\left(\begin{matrix} d, 2\,pn \\ d, 2\,np \end{matrix}\right)\right]}{\sigma^{28}} < 1 \text{ and } \frac{\sigma^{37}}{\sigma^{28}} < 30$$

Secondary

$$\frac{\sigma(n, 2n)}{\sigma^{28}} < 0.4 \quad \frac{\sigma^{37}}{\sigma^{28}} < 30$$

The measurements confirm the upper limits estimated and show that the isotopic composition should not be unfavorable for the Pu^{239} case. It should be possible to increase the sensitivity of these measurements so that the actual ratios may be measured.

In order to determine the contribution of the U^{237} produced by the U^{238} (d, 2 np)U^{237} and U^{238}(d, 2 pn)Pa^{237} β^- U^{237} reactions in 4-12 target configurations, the excitation function for the formation of U^{237} from U^{238} has been determined. The results are given in Fig. 7, and represent the contributions of both the (d, 2 np) and (d, 2 pn) reaction paths.

The nuclide Pa^{237} had not been observed previously and was thought to have a short half-life. In order to separate the contribution of the (d, 2 pn) reaction a search was made for the Pa^{237} radioactivity. A series of short bombardments were run and an activity with a half-life of 12 minutes was observed in the protactinium fraction. Assignment of the activity to Pa^{237} was made by milking the 6.6 day U^{237} from purified protactinium fractions. The newly observed nuclide Pa^{237} has a half-life of 12 minutes and undergoes negative beta emission to U^{237}. The excitation function for the U^{238} (d, 2 pn)Pa^{237} reaction is shown in Fig. 8.

Fission Product Distribution at High Energies for Uranium and Thorium

M. Lindner and R. N. Osborne
CRRC

Excitation functions for Zr^{97}, Ag^{111}, and Ba^{139} formation in fission of thorium and uranium have been run for proton-, deuteron-, and helium-ion-induced fission. Figs. 9 through 17 show these plotted as cross-section

vs. energy. In addition to the observations noted in the last quarterly report, it may be seen that helium-ion and deuteron cross sections are nearly alike for all these nuclides, while the corresponding proton cross-sections are somewhat lower. It can, therefore, be said that cross sections for isotopes of this type in deuteron-induced fission reactions at 350 Mev should be very comparable to those for alpha particles of the same energy.

Similar functions are being determined for the nuclides Rb^{86} and Ba^{131}, these being supposedly more energy-sensitive than those mentioned above. The Ba^{131} is being observed through its daughter Cs^{131} which decays by electron capture. No data are yet available for Ba^{131} but the excitation functions for Rb^{86} formed in U and Th from proton bombardment indicate a threshold of about 40 Mev, with an almost constant slope to 350 Mev, at which energy the cross section was about 1.0 mb. An analogous excitation function for Th with alpha particles indicates the same threshold with somewhat higher cross sections at increasing energies. When all results are complete these data will be reported in more detail.

Excitation Function for the Reaction Al^{27} (α, α 2 pn)Na^{24}

A stack of aluminum foils was bombarded on the 60-inch cyclotron with 40 Mev alpha particles and the activity of Na^{24} determined. As a result, the curve shown in Fig. 18 was obtained, the beam current being integrated with a Faraday cup. This excitation function near threshold permitted the more precise determination of the energy definition for the overall excitation function reported previously. As a result, the revised excitation function is as shown in Fig. 19. In spite of this, it is likely that the function below 100 Mev is still subject to considerable uncertainty because of non-homogeneity of the alpha particle beam of the 184-inch cyclotron.

The experimental threshold appears (Fig. 18) at about 33 Mev, in reasonable agreement with a calculated threshold of 34 Mev.

Excitation Function for the Reaction C^{12} (α, α n)C^{11}

Polystyrene stacked foil bombardments were made in the internal deflected beam of alpha particles and, as in the case of the aluminum stacked foils, a "Faraday cup run" made, one in which the cross section was carefully determined for one energy. The uncertainties in energy at the lower energies were minimized with a Faraday cup run on the 60-inch cyclotron, using ground graphite discs 3 to 5 mils thick. Fig. 20 gives the excitation function near threshold as determined on the 60-inch cyclotron. The observed threshold of 21 Mev is in satisfactory agreement with a calculated threshold of 24 Mev.

The over-all excitation function is shown in Fig. 21. It will be noted that the determinations on the 60-inch and the 184-inch cyclotrons overlap considerably. This is in contrast to that observed for the Al^{27} (α, α 2 pn)Na^{24} reaction, and is due to the lower threshold for the C^{12} (α, α n)C^{11} reaction.

One of the excitation runs made on the $C^{12}(\alpha, \alpha n)C^{11}$ contained an aluminum monitor foil, the value being based upon the $Al^{27}(\alpha, \alpha 2pn)Na^{24}$ study. This monitor gave values for the cross sections of the C^{12} reaction in satisfactory agreement with an experimentally determined Faraday cup run for the $(\alpha, \alpha n)$ reaction.

Induced Activities

$Be^9(d, p 3n)Be^7$ Reaction. (R. E. Batzel and G. H. Coleman, CR&D)

The cross section for formation of Be^7 from deuteron irradiation of beryllium has been measured as a function of deuteron energy from 70 to 190 Mev. This activity would be important in shielding and heat load considerations if a beryllium target were to be used for an A-12 primary target. The results are listed in Table 4.

Table 4

Cross Section for $Be^9(d, p 3n)Be^7$ Reaction

Deuteron Energy (Mev)	70	100	160	190
Cross Section (Mb)	11	11	12	11

Experiments are under way to determine the number of Be^7 recoils to be expected from a beryllium target irradiated with high energy deuterons.

The cross section for formation of C^{11} from deuteron irradiation of oxygen is important in shielding considerations for the cooling water of a water cooled primary target. Preliminary results show that the cross section for formation of C^{11} by 190 Mev deuteron irradiation of oxygen is ~16 mb.

Corrosion of Zirconium. (L. Lits, S. A. Ring, and W. R. Balkwell, CR&D)

Four runs were made in which 190 Mev deuteron bombarded zirconium foils were immersed in water at 300° C. The amount of radioactivity transferred from the foils to the water and the stainless steel container fell off rapidly with increasing time of immersion. In one series of three consecutive runs with the same set of foils, the activity on the container after the second run of 8 days was 14.3 percent of that after the first run of 6 days and was 4.0 percent of the initial run after the third run of 13 days.

Very little zirconium was found either on the walls of the container or in the water. The major activity was due to strontium with smaller amounts of yttrium and selenium. A trace of niobium was found in some cases.

The majority of the activity appears to absorb on the walls of the containing vessel and is very difficult to remove entirely. Techniques for removing this activity are being investigated.

The weight gain of the zirconium foils in the first run after 8.2 days was 0.051 mg/cm^2. The weight gain after the second set of three runs with another group of zirconium foils was 0.079 mg/cm^2. The results indicate that there is a high initial corrosion accompanied by high loss of activity to the solution after which both the corrosion rate and rate of leaching of activities from the corrosion film drops off rapidly. Quantitative comparisons of the ratio of activity lost from the foil to that in the foil are not available as yet.

The study of the distribution of zirconium spallation products is continuing. The following isotopes have been identified among the longer-lived products from the bombardment of zirconium foils with 190 Mev deuterons - Nb-90; Zr-88,-89; Y-85, 86, 87, 88, 90, 93; Sr-82, 83, 85, 87, 91; Rb-82, 84; Br-76, 77; Se-72, 73; As-71, 72, 73, 74; Ge-69; Ga-67.

Absolute Beta-Counting. (P. C. Stevenson, UCRL - R. S. Gilbert, H. G. Hicks, and W. H. Hutchin, CWRD)

In order to improve the accuracy to be obtained from beta-counting of weighably thick samples on heavy backings, a program of investigation of the self-scattering, self-absorption, back-scattering, and sample-backing interaction has been initiated. A sample of Ag^{111} (7.5 days, 1.06 Mev β^-, no gamma, no daughter activity) was obtained from Oak Ridge in the form of pile-bombarded palladium foil and was separated carrier-free. The tracer solution so obtained was assayed on a very thin backing (~10 micrograms/cm^2) and a small amount of high-specific-activity silver metal was prepared. Using this, alloys were prepared of ~99 percent Cu, 1 percent Ag, and of ~99 percent Au and 1 percent Ag. Samples of these alloys and of silver metal were prepared in various thicknesses and counted on various backings. Similar measurements were made using the tracer Cu^{67}. Work is still in progress. It seems possible that a general formula for the necessary correction factor for the combined influence of sample and backing will be developed.

As the decay scheme of Cu^{67} was not known prior to the start of this investigation, the tracer used in our investigation was investigated with a scintillation gamma spectrometer and with a circular double-focussing magnetic beta-ray spectrometer. Gamma rays of energy 96 Kev and 191 Kev were observed using both the scintillation spectrometer and the beta-ray spectrometer. Allowed-shape beta spectra of upper energy limits 388 ± 5 and 570 ± 10 Kev were observed. The following decay scheme is tentatively postulated pending further investigation. (See Fig. 22.)

The backscattering by thick backings of various energies of beta radiation from various media was measured, following the technique used by Burtt (Nucleonics, August, 1941). In every case the backscattered radiation intensity (i.e. the increment of the counting rate due to the presence of the backing) was found to depend on the atomic number of the backing according to the relationship,

$$I_B = K(E)(\sqrt{Z} - 1)$$

where I_B is the intensity of backscattered radiation, Z is the atomic number of the backing material, and K is a function of the maximum beta energy E. Gamma-emitting tracers were not used in order to avoid effects due to secondary emission.

Instrumentation

G. D. O'Kelley, J. L. Olsen, and J. R. Tarrant
CRDC

The long magnetic lens beta spectrometer has been completed, and preliminary tests of the apparatus have been made. Axial focusing is used; the transmission and resolving power of the instrument being determined by a single annular slit midway between the source and the detector. Using the beta and internal conversion electron spectrum of Cs^{137}, the transmission and resolving power were determined for three slit widths. Results are given in Table 5.

Table 5

Slit Width	Transmission	Resolving Power
1 inch	2.6 percent	5.5 percent
3/4 inch	1.9 percent	4.3 percent
1/2 inch	0.91 percent	3.5 percent

It is anticipated that modification of the baffle system to permit ring focusing instead of axial focusing will improve the resolving power for a given transmission by a factor of two. Photographic films exposed in the region of the detector indicate that good axial focusing is obtained. With this assurance that the magnetic field shape is satisfactory, a series of photographic experiments is under way to determine the optimum position of the ring baffles.

A dry box for handling thallium activated sodium iodide crystals has been assembled, and considerable experience in cleaving sodium iodide crystals has been obtained. The resolution and efficiency of several crystals are being studied as a function of energy. Under conditions of high resolution, the Np L x-rays from Am^{241} decay (17 Kev) are resolved from the 59.8 Kev gamma ray with a "peak-to-valley" ratio of about five, and occasionally the 33 Kev gamma transition of low intensity can also be seen. Krypton x-rays of 13 Kev have been resolved, although photomultiplier noise severly limits the precision of such measurements.

A coincidence apparatus has been tested with which the gamma-ray spectrum in coincidence with beta particles can be recorded. An anthracene beta counter is used in coincidence with the scintillation spectrometer, and preliminary results with a sample of Np^{238} indicate that equipment performs satisfactorily.

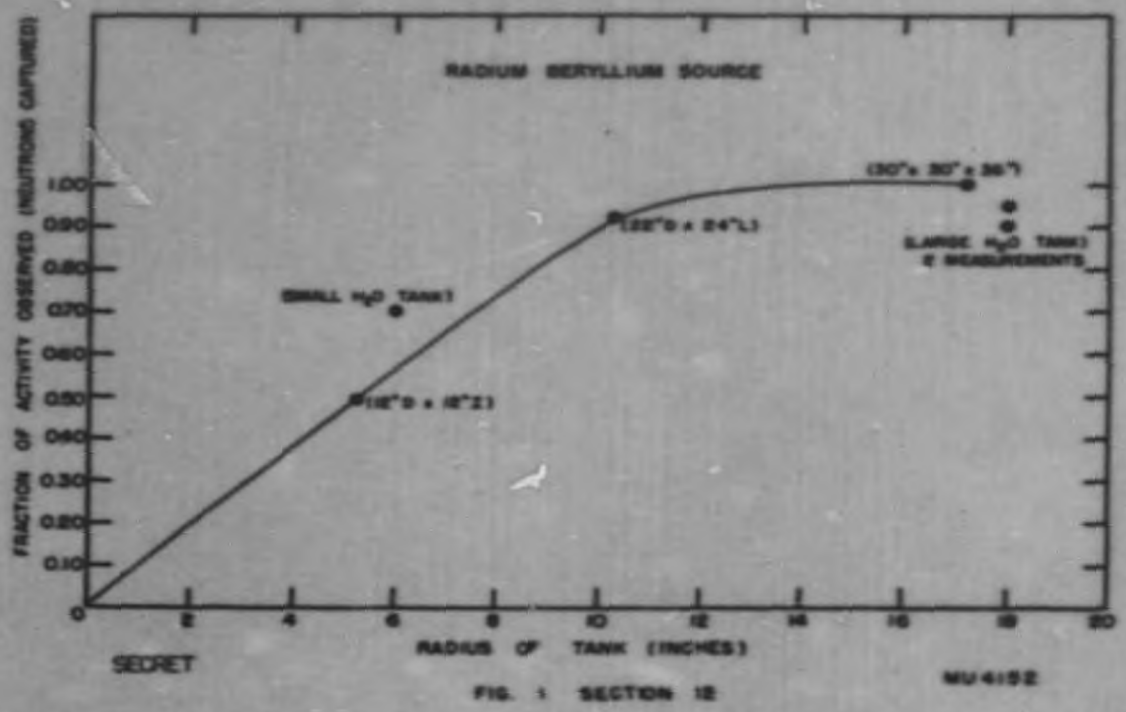

FIG. 1 SECTION 12

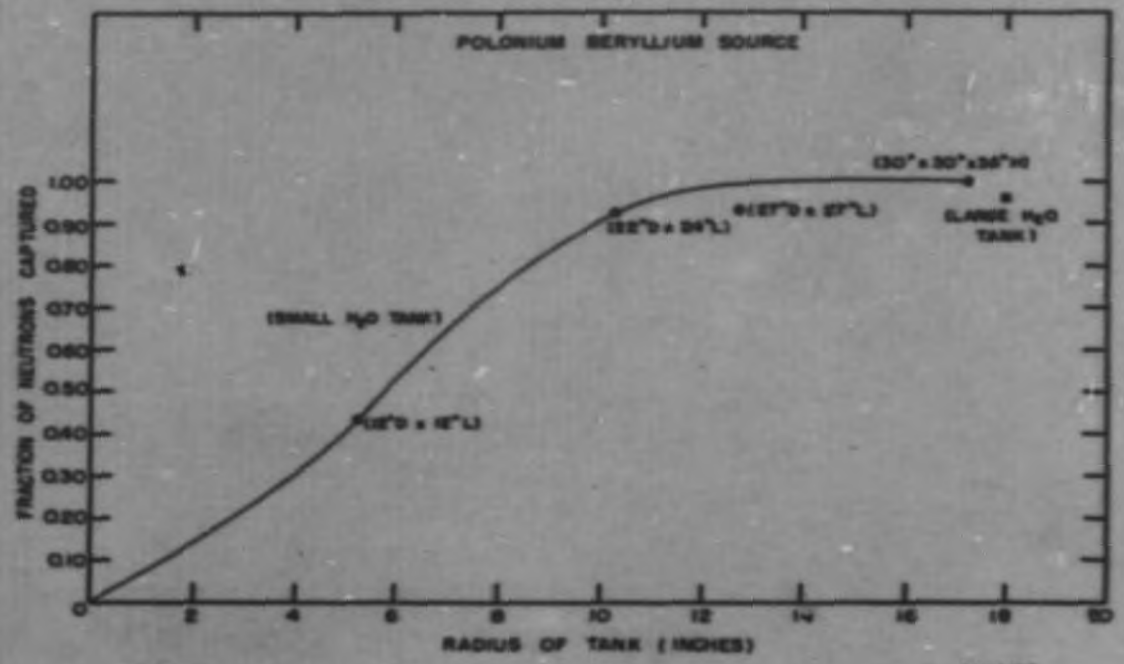

SECRET

MU4153

FIG. 2 SECTION 12

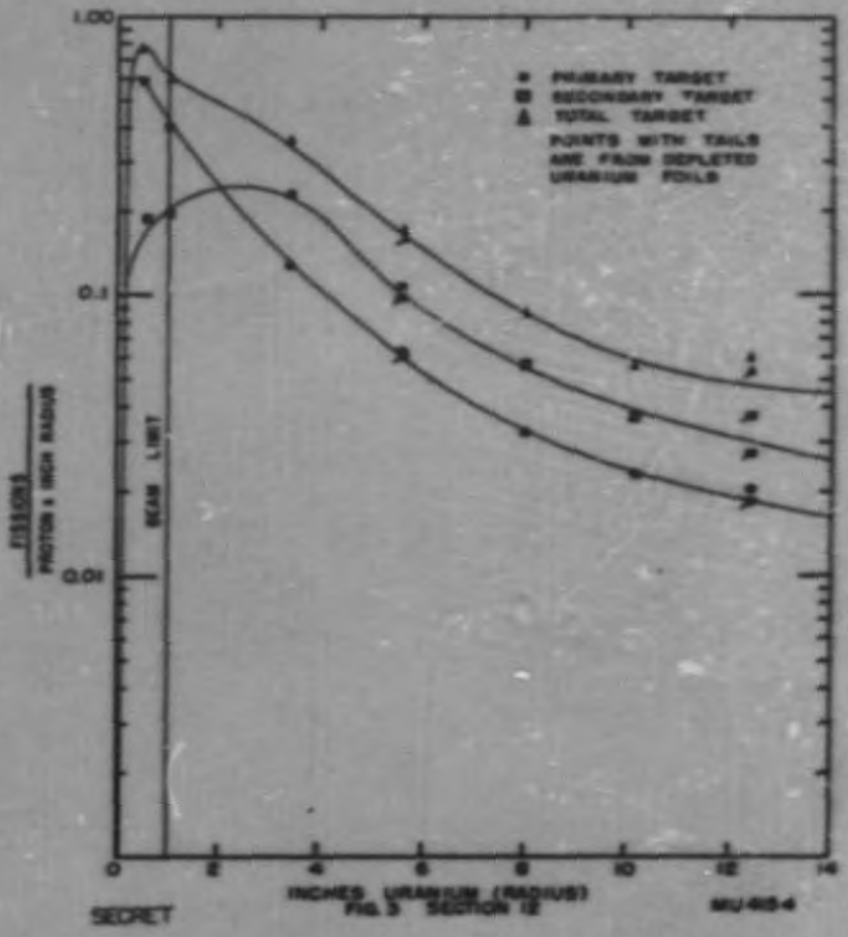

Weighted (with radius) radial distribution of fission events per proton occurring in an uranium block 24 in. x 24 in. x 13 in. deep bombarded with 350 Mev protons at the approximate center of the 24 in. x 24 in. face.

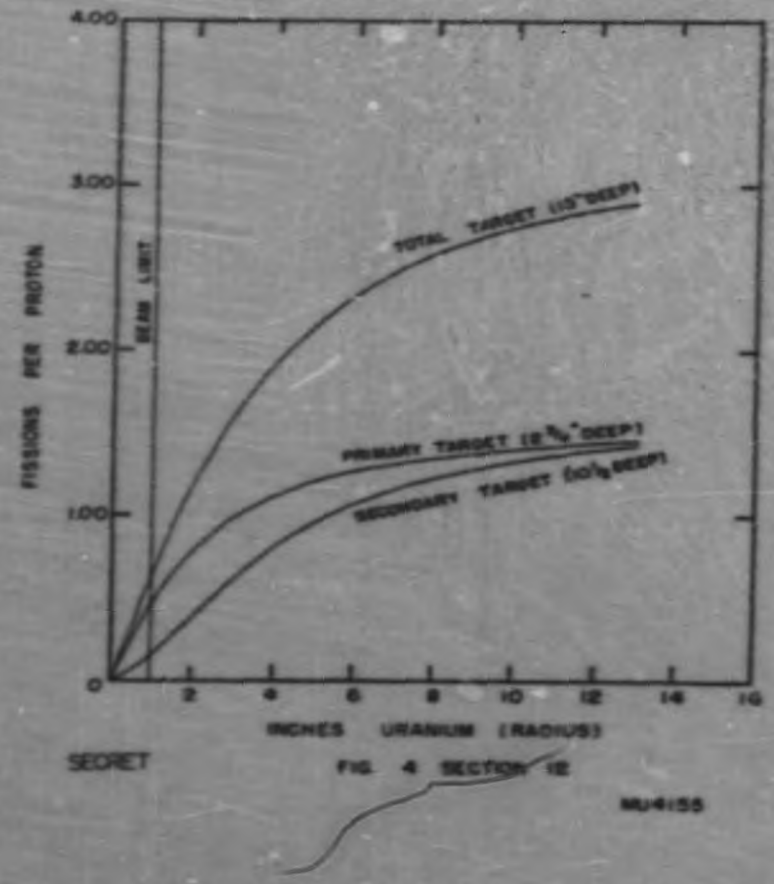

Total number of fission events per proton as a function of radius in a 24 in. x 24 in. uranium block bombarded with 350 Mev protons, integrals of curves in Fig. 1.

18-3-156

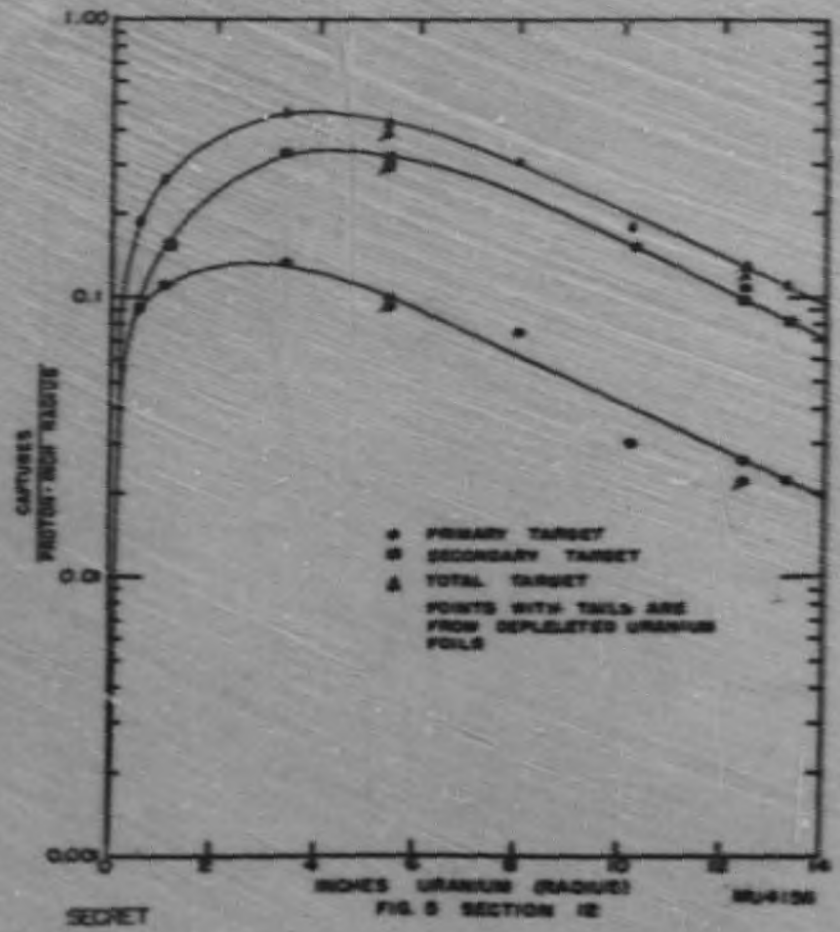

Weighted (with radius) radial distribution of capture events per proton occurring in an uranium block 24 in. x 24 in. x 13 in. deep bombarded with 350 Mev protons at the approximate center of the 24 in. x 24 in. face.

1903-137

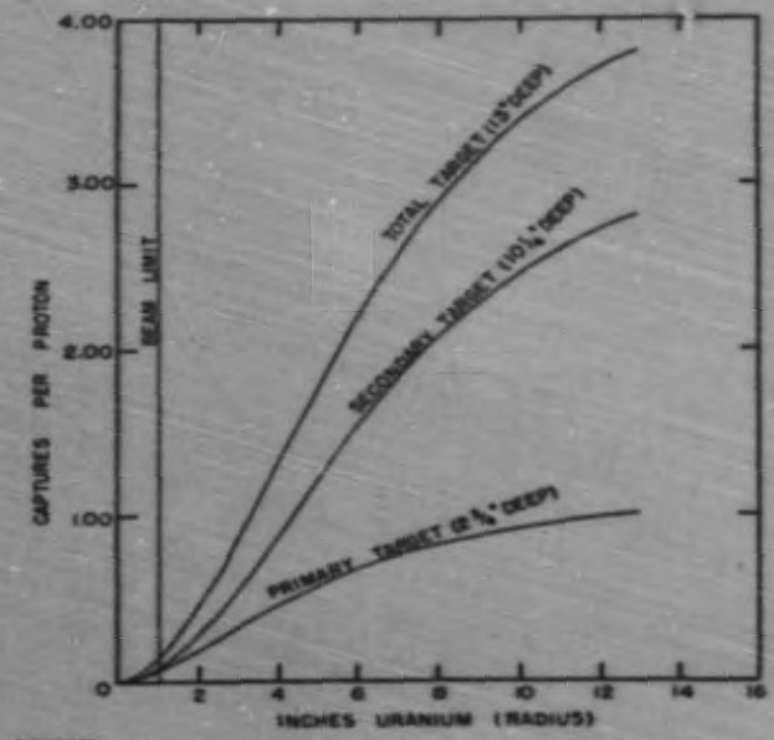

SECRET

FIG. 6 SECTION II

MU-4157

Total number of capture events per proton as a function of radius in a 24 in. x 24 in. uranium block bombarded with 350 Mev protons, integrals of curves in Fig. 3.

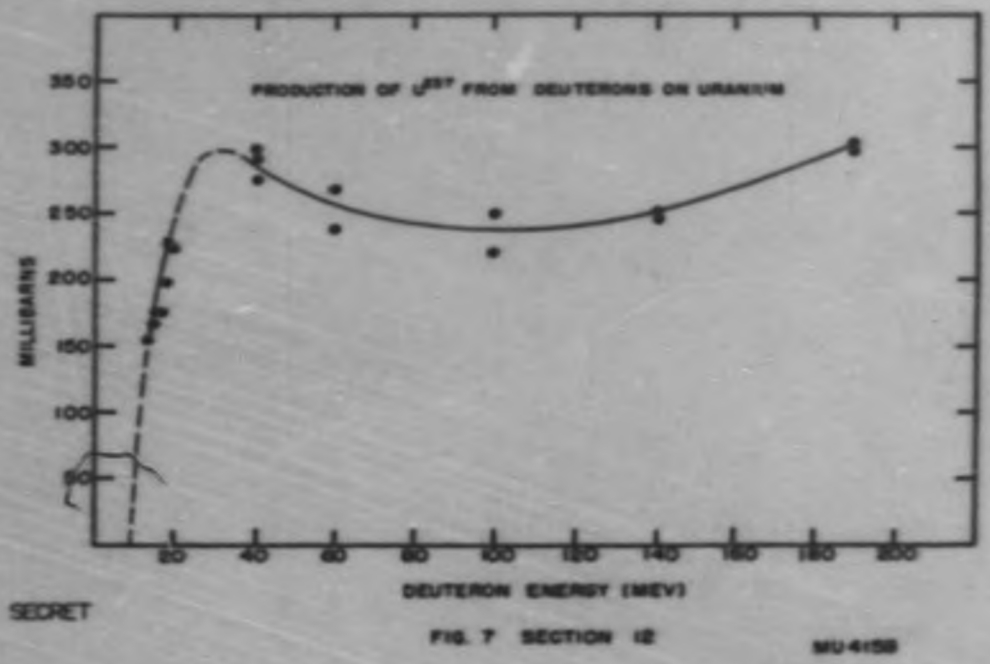

SECRET

FIG. 7 SECTION II

MU-4158

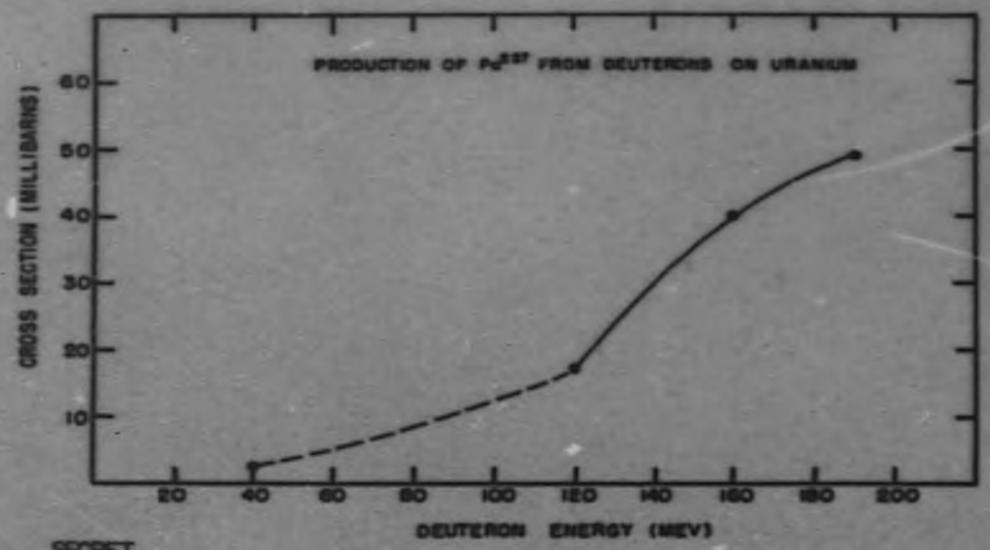

FIG. 8 SECTION 12

MU-4159

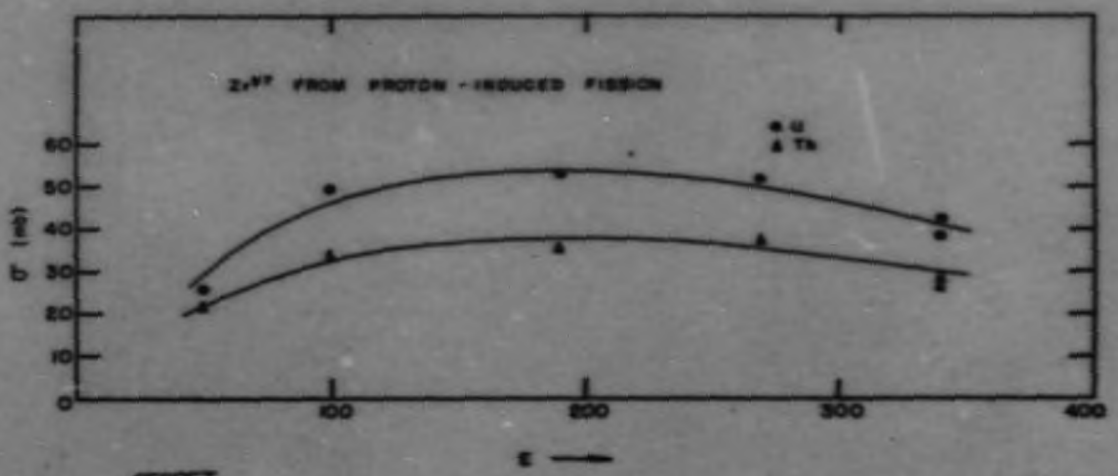

SECRET

FIG. 9 SECTION 12

MU4180

1503-141

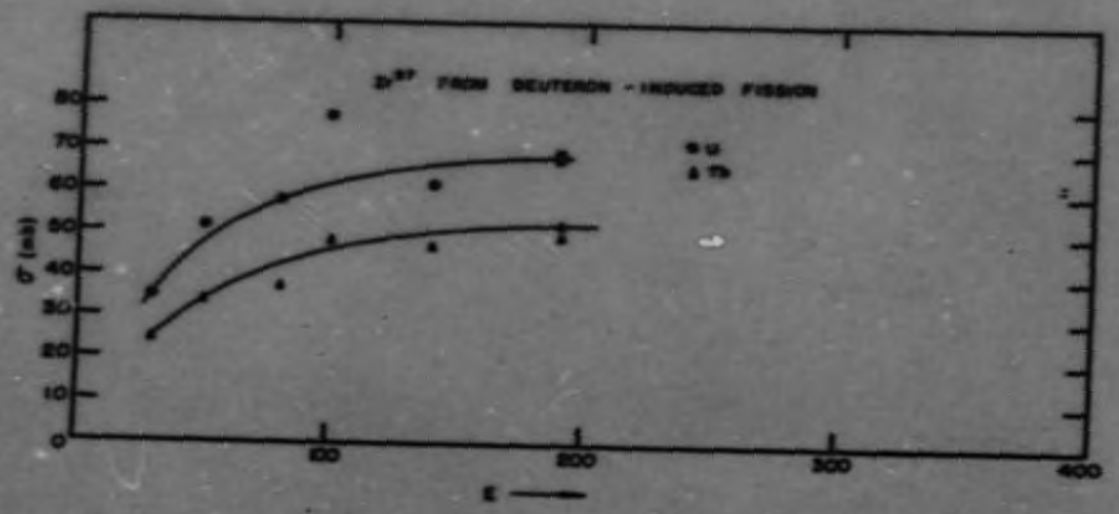

SECRET

FIG. 10 SECTION 12

MU-4161

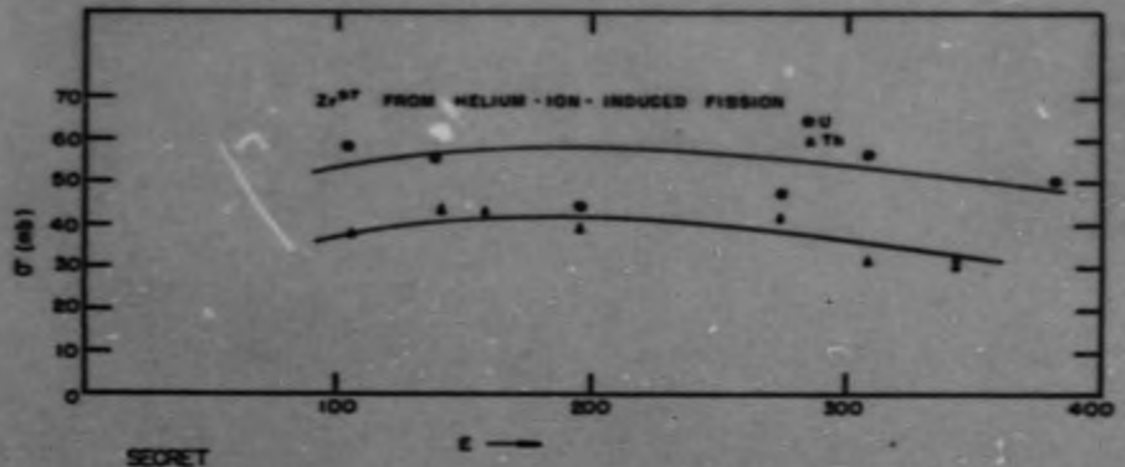

SECRET

FIG. 11 SECTION 12

MU4182

1903-143

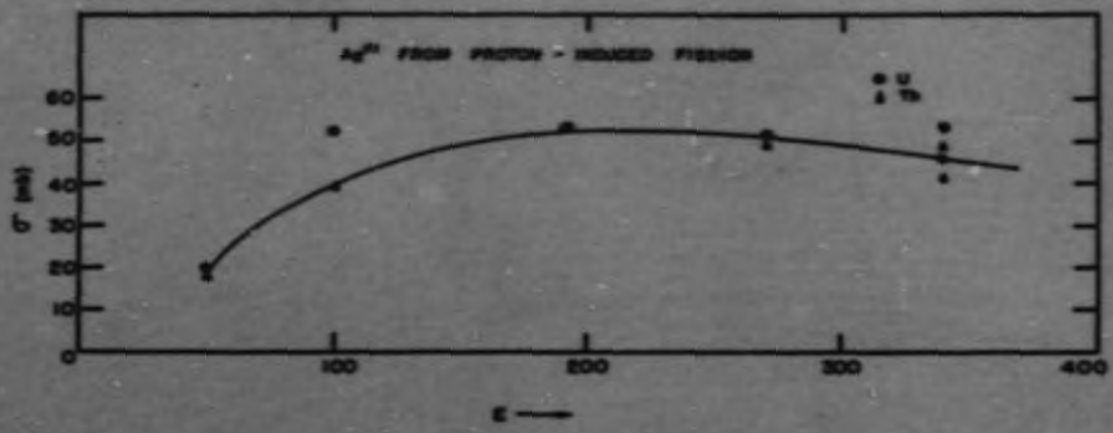

FIG. 12 SECTION 12

SECRET

MU-4163

1903-1X4

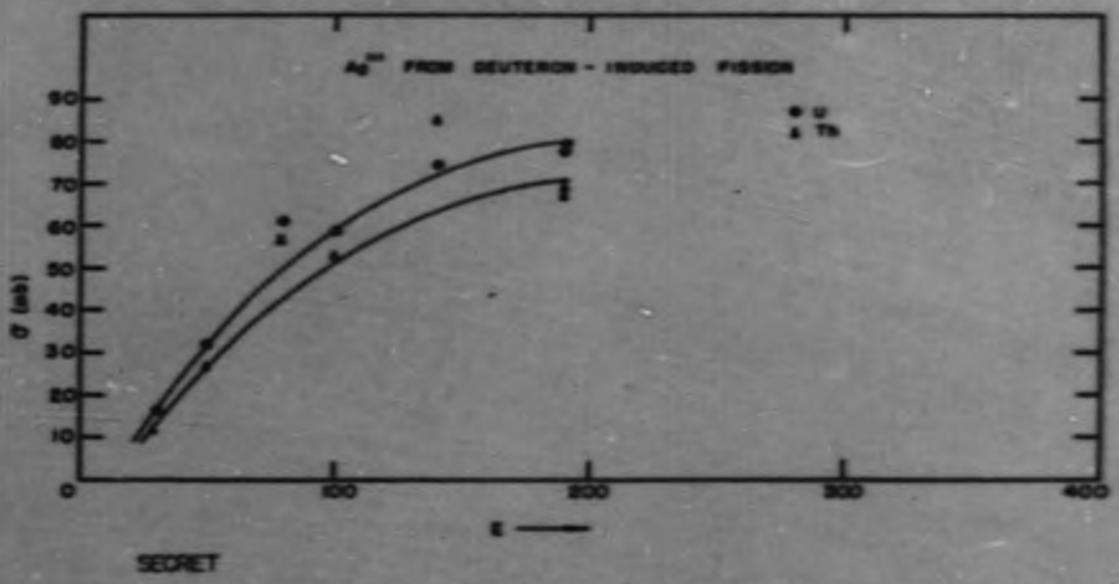

SECRET

FIG. 13 SECTION 12

MU4184

1903-145

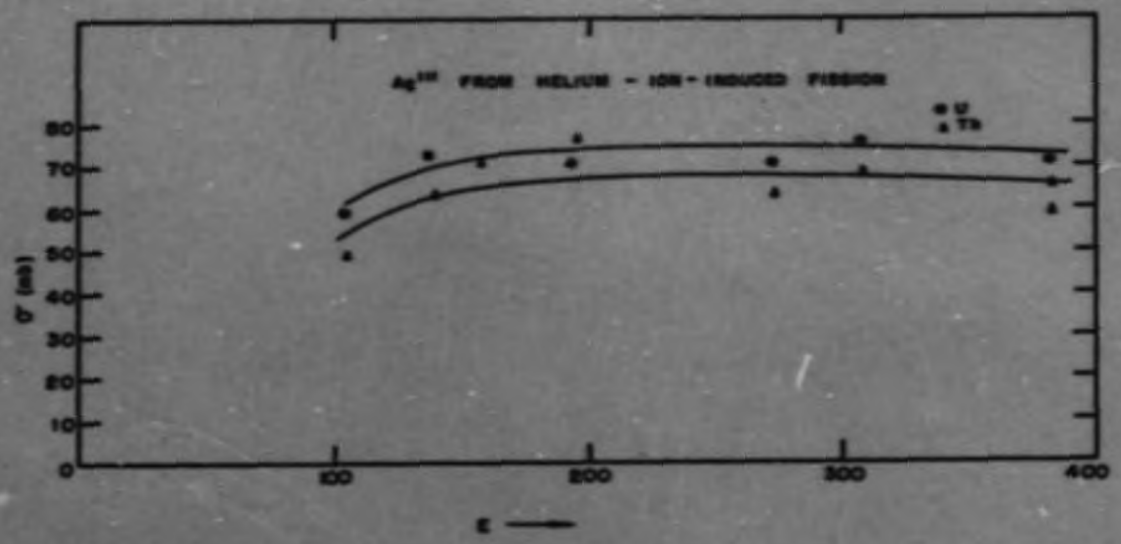

SECRET FIG. 14 SECTION II MU4165

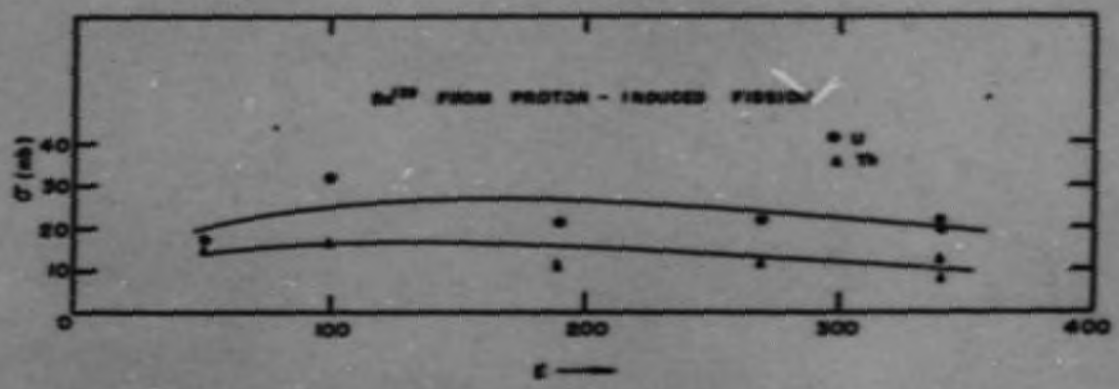

FIG. 15 SECTION 12

1903-147

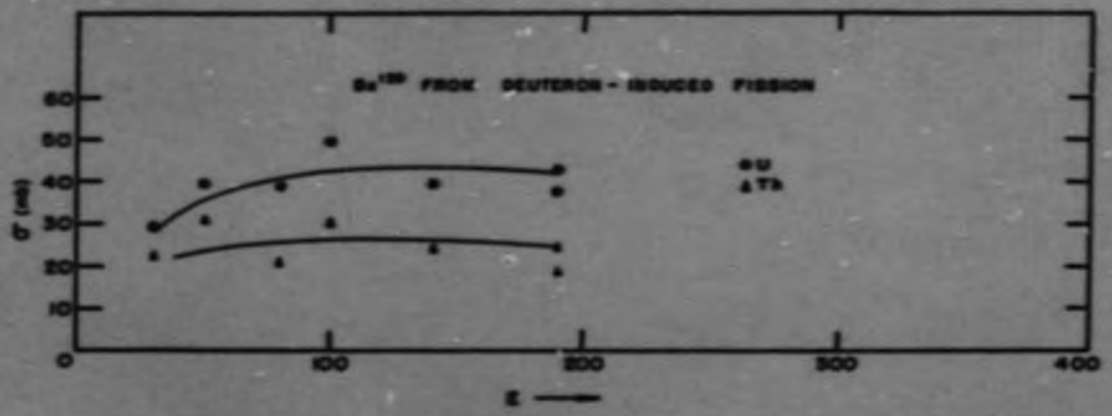

FIG. 16 SECTION 12

SECRET

MU4167

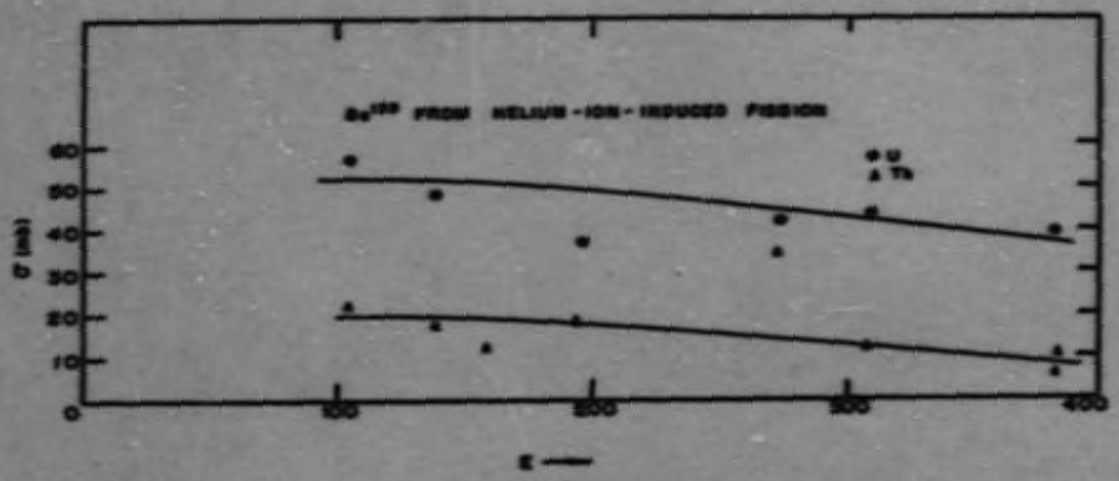

FIG. 17 SECTION 12

SECRET

MU-4189

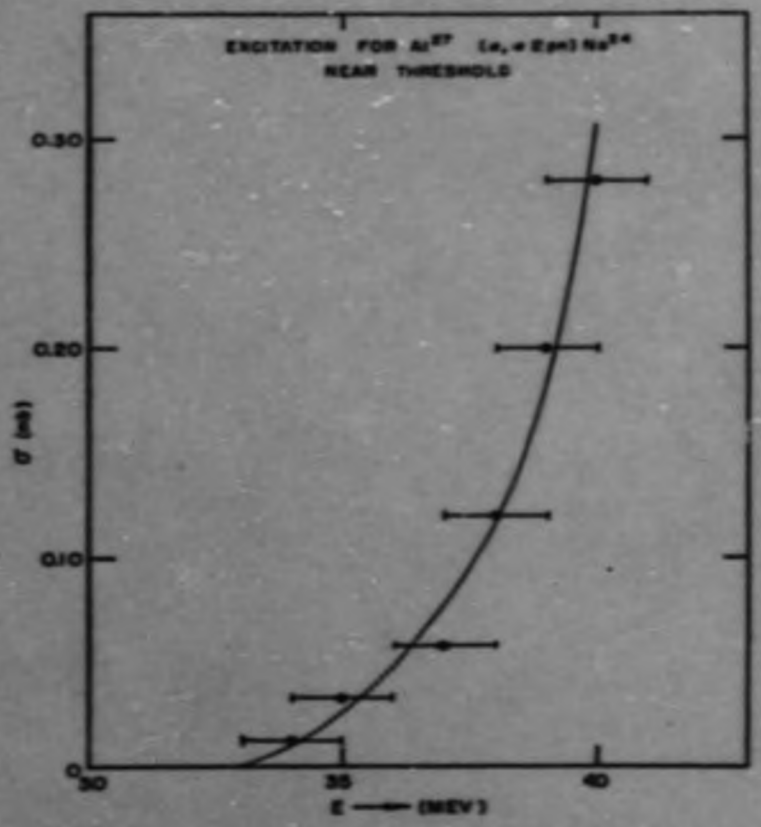

SECRET

FIG. 18 SECTION 12 MU4169

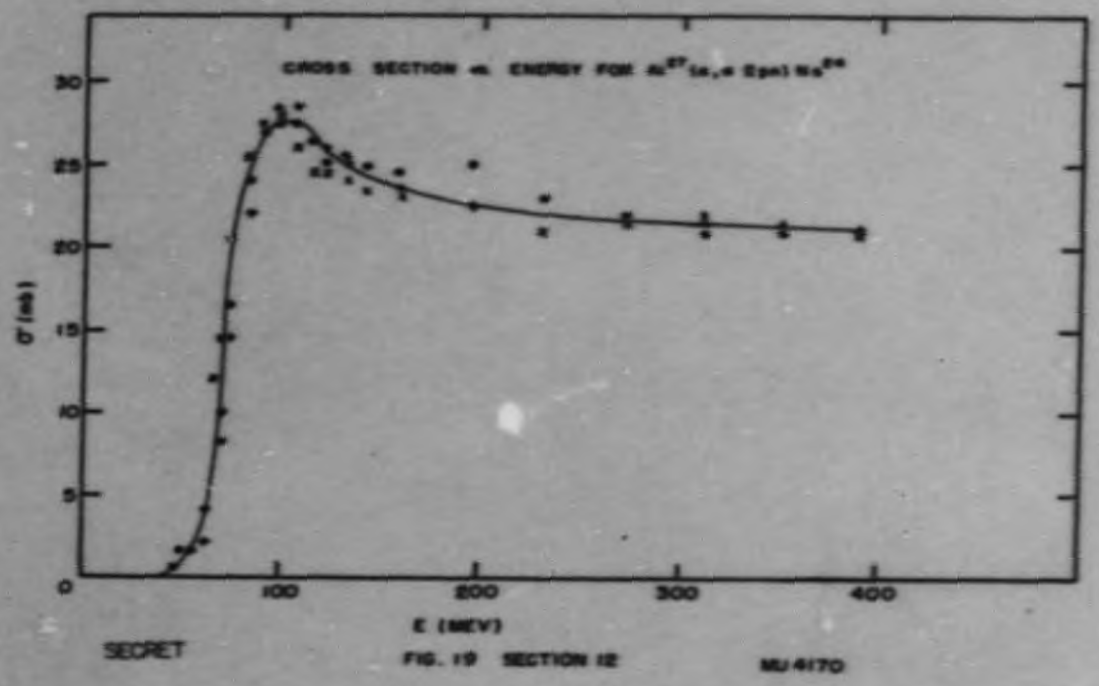

SECRET

FIG. 19 SECTION II

MU-4170

1603-151

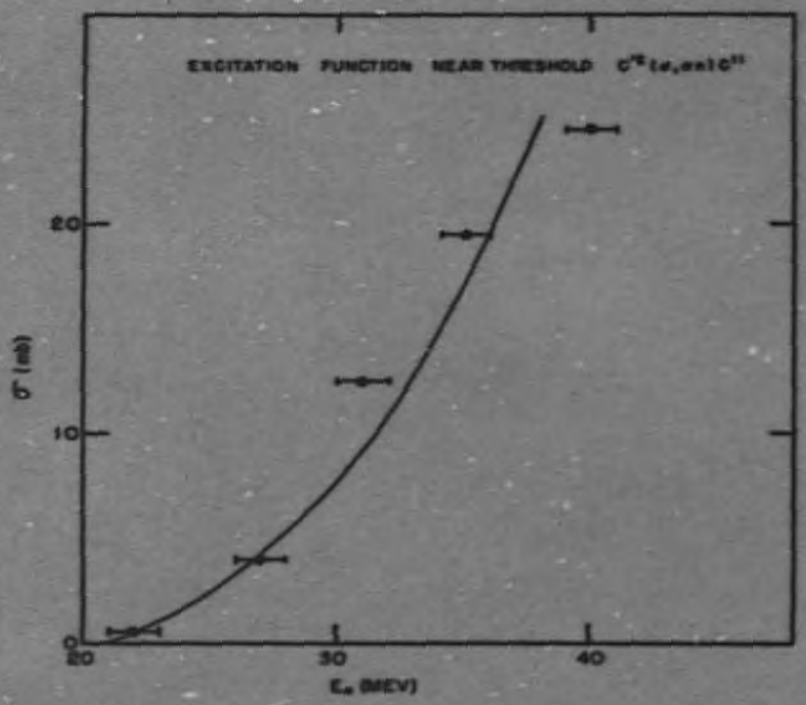

SECRET

FIG. 20 SECTION II

MU-4171

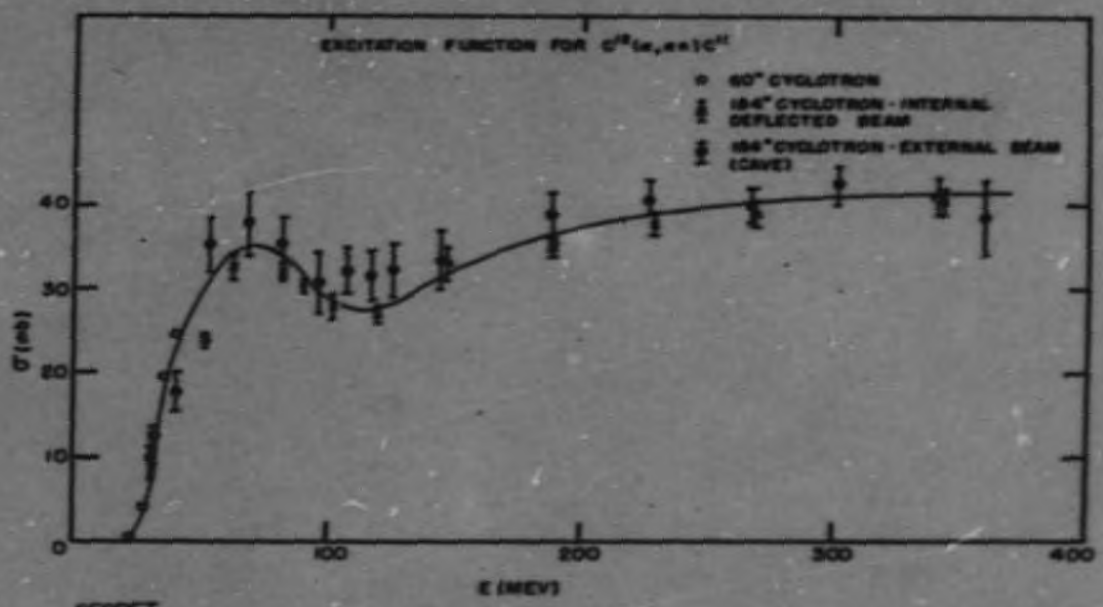

SECRET

FIG. 21 SECTION 12

MU-4172

1903-153

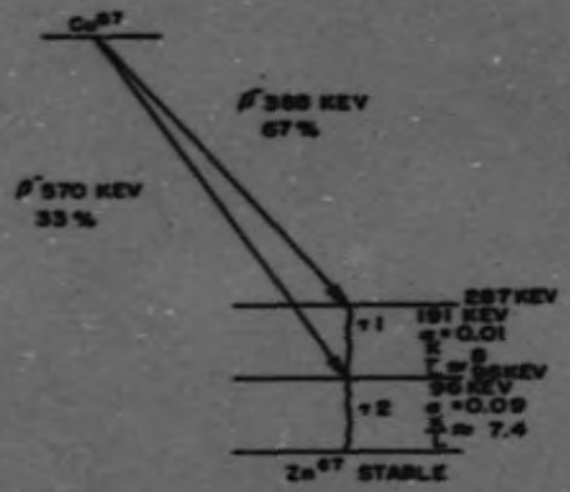

FIG. 22 SECTION 12

13. A-12 TARGET DEVELOPMENT

E. D. Kane
UCRL

Target Analysis

R. L. McKisson, M. E. Kaiser, E. G. Cope,
J. A. Quinville, N. R. LeRoy and R. M. Horning
CRDC

Beam Sweeping Studies

Spiral sweeping studies have been continued with emphasis on the full sine spiral because this is the pattern most easily obtained in practice. An optimization study has been completed with reference to the following parameters: target size, 12 ft. to 18 ft.; beam diameter, 2 ft. to 8 ft.; diameter of unswept center ("hole") 0 ft. to 6 ft.; and central overlap diameter, 0 ft. to 2 ft.; all with the 33/1 peak-to-average beam.

Several modes of optimization were found, viz.,

a. If beam size and target size are fixed, there is an optimum size of overlap or hole to minimize the peak heat load, $\overline{U}_{max}$ microamps/sq. in.;

b. If target size and hole size are fixed (for example to allow for central coolant duct,) there is an optimum beam size to minimize $\overline{U}_{max}$; and

c. If the target size only is fixed, then there is a range of optimum beam sizes and hole sizes for minimum $\overline{U}_{max}$.

Table 1, taken from report CRD-TI-114 for 12 ft. and 14 ft. targets, clearly illustrates the modes of optimization listed above.

Examination of Table 1 shows that optimum $\overline{U}_{max}$ values for a fixed target size are obtained for beam sizes requiring an unswept area at the target center. For beam diameters greater than 0.4 times the target diameter, optimum $\overline{U}_{max}$ values are obtained for overlapping sweeping conditions. It is of interest to note that the minimum $\overline{U}_{max}$ can be developed by several different sweeping patterns and beam sizes. This means, of course, that spiral sweeping allows maximum flexibility in accomodating for possible variations in beam size at the target.

Table 1

Values of Maximum Current Intensity*

Target Diam. Ft.	Beam Diam. Ft.	Diameter of Overlap Ft.		Diameter of Unswept Central Area Ft.			
		2	1	0	2	4	6
12	2.0	-	-	173	110	94	107
	3.0	-	-	120	91	104	187**
	4.0	138	105	97	104	158**	-
	5.0	109	103	105	145**	-	-
	6.0	118	-	141**	-	-	-
14	2.0	-	-	-	-	76	71
	3.0	-	-	100	73	68	82
	4.0	-	-	77	68	84	126**
	5.0	-	73	72	82	113**	-
	6.0	79	78	84	106**	-	-
	7.0	88	91	103**	-	-	-

* Values are estimated to have a probable error of 5 percent.

** Circular Sweeping.

Table 2

Tube Heat Load Comparison

Type of Sweeping	Target Size Ft.	Beam Diameter Ft.	"Hole" Diameter Ft.	Qmax Microamp inch / Width Tube
Opt. 5:4 Lissajou	12	6	-	6150 ± 8 %
Opt. Full Wave Spiral	12	4	0	7250 ± 8 %
	14.4*	4	2	5670 ± 8 %

* A 14.4 ft. spiral pattern target compares directly with a 12 ft. square Lissajou target in overall dimensions.

1503-156

While the $\bar{U}_{max}$ values are important target parameters in that they determine the point heat transfer loads, the total heat delivered to a tube is equally important. The Q values, which are proportional to this total heat, have been determined for several cases of spiral sweeping and are compared in Table 2 with the Q values computed for the optimized 5:4 Lissajou sweeping case.

The data in Table 2 show that the computed Q_{max} for spiral sweeping on a 14.4 ft. target is lower than that for the corresponding optimized 5:4 Lissajou sweeping, although the difference is of the order of the estimated error.

A third quantity useful in the comparison of sweeping patterns is the peak-to-average ratio in the target, $\bar{U}_{max}/U_T$. This value is indicative of the degree of uniformity developed by the sweeping method. Data for various types of sweeping and various target sizes are given in Table 3.

The effects of various beam shapes and peak-to-average ratios on $\bar{U}_{max}$ for circular sweeping have been surveyed. It has been found that for the center-peaked beams a reduction in peak-to-average beam intensity from 11/1 to 10/1 is much less effective than a further decrease from 10/1 to 3/1 for sweeping at $\rho = R_{max}$. The values of $\bar{U}_{max}/U_{ave}$ for these ratios are: 1.145 for 33/1; 0.82 for 10/1; and 0.46 for 3/1. It was also found that a beam with a central "dimple" (i.e., zero intensity at center) gives about a 5 percent decrease in the $\bar{U}_{max}/U_{ave}$ ratio for sweeping at $\rho = R_{max}$ with peak-to-average ratios of 10/1 and 5/1.

The $\bar{U}_{max}/U_T$ values for these beams are also given in Table 3 for comparison.

Table 3

Peak-to-Average Current Intensities on Target

Type of Sweeping	Target Size Ft.	Peak / Ave In Beam	Beam Diameter Ft.	"Hole" Diameter Ft.	$\bar{U}_{max}$ Microamps / Sq. In.	$\bar{U}_{max}/U_T$*
		Center Peak				
Opt. 5:4 Lissajou	12 Sq	33/1	6	-	91	3.57
Fund 5:4 Lissajou	12 Sq	33/1	6	-	107	4.20
Opt. Full Wave Sine Spiral	12 Circ	33/1	4	0	97	3.16
	14 Circ	33/1	4	2	68	3.18
Circular	12 Circ	33/1	6	-	142	4.62
	12 Circ	10/1	6	-	101	3.28
	12 Circ	5/1	6	-	80	2.61
	12 Circ	3/1	6	-	67	2.18
		Center 'dimple'				
	12 Circ	10/1	6	-	95	3.10
	12 Circ	5/1	6	-	75	2.44

* U_T is computed as the average current intensity in the swept area of the target.

1903-157

The data of Table 3 indicate that sweeping the beam produces significant reductions in $\bar{U}_{max}/U_T$, even for beams whose peak-to-average is already down to the order of 5/1 or lower.

A-12 Window Studies

An estimate of the effect on ultimate neutron production of a "window" inserted in the A-12 beam has been made. The window was taken to be a cylindrical aluminum shell 5 ft. in radius and 0.144 inches thick, backed by a series of trapezoidal water channels about 1.7 inches x 0.375 inches in size formed by a shaped aluminum sheet 0.144 inches thick welded to the first shell.

Assuming full-wave sine spiral sweeping pattern, the average loss in beam energy and the beam attenuation were calculated. There was a 7.5 percent decrease in beam power, from 175 megawatts to 162 megawatts, and an estimated net loss in potential neutron production of 8.5 percent. While the latter value was computed for a specific case, it is reasonable to regard it as generally representative of the loss in potential neutron production for such windows.

Blister Problem in Clad Plates

The influence of blisters upon the heat transfer characteristics of clad plates and upon the related thermal stresses is being studied. The solution of this problem is not yet available. A detailed analysis is now in progress and is about 50 percent complete.

Gas-Cooled Primary Target

The gas-cooled uranium primary target study is complete. Both conical and flat plate elements were studied, and the flat plates appeared more favorable. The best design is one in which the plates are completely tailored in thickness such that all coolant channels receive an equal heat duty. With such tailoring, the total weight rate of helium for the dissipation of 180 megawatts is 200 lb/sec compared to 400 lb/sec for the two-step tailoring system originally proposed. Gas-cooling studies of uranium targets have been deferred because of the unpredictable growth problem at high temperature. If this problem can be solved, gas cooling should be seriously considered for a production target with the use of a window. The loss in potential production caused by a window is now estimated to be about 8.5 percent; and since a gas cooled target can be made very efficient, it seems possible to design a high production target using this combination.

Calorimetric Heat Release Feasibility Study

A feasibility study of a direct experimental measurement of the heat release in a primary target for 190 Mev deuterons is in progress. Computations indicate that the heat release of the 190 Mev deuteron beam of the 184-inch UCRL cyclotron in a uranium primary target is measurable, the rate of temperature rise being estimated as 1 degree F in 4 minutes. The estimated accuracy of measurement is ± 10 percent.

Experimental Probe

The design of the experimental probe for the Mark 0 beam for the study of radiation effects is about 60 percent complete. The most probable peak heat duty is now estimated to be 300,000 BTU/hr. ft.^{2} or half of the originally quoted estimate. This reduction is caused by two effects: 1) the beam is now being allowed to penetrate the outer shell and to dissipate a significant part of its energy in the water coolant; and 2) the design time average beam intensity is 42.5 microamps/sq. in which is a 25 percent decrease in current intensity. This decrease in current intensity would result from the use of the most efficient beam sweeping for the assumed beam shape.

The currently conceived probe consists of a stainless steel thimble supported at the upper end of a D-8 vessel nozzle and extending about 4 ft. into the vessel cavity. The exposed end consists of a semi-permanent 11-1/2 in. o.d. waterjacket in which an opening about 1 inch in width and 24 inches long will be cut. A double-walled helium-cooled window is aligned behind the opening in the water jacket. This window allows the useable particle beam to pass into the sample chamber. The samples are mounted in a sample carrier which is inserted and removed from the probe through the nozzle opening. The carrier is positioned by means of guides so that the gauge lengths of the samples are held in position in the particle beam.

It now appears that window designs are a very important feature of the probe design, and a series of tests is planned to establish window limitations and specifications since long probe life is necessary for efficient use of accelerator time.

Experimental Engineering

P. J. Charley and D. F. Casey
CRDC

A 1/48 scale model of the base case target and lattice arrangement has been completed.

All equipment required for the construction of the 500 KVA resistance thermal cycler has been requisitioned. This apparatus will be located in Building 21 until the proposed new building is available. It is now anticipated that this cycler will be ready for operation in October, 1952.

O.R.N.L. has been requested to ship the small resistance cycler (without power transformer) to Livermore this July. A low voltage-high current transformer for this equipment has been purchased. This apparatus has been used in an effort to establish an "endurance strength" curve for a water-cooled uranium sample in which the alternating (thermal) stresses are

imposed by pulsed resistance heating. Uranium corrosion due to the water environment has partially obscured the test results. Corrosion tests of uranium in "Aroclor 1248", a hydrocarbon used for heat transfer, are being planned. Should the samples prove resistent to attack therein, this liquid will be used as the coolant.

An in-pile irradiation test of an A-12 target element is being planned by the materials group. Preliminary to this test, it is necessary to establish that the elements will not fail prematurely due to improper fabrication or radiation damage. The Experimental Engineering Section has designed an apparatus to subject elements to thermal cycling as the best available pre-test and purchasable equipment has been ordered.

Target Design

J. E. Viscardi, B. W. Kia, J. Ekvall and P. W. Osborne
CRDC

F. J. Sterbentz
Bechtel

R. Spies
UCRL

Base Case

Pu producer utilizing depleted U[redacted] in both primary and secondary targets, as well as in the lattice, moderated and cooled by light water which also serves as the neutron reflector and biologic shield.

General

During the early part of this quarter, it was decided to proceed with the elaboration of a definite target design for what is designated as the base case, viz., for a Pu producer using depleted U[redacted] in both primary and secondary target sections, as well as in the lattice, entirely moderated and cooled with light water which will also serve as the neutron reflector and biologic shield.

All the target components (primary, secondary, and lattice) will be stationed under water. An important simplification is achieved by this arrangement in so far as the water serves as a neutron reflector and biologic shield besides functioning as a moderator and heat transfer medium.

The design will provide for accessibility of all targets constituents to permit replacements, repairs, or substitution of modifications by remote handling.

Excepting the fuel elements, most parts will be made of aluminum.

Primary Target

The primary target will be vertically inserted in a horizontal cylindrical vacuum vessel at a point near the flat closed end of the latter opposite the opening for the beam from the accelerator. The fuel elements in this target section will be in the form of long flat rectangular plates consisting of a 45-mil core of Zr-U alloy (2 percent Zr) with 10-mil Zr cladding on each side and somewhat more at the edges. These plates will be hung in bundles on the internal open-ended cylinders of bayonet tubes, and they will occupy both the inner circular and the outer annular channels with uniform interplate spacing so proportioned as to equalize the areas for the flow of cooling water through the two channels in series. The cooling water circulated in a separate closed system will be deaerated and treated to minimize corrosion and surface deposits.

Alternative manifolding arrangements for the two-row bayonet tube bank are still under consideration. The first design, originally devised for the U^{233} breeder, can be readily adapted to the base case. It comprises 21 separate manifolds each accomodating two bayonet tubes. Either the separate manifolds with their respective pairs of tubes in place or the plate bundles in particular tubes can be handled, as might be desired. Each bayonet tube has its own water flow controller, and each manifold has shut-off valves for use in the removal operation. The second design has a common manifold for all the bayonet tubes. With this arrangement, the entire assembly must be transferred to the handling area before individual tubes and plate bundles can be withdrawn. Comparative outage time and relative adaptability to various anticipated operating contingencies must be carefully studied before a choice can be made between the two arrangements.

The estimated weight of the whole primary target is around 42 tons. The weight of one bayonet tube, including its plate bundles, is about 1,600 pounds.

Secondary Target

The secondary target, contained in its own rectangular tank, will be located outside the cylindrical vacuum vessel, very close to the flat end of the latter, and axially in line with the primary target. The external location of the secondary target is preferred mainly because it will facilitate modifications likely to be required owing to uncertainties in theoretical predictions of its performance, but also partly because it reduces the structural difficulties occasioned by extremely large openings in the vacuum vessel. The tank will be divided by aluminum partitions into rows of long rectangular cells 4 inches deep and 8-3/4 inches wide, containing spaced Zr-clad U plates, made like those in the primary target but with thicker cores and sufficient in number to provide 6 inches of equivalent uranium thickness.

There will be 21 plates in depth. Of these the first nine, which are designed for the peak heat load of 4.1 kilowatts per cubic inch, will each be 220 mils thick and uniformly spaced 150 mils apart for water cooling; the remaining 12, which are designed for the average heat load of 1.9 kilowatts per cubic inch, will each be 340 mils thick with 150-mil interspaces. Approximately 110 tons of uranium will be required for this target.

The total heat load in the secondary target is estimated at 221 megawatts with a peak-to-average ratio of 2.16. The necessary cooling water flow rate is about 43,000 gallons per minute with a 35° F rise in the bulk temperature. The design calls for a water pressure of 120 psi at the inlet and 50 psi at the outlet. Like the primary, the secondary target has an independent coolant system circulating deaerated treated water.

Between the flat rear end of the vacuum vessel and the front face of the secondary target tank, there will be a 1/4 inch gap which appears adequate to cool this vacuum vessel wall by local natural convection of the general immersion water.

It is planned to make the rear lattice structure integral with the secondary target tank. The arrangement will comprise rectangular cells containing flat zirconium-clad uranium plates, each 340 mils thick spaced 340 mils apart for the circulation of cooling water, which will amount to about 12,000 gallons per minute.

The plate bundles in both the secondary target and in the connected rear lattice will be handled by crane from overhead.

Lattice

Apart from the auxiliary rear lattice just mentioned above, the main lattice will be placed cylindrically around the vacuum vessel and will extend backward to the secondary target. The fuel elements in this lattice will consist of 1-inch o.d. aluminum-clad round rods of depleted uranium [redacted] 48 inches long. To facilitate handling, these rods will be semi-jacketed together parallelwise in chains which will be supported twelve layers deep in lateral semi-circular guides in C-shape frames. The spacing of these rods in the bank will approximate the 1.25 inch equilateral triangular setting of centers with one side parallel to the vacuum vessel surface, such as was assumed in the theoretical calculation of Pu production in this part of the system. The overall length of the cylindrical lattice will be about 50 feet. The inside diameter of the semicircular C-frames will be approximately 18 feet. Beyond this the breeder rods will occupy 15 inches of radial depth, and 3 additional feet will be taken up by water for neutron reflection and by metal structure.

The sides and back of the C-frame will be closed, while the front will be left open in order to promote water cooling of the vacuum vessel wall. The design will provide for adjustment of the gap between the front tubes and the vessel surface, so as to hold the water blanket thickness there down to values that will prevent excessive neutron capture and consequent Pu production losses. Special experiments are now under way by other groups to evaluate these blanket-induced losses.

Cooling water from a closed circulation system will be introduced from a header into each C at quarter arc points midway between the vertical and horizontal axes and will exit at the top and bottom. To prevent grossly unequal liquid sweeping of rod and vessel surfaces, it appears necessary to install lateral gaskets between the side of the C and the vacuum vessel.

Two or three important effects have not yet been taken into account quantitatively in the above-outlined estimate of the lattice cooling load, namely,

1. The variation of the film heat transfer coefficient around individual rods may entail a maximum-to-average ratio of 2/1 in the local temperature difference between the surface and the water.

2. It may be possible to permit the rod surface temperature to rise appreciably above present contemplated levels at various points in the lattice and still maintain non-boiling conditions.

3. Water velocities, pressures, and temperatures must be adjusted in such a way as to prevent cavitation, especially since many of the rods will have to remain in the lattice for long periods of time.

In calculating the above-cited cooling data, it was assumed that effects (1) and (2) roughly counterbalance.

Each C-frame will be mounted on a four-wheeled flat car which can be rolled perpendicularly toward or away from the vacuum vessel by means of a mechanism attached to a gantry crane traveling parallel to the vessel. This crane will be equipped to load and unload the C-frames and transport them to and from the handling or service areas. The gantry will be driven by electric motors from above the water tank level through a system of gear and chain drives. The electric power for this purpose will be supplied from a rail-type installation outside the water tank. There will be a slip joint between the piping on the C-frame and the cooling water header, so that remote disconnection can be effected when the frame has to be moved.

The average value of the heat generation rate in the lattice rods is estimated at approximately 61.5 BTU per cubic inch per hour, equivalent to about 210 watts per cubic inch. The radial variation of the heat flux in the individual C's has been calculated, and the ratio of maximum to average is indicated to be around 2/1. The heat load variation from C to C axially along the vacuum vessel has not been determined yet, but maximum-to-average ratios from 3/1 to 5/1 have been envisaged in computing the possible cooling requirements.

With 4-foot rods, there will be 26 C-frames altogether. The average heat evolution per C will amount to approximately 25 million BTU per hour. The cooling design is based primarily upon the avoidance of boiling at any point, so that, for example, a maximum surface temperature of 232° F would be tolerable at a spot with a hydrostatic head of 16 feet. The following tabulation summarizes the calculated cooling data for the case in which the axial maximum-to-average ratio of heat load is 4/1:

Inlet Water Temp., F	80	100	120
Av. Water Temp. Rise, F	40	32	27
Inlet Water Press. psia	15	15	15
Outlet Water Press., psia	30	32	35
GPM	33,600	41,000	49,000

Alternative Designs

During the last part of this quarter, a subgroup (Mahlmeister, J. Smith, H. Hollister, T. Batser, C. Hay) was organized within the Target Design Group to investigate other possible arrangements of the primary target, secondary target, and lattice as well as complete alternatives to the base case. The following is a summary of the various proposals thus far studied:

Window for 350-Mev 0.5 Ampere Beam. It appears that the design of a window to pass the 350-Mev 0.5-ampere deuteron beam is theoretically feasible. This study covered preliminary studies of fabrication, heat, transfer, and fluid flow. The window would be located down-stream from the beam sweeping equipment and in front of the lattice water tank. It would be of aluminum construction with design features permitting removal by remote control. The irradiated area consists of three aluminum plates with water coolant passages. The loss of production is approximately 9 percent for a differential coolant pressure of 50 psi with an allowed design stress of 15,900 psi.

The current effort is to devise suitable performance tests on typical sections of the envisaged design.

Helium-Cooled Beryllium Plate Primary. The use of beryllium plates in stainless steel tubes is tentatively considered a promising alternative to the base case design. This study, using the bayonet tube with plates in the internal tube only, may prove to be a desirable arrangement. One serious difficulty is occasioned by the low thermal capacity of helium and its relatively poor heat transfer characteristics. According to present indications, the required pumping power would be greater than for the water-cooled uranium target. Work is continuing on other arrangements.

Helium-Cooled Secondary Target. Theoretical and mechanical design studies of a gas-cooled uranium secondary target indicate that the uranium plates would be subjected to temperatures as high as 1000° F. Mechanical layouts have been completed to show possible arrangements using a water-cooled lattice or a graphite, moderated, helium-cooled lattice behind the secondary target. These appear to be feasible arrangements but many aspects, such as the dimensional stability of the uranium plates, production estimates, and handling problems, remain to be examined.

Fixed-Dust Type Lattice. A study has been made of lattice arrangements with fuel rods located in passageways formed by external ribs. In this connection, the advantages and disadvantages of charging and discharging the fuel rods in the lattice area have been evaluated. The ribs in this scheme would also reinforce the vacuum vessel. Although this arrangement does not appear desirable, some features might be applied advantageously to the base case.

Packed-Bed Lattice with Spherical Fuel. A heat transfer and fluid flow study of the performance of a lattice with a packed bed of spherical fuel elements indicates feasibility of such a design. The heat load conditions in this type of lattice permit reasonable bed lengths and pressure drops. Work is continuing on mechanical layouts, the optimization of ball diameter and cladding, and the study of heat distribution.

Target Specifications

R. C. Gerber, L. B. Robbins, F. J. Duvall
CRDC

Handling and Storage

Preliminary design studies have been started on a handling and storage area to handle C-frames and rod crates from the lattice and plate assemblies from primary and secondary targets. Water shielding promises to provide the simplest type storage area and handling equipment. The water tank built around the targets, in the "base-case" design, would be extended to furnish sufficient area for cooling, storage, partial assembly and disassembly of the targets and C-frames.

Estimates have been made on shutdown heat loads for primary, secondary, and lattice targets as a function of time after removal from the operating position. The removed lattice C-frames can be effectively cooled by natural convection of water in the storage area tank. Work has been started on a forced water cooling system to remove heat from primary target plate assemblies.

The primary header design has been revised to provide for removal of plate assemblies while the outer tubes are left in place and vacuum seals remain tight. Containers are being designed to receive plate assemblies at the target, to maintain shutdown cooling and shielding, and to transport the assemblies to the storage area.

Vacuum Vessel

Preliminary design specifications for the vacuum vessel have been written to guide studies on its definite design. Work has been started to obtain weight estimates, to determine the shape, material, and location of supports and reinforcing members, and to determine the magnitudes and nature of possible deformations. Estimates have been completed on heat generation in vessel walls during accelerator operation and on the corresponding temperature distribution and thermal stresses in typical stiffening rings (published in CRD-TI-116).

14. MATERIALS RESEARCH

C. C. Woolsey, Jr., M. H. Boyer, W. E. Browning,
J. P. Frankel, H. Majors, Jr., R. B. Small
CRDC

Introduction

Progress in materials research at Livermore has been limited rather severely by the lack of laboratory facilities. Most work has been limited to extensive searching of the literature preparing for the experimental research work which will get under way as soon as these facilities become available. Some limited experimental work has been carried on with facilities at the Standard Oil Materials Laboratory and at the University of California Radiation Laboratory.

Reasonable success has been achieved in the fabrication of zirconium clad uranium fuel plates by edge welding techniques. The process involves the rolling of a sandwich of uranium and zirconium, jacketed in titanium killed steel evacuated prior to the heating and rolling. The resulting uranium-zirconium sandwich is sheared into strips of the desired size, and the edges are grooved by acid pickling, which removes the core material to a uniform depth. A zirconium-nickel alloy filler wire is placed in the groove and the edge is welded by the heliarc method. Use of the alloy filler wire was found necessary to reduce the melting point and thus reduce the uranium dilution of the weld head. This work has been performed by CR&D personnel at Oak Ridge National Laboratories.

In addition to numerous samples produced in developing welding techniques and for corrosion testing, a plate, 2-1/2 in. by 40 in. with 9 mils of cladding on both sides of a 0.047 in. uranium core, has been produced by this rolling and edge welding technique.

Resistance Cycler

Tests are continuing on uranium rods at various power levels so that a fatigue type curve may be obtained. Cycling conditions were: total cycle time, 150 milliseconds; duration of pulse, 50 milliseconds; duty cycle, 33-1/3 percent, pulse power input varied from maximum obtainable downward; coolant, distilled water at about 90° C, water velocity 17.7 ft./sec. For power levels of 48,44, and 40 kw/in^3, little change in number of cycles to failure was observed. Tests were then made at 30 and at 25 kw/in^3.

In the case of the 30 kw/in^3 run, a crack was noticed after about 16,000 cycles. At 262,000 cycles two spines were apparent and at 284,000 cycles the sample was very rough. As more spines appeared, it became apparent that the cross sectional area of the rod was decreasing, as indicated by an increase in electrical resistance; thus, the power density was

increasing since the input was being held constant. After 806,920 cycles, the power input was decreased in proportion to this change in resistance to bring the power density level to the intended 30 kw/in^3. Sample failure occurred at 862,120 cycles.

In the case of the 25 kw/in^3 run, power input adjustments were made daily to compensate for the change in resistance. The run was terminated after 2,134,800 cycles, with no failure indicated. The electrical resistance increased by a factor of nearly 4 and further running did not seem practical. The sample was very rough and badly splintered at the end of the run.

The next runs will be made at 30 and at 35 kw/in^3 with adjustments in power input to provide consistent data which can be used in plotting a fatigue curve.

15. A-12 CHEMICAL PROCESS STUDIES

Process Research

W. H. McVey, P. O. Amar, F. J. Brutschy, R. H. Gerke,
S. J. Horn, D. Lewis, K. L. Mattern, W. H. Ludewig
CRDC

Corrosion

Work was extended on the corrosion of stainless steels capable of being used for equipment to dissolve zirconium clad uranium or thorium elements. For simultaneous dissolution of both cladding and fuel, a mixture of 20 percent HNO_3 - 3 percent HF by weight gives satisfactorily rapid dissolution rates at 57° C for total hydrofluoric acid to zirconium ratios of 10 to 1; but all tank construction materials tested so far show corrosion rates > 500 mils/year in this solution at 57° C. Stainless steels of types 302, 304, 316, 321, and 347 have been tested. However, in preliminary tests 309 Cb and Durimet-20 have shown favorable corrosion.resistance. A status report on corrosion is being prepared.

Nitric Acid Recovery

A proposed solvent recovery system for the chelate process included an oxalic acid-nitric acid strip of zirconium from the waste organic-TBP stream before recycling this stream. The strip solution was to be combined with all other waste aqueous acid streams for nitric acid recovery by distillation. Experiments were carried out to determine if the recovered nitric acid would be contaminated with oxalic acid which could cause plutonium oxalate precipitation when recycled in the process.

It was found that the nitric acid could be distilled until the concentration of nitric acid in the still was 6 M without contamination of oxalic acid (limits of detection were 0.1 percent of total oxalic acid). No oxalate decomposition was observed under these conditions. However, at nitric acid concentrations of 8-9 M, there was considerable oxalate decomposition (~ 50 percent) and 1-2 percent of the total oxalic acid was found in the distillate.

Thorium-Uranium Separations

Calculations were made for a three column Thorex-type process flowsheet for the extraction, decontamination, and separation of thorium and uranium-233 from neutron irradiated fuel elements. This flowsheet is similar to a flowsheet proposed by ORNL except that a water scrub is used in place of an acid deficient aluminum nitrate scrub. Since previous experience, reported last quarter, has indicated a close correspondence between calculated and actual columns in this system, it is felt that the following calculations have real significance.

The conditions and calculated results are:

IA Column: 6 extraction stages
6 scrub stages

Feed: 1 Vol. 1.4 M $Th(NO_3)_4$,
0.0028 M $UO_2(NO_3)_2$
0.3 M HNO_3

Scrub: 0.6 vols. water

Extractant: 6 vols. 35 percent TBP
0.5 M HNO_3

Waste: 1.6 vols. 2×10^{-4} M Th,
2.17 M HNO_3
10^{-6} M U

IB Column: 6 scrub stages
6 extraction stages

Feed: 6 vols. 0.233 M Th
4×10^{-4} M U
0 M HNO_3

Extractant: 6 vols. 0.2 M HNO_3

Scrub: 1.2 vols. 35 percent TBP
0 M HNO_3

The Product: 0.233 M Th,
0.1 M HNO_3
10^{-7} M U

IC Column: 6 extraction stages

Feed: 6 vols. 35 percent TBP
10^{-7} M Th
4×10^{-4} M U
0.05 M HNO_3

Extractant: 2 vols. water

In addition to achieving excellent separation and recoveries for uranium and thorium, this scheme, of course, requires no solid salt or additional nitric acid for the scrub section of the 1A column. Since this system uses a low thorium distribution ratio in the scrub section, which allows thorium to reflux in the column, the distribution ratio of fission products should be lower also in the scrub section. This would result in more efficient scrubbing than is achieved in a salted scrub, provided certain fission products do not form highly organic extractable species at low acidities. Little data are available for calculating fission product and protactinium behavior, and these points will be investigated experimentally, as well as the actual stagewise Th-U behavior.

Uranyl Nitrate-Nitric Acid-TBP Interactions

The effect of nitric acid on the extraction of uranyl nitrate by TBP at high uranium concentrations has been investigated. It was found that the extraction of uranium is depressed by the addition of nitric acid in the high uranium range due to a competition between nitric acid and uranium for TBP. This effect is not evident at lower uranium concentrations since, far from saturation, the second power nitrate dependence on the extraction is nearly approximated and increasing nitrate ion concentration increases the extraction. A similar depression has been reported previously for thorium extraction by TBP.

Protactinium Extraction

The extraction of protactinium by TBP has been shown to follow a direct second order nitric acid concentration dependence. Since this is probably a combined hydrogen ion and nitrate ion dependence, it has not been possible to separate the effects, nor has it been possible to draw definite conclusions concerning the protactinium species in either phase from these data alone. Nitric acid concentrations in excess of five molar are required for extraction coefficients of the order of unity. The extraction of Pa-233 from thorium with TBP is not possible although thorium may be extracted from protactinium.

Dissolution of Zirconium and Uranium

The dissolution of zirconium clad uranium has been simulated. Attempts were made to dissolve metallic zirconium and uranium in nitric acid-hydrofluoric acid mixtures to give, on complete dissolution, a solution 1.35 M in uranium (UO_2^{++}), and 0.4 M in zirconium and hydrofluoric acid (ZrF^{+3}). The metals went readily into solution, though with some hydrogen gas evolution. However, most of the zirconium precipitated leaving the solution only 0.04 M in dissolved zirconium. The precipitate contained only zirconium and no uranium as shown by spectral analysis. The x-ray diffraction pattern did not correspond to that of either ZrO_2 nor ZrF_4. At the

present time the composition of this solid is unknown, though from steichiometric considerations alone a consistant formula is $Zr(OH)_n(NO_3)_{3-n}F$. Even though the first aqueous zirconium fluoride complex is very stable, that is

$$Zr^{+4} + HF = ZrF^{+3} + H^+, \quad K = 6 \times 10^5,$$

the solid is apparently stable in solutions in which the HF to Zr ratio is unity. A stable zirconium solution may be prepared by using higher HF to Zr ratios as has been observed elsewhere (ANL).

Both H_2SiF_6 and HBF_4 are as equally good sources of fluoride HF, though there is some silica precipitation in the case of H_2SiF_6.

Effects of High Energy Fission and Spallation Products

Because the presence of high energy fission and especially spallation products in deuteron bombarded uranium may necessitate considerable changes to existing separations techniques, some preliminary work has been done to evaluate these problems.

A uranium target which was bombarded with 350 Mev protons (actually performed for other than subject experiments) was subjected to a Purex separation. Because of an unduly long cooling period of six months, the only readily identifiable spallation product was thorium 228. Counting rates on fission products were too low to give conclusive results. As anticipated, thorium 228 tends to follow the plutonium. However, this may not be too serious because a decontamination factor in the order of 100 is all that is required.

A second uranium target was bombarded with 32 Mev alpha particles. After a 21 day cooling period, the Purex separation method showed iodine, zirconium, and ruthenium as the chief contaminents in the product stream. This is as one might expect. High energy fission products, such as tin and tellurium, did not contribute appreciably to the activity of the product stream although these were identified in this stream and particularly in the original uranium solution. Another experiment on the same materials was run after 45 days cooling to check the action of tellurium. Here again it was indicated that this element was not present in sufficient amount to be serious.

Higher current bombardment and shorter cooling period for the first target would have given more comprehensive information. Control of conditions, of course, will be possible in proposed future work.

Process Development

T. R. Hicks, J. L. Bloom, L. D. Christensen,
J. M. Davis, L. M. Guenther, J. Jost, R. A. Lewis,
A. L. Lindsay, R. W. Robinson, B. Rubin, G. R. Tully
CRDC

The Chelate Process

Process work was continued on the TTA chelation process for the recovery and decontamination of plutonium from Hanford material. Since niobium — 95 (which decays from zirconium — 95 during the zirconium transit time in the first column) limits the plutonium decontamination factor, the feed to the first column was scavenged with TTA to remove zirconium.

This feed was treated with ferrous ion and sulfamic acid to reduce plutonium to the unextractable plutonium (III) state. Zirconium is unaffected by this treatment and is extractable in the scavenging column, leaving the plutonium in the aqueous stream. The aqueous stream leaving the scavenging column was treated with nitrite to oxidize plutonium before being fed to the extraction column where the plutonium (IV) was extracted away from uranium and fission products.

In the first run, the use of carbon tetrachloride for a TTA carrier resulted in hydraulic difficulties which were not readily corrected in the existing equipment. In subsequent runs, secondary-butyl-benzene was substituted as the solvent and no further hydraulic difficulties were encountered. It was also discovered that excess nitrite in the extraction column feed reacted with the TTA causing malfunctioning of the plutonium extract on column. In later runs, steps were taken to destroy the excess nitrite.

Of the zirconium, 95 percent was removed in the scavenging column. Plutonium losses were 0.2 percent in the scavenging column and 0.3 percent in the extraction column. Since the re-extraction of plutonium has been successfully proven and since there were not enough mixer-settler stages to run a scavenging column, an extraction column, and a re-extraction column, the re-extraction column was not run.

Midi Mixer-Settler Prototype

A flexible midi-scale mixer-settler prototype has been assembled to aid in the design of future multi-stage midi-scale mixer-settlers. Studies of mixing and settling chamber designs, stirring speeds, and pump-paddle designs have already indicated significant improvements in mixer-settler designs.

Systems involving CCl_4 have hydraulics which differ from hydrocarbon systems. Physical designs and flow rates must take into account the hydraulics and slow separation of phases characteristic of CCl_4. The poor operating values for CCl_4 are manifest by a rise in the interface, followed by rapid cascading through stages of the heavy organic layer. Kerosene systems appear much easier to operate, displaying more predictable behavior and considerably less physical entrainment than CCl_4 systems.

Mini Mixer-Settler

The miniature mixer-settler, designed for small scale experimental separations on high activity samples, was assembled and is now being tested on cold solutions. The new pump mix paddles for the unit operated satisfactorily with hydrocarbon systems, but the interfacial tension and hydraulic effects of TBP-CCl_4 solutions prevented completely satisfactory operation with the CCl_4 system. A new mixing box on 3/8 in. scale was built and is now being tested with TBP-kerosene systems, where mixing, flow rate, and surface tension problems are less troublesome.

Horizontal Pulse Column

A novel experimental 5/8 in. by 18 in. laboratory model horizontal pulse column was successfully operated with a H_2O-CCl_4 system. The column acts as a series of mixer-settler stages giving good mixing and settling in each of the stages. At high pulse rates and low flow rates emulsification of the two phases occurred as expected, but at lower pulse rates and proper operating conditions the column is self compensating. A larger unit (1 in. x 4 ft.) of improved design has been built and is being tested.

Solution Agitation in Tanks

The feasibility of using air as a means of agitating tanks of 50 gal. capacity was studied and a suitable series of inlet tubes and conical baffles designed to give adequate mixing with small amounts of low pressure air.

Process Design

L. R. Michels, R. D. Chaffe, D. L. Fry, M. C. Feldman,
E. J. Haven, R. J. McCarter, H. Schneider,
J. L. Schuenemeyer, K. G. Steyer, J. W. Unverferth
CRDC

A study regarding methods of handling dissolver off-gases to avoid discharge of radioactive noble gases into the atmosphere was begun. Preliminary results indicate that the most economical method of operation is to dissolve in an oxygen atmosphere and to compress and store the entire off-gas output. This method differs from that considered for other A.E.C. installations in that H_2O destruction and charcoal absorption of the radioactive noble gases at low temperatures is not required. Further evaluation is contingent upon receipt of more detailed and reliable data on inert gas volume ratios.

A new type of horizontal pulsed liquid contactor has been proposed. A report is being prepared describing this contactor and its possible advantages for radioactive separations work. Preliminary designs were transferred to the Process Development Group for further development.

Work was initiated on preliminary process designs for the extraction of U-233 from long cooled, irradiated thorium by the ORNL, 23 Process (hexone solvent). A materials flowsheet for this process has been prepared.

A revised materials flowsheet based upon the ORNL Purex No. 3 flowsheet and including the necessary feed preparation, acid recovery, waste disposal, solvent recovery, and fuel recovery steps to give an integrated process flowsheet has been completed. Scoping efforts for a Purex-type chemical separations plant for an MTA facility are currently under way using the above work as a general guide. Preliminary to the scoping studies, equipment schematic and engineering flow diagrams are being developed for the various unit operations.

Uranium recovery from a Purex solvent extraction process is described in a recent report. In addition, the study of UNH decomposition has continued and a flowsheet similar to one in use by Hanford has been developed. The study is continuing to develop possible economic incentives for changing the batch type portions of the process to continuous.

A graphical method has been developed for assisting in the calculation of equilibrium relationships in solvent extraction contactors in the extraction of uranium and nitric acid from uranyl nitrate - nitric acid - water systems with tributyl phosphate - kerosene solvent mixtures. This method makes use of the Moore equation which expresses uranium and nitric acid distribution coefficients in terms of aqueous phase nitrate ion concentration and organic phase, uncomplexed tributyl phosphate concentration.

A number of economic studies by the Process Design Group on various process alternatives have continued with the following results:

(a) The effect of A-12 operating costs vs. g/t level in the lattice for the base case over the range of uranium fuel costs from $10 to $30 per pound has been initiated. Preliminary results indicate a considerable incentive for operating at higher g/t levels in the lattice.

(b) Assuming product inventory as capital with delayed return, the yearly operating costs for a new MTA case, similar to the base case except for a lithium alloy lattice, were estimated to be about 2 percent less than the base case (metal costs neglected).

(e) The economic comparison between the proposed Chelate process and the Purex process is being modified in the light of recent cost information obtained on the Hanford Redox plant.

Technical assistance has been given the groups charged with the design of the Livermore site Waste Disposal Facility. Drawings, (Equipment Schematic Flowsheet, and Materials Flowsheet) for the facility have been prepared to serve as a preliminary basis for design. Preliminary design of the Waste Facility evaporators and deentrainment towers has been completed.

Detailed drawings for all process tankage in the cells of the Unit Operations Laboratory have been completed. Design specifications for the solvent extraction pulse columns have been forwarded to the Process Engineering Division. Work is continuing on the development of materials handling devices, sampling techniques, flow control schemes, and instrumentation

A three day visit to the Hanford Works was made in April by Messrs. H. W. Crandall, A. C. Miller, L. R. Michels, R. J. McCarter, and E. J. Haven. The Redox and Metal Recovery plants were inspected. Design, operating and cost information was obtained on these and allied processes. Scoping work on various projected Purex alternatives was reviewed.

The Process Design Group's representatives assigned to Oak Ridge have investigated the problems of decontamination fluid recovery and INT-23 plant operation and have kept abreast with process developments from that site.

16. ELECTRON MODEL CLOVERLEAF CYCLOTRON STUDIES

Electron Model II

Robert V. Pyle
UCRL

It was mentioned in the preceding report that rod type dees do not provide the field-free regions necessary for space charge neutralization, and that solid tips, 100° wide at their outer radius, had been cut from 6 in. radius disks and attached. The beam was clipped vertically from 3 in. to 5 in. radii and examined for possible defocusing effects at the transition radius of 6 in. There did appear to be a tendency for the beam to blow up vertically at about 6 in.

This examination was made with the clipping gap fixed and has been repeated with adjustable clippers on the chance that the beam was not being started in the magnetic median plane. It was in fact found that with proper positioning of the clipping gap, there was no indication of defocusing of the beam at 6 in. radius. The threshold was also determined and found to be slightly lower than without the solid tips, presumably because of the larger energy gain per turn at small radii.

Another attempt was made to investigate the effects of accelerating systems which tend to drive the orbits off center. The electrode system consisted of three sets of rod dees, one in each volley, connected at 6 in. radius to two solid 180° dees. Two rod dees were connected to a single 180° section in this arrangement. We were unable to accelerate electrons beyond a radius of 8 in.

A single, solid 90° dee was then installed. This had the same energy gain per turn (1.3 V_0) and the same impulse tending to drive the orbits off center as the dees described in the preceding paragraph, but without the complication of the change in dee structure at 6 in. The threshold peak rf voltage for accelerating electrons to full energy was 500 V, or about three times the dee to ground voltage necessary in a three phase system with the same energy gain per turn. The orbits could be well centered by appropriate adjustment of the "C-term" coils, but the radial oscillations were large, about 1/2 in. at the larger radii.

An attempt was made to excite rod dees at a frequency three times the cyclotron frequency, but considerable difficulty was experienced in the tuning and tailoring of the dees to get reasonable voltage distributions, and this project was abandoned in favor of beam extraction techniques.

A segment of maximum depth 2-1/2 in. and with a chord length of 24 in. was cut from each of the poles at one of the hills to provide removable pieces of iron in which magnetic channels could be machined. A channel designed by H. Keller was cut in these pieces, and the spill beam distribution was examined with fluorescent probes. Several modifications of the magnetic field appeared to be desirable and are being made.

Electron Model III

E. L. Kelly
UCRL

The new electron model construction has been largely completed. The tank and poles have been assembled and magnetic measurements started. The vacuum system is 95 percent completed and should be ready for testing soon. Design work on the dees is complete and construction started. The electronics installation is on schedule and should be ready and tested by the time it is needed.

Preliminary results indicate the magnetic field before shiming is within one percent of the theoretical values desired. Operational data should be available by the end of the next quarter.

17. 20-INCH CYCLOTRON PROJECT

Mark Jakobson and Lawrence Ruby
UCRL

Off Center Source

Through advice from the cyclotron group at Oak Ridge, the ion source was moved to a radius of 1-3/4 inches and adjacent to one dee. A hood patterned after an Oak Ridge design was used over the arc. Considerable work was done to find a good injection radius, source, and dee slit design. With the geometry as shown in Fig. 1 it is typical to have between 6 and 7 ma. at 1 Mev. This current does not change with 450 volts of d.c. positive bias on the probe. However, when the current probe is moved into 6 inches, the beam begins to increase rapidly and is lowered by positive bias on the probe, indicating some loss of electrons by secondary emission. The beam is a linear function of the d.c. input power, of which about 40 kv is available, and also of the rf voltage, of which up to about 30 kv is held when loaded.

Neutralizing Lines Added

The amount of inter-dee coupling and consequent instability in the servo system was very sensitive to either removing any part of the dee shields or changing the size of the dee tips. Some improvement was secured by adding a variable speed of response to the servos in the form of an adjustable coupling pulley system between the servo motors and dee tuning capacitors. However, the problem was effectively solved only when a neutralizing system was installed. This involved a set of inductively coupled transmission lines between each dee stem. The coupling loop on one end of each transmission line is rotated by a motor controlled from the console. By exciting one dee only and adjusting the neutralizing loops, the voltage appearing on either of the other dees can be reduced to less than 5 percent. The process is then repeated by exciting only the second dee and further adjusting. When the third dee alone is excited, it is found that the system is already neutralized, i.e., no induced voltages appear, and this is used as a check. The entire operation must be done at atmospheric pressure to prevent small induced voltages from being obscured by ion-lock. It takes about 45 minutes to let the cyclotron down to nitrogen, neutralize, and pump down again. This would be impractical on a large machine and a new method for neutralizing is now being designed.

At times there was considerable sparking and it was repeatedly necessary to restore the excitation which was removed by the rf-dc fault circuit. Hence, a recycler was added which would do this automatically, after a time delay which could be set by the operator. Recycling would often be repeated continuously requiring several attempts before the rf came on, especially if the voltage was high, and it was found that during this period the servos received spurious signals and tended to creep away. So, an additional time delay was added, also adjustable, which would deactivate the servos during the recycling periods and until the rf had been on a short while.

At high beam levels, the servos picked up, in addition to the rf signal, a large quantity of "arc hash". This "hash" has considerable audio component and rendered the servos inoperable. A special filter network added to the servo amplifiers was necessary to eliminate this interference.

Settings of the tuning capacitors are quite different for operating with high beams and operating with no beam (due to change of capacity with heating of the dees), so that shutting down after having the beam on requires retuning before the rf can be made to come on again. A device to do this automatically is now being designed.

Further details of the rf system are to be found in the report UCRL-1884 by B. H. Smith.

After about 8 months of operation, the deposit of cracked oil on the dees and inside the tank had increased to such an extent that it became difficult to hold full voltage on the dees. A glow discharge would occur in the tank. The liners, dees and probe were then removed and sand blasted to remove the deposit. This eliminated the glow discharge in the tank.

Programming the Beam

It has been possible to program the beam for two complete turns by putting graphite slits on the dees. No decrease in the beam at large radii was observed. The first turn passes over the center of the cyclotron and misses one dee entirely, then comes around and skirts the ion source. The programming slits run cool only through a narrow range of rf voltage. Figure 2 is a plot of the ion paths for the first two turns.

Unfinished Experiments

One of the questions still unanswered at the end of the operating period is that of the effect of the beam coupling on the phase of the dee voltages. The resistive component of the beam load will reduce the Q of the tank and reduce the problem of phase control, since low Q circuits are easier to control than high Q circuits. The effect of the reactive component of the beam is more obscure and difficult to predict. The operation of the machine has indicated no effect other than the phases appear slightly more stable with the beam on than off. This would indicate either the reactive component is negligible for beam levels of the 20-inch, or that it is not detrimental.

The difficulty associated with neutralising with the tank at air has been described above. An alternate method which has been suggested but not completed would be to neutralize under vacuum at high voltages. This would be done by modulating the 2E26 buffer plate on one dee with 60 cycles, and then adjusting the neutralization until the 60 cycle component on the other two dees would be a minimum. This would be done successively for the other two dees.

IV. SUMMARY OF INFORMATION OBTAINED WITH THE 20-INCH CYCLOTRON

A hooded arc operated 1-1/2 inches off center has provided the most beam with a minimum of rf power lost in defocused beam. A curved accelerating slit to pull out the ions is attached to B dee. The hood helps to shield portions of the plasma from the rf fields. Off-center operation provided a better focusing geometry for the starting ions. The first few turns in the cyclotron are discrete and off center about 3/4 inch. They can be made to pass through accelerating slits on the dees with negligible loss in beam.

A phase control system has been necessary for satisfactory operation. In addition, in order to operate the cyclotron with no hunting of the phase control system, and equal dee voltages, it has been necessary to neutralize the dee-to-dee capacity. Even with the neutralizing lines, there is a slight asymmetry in the dee voltages due to the fact the accelerating slit for the source is attached to B dee. As a result B amplifier is more heavily loaded. With a larger machine, this extra load should have less effect.

Stable operation has been maintained with 6 ma of 1 Mev protons for dee voltage of 28 kv. From the programmed orbits the gain in energy per turn has been found to be about 2.5 eVo. By changing the phase sequence from ABC to ACB and using deuterium gas in the source, 6.5 ma of 0.5 Mev deuterons have been obtained. Similarly, using helium gas in the source, 1.5 ma of 1 Mev alpha particles were obtained. The gain in energy per turn for this mode is approximately 5 eVo. A more complete report on the operation of the 20-inch cyclotron is given in UCRL-1889.

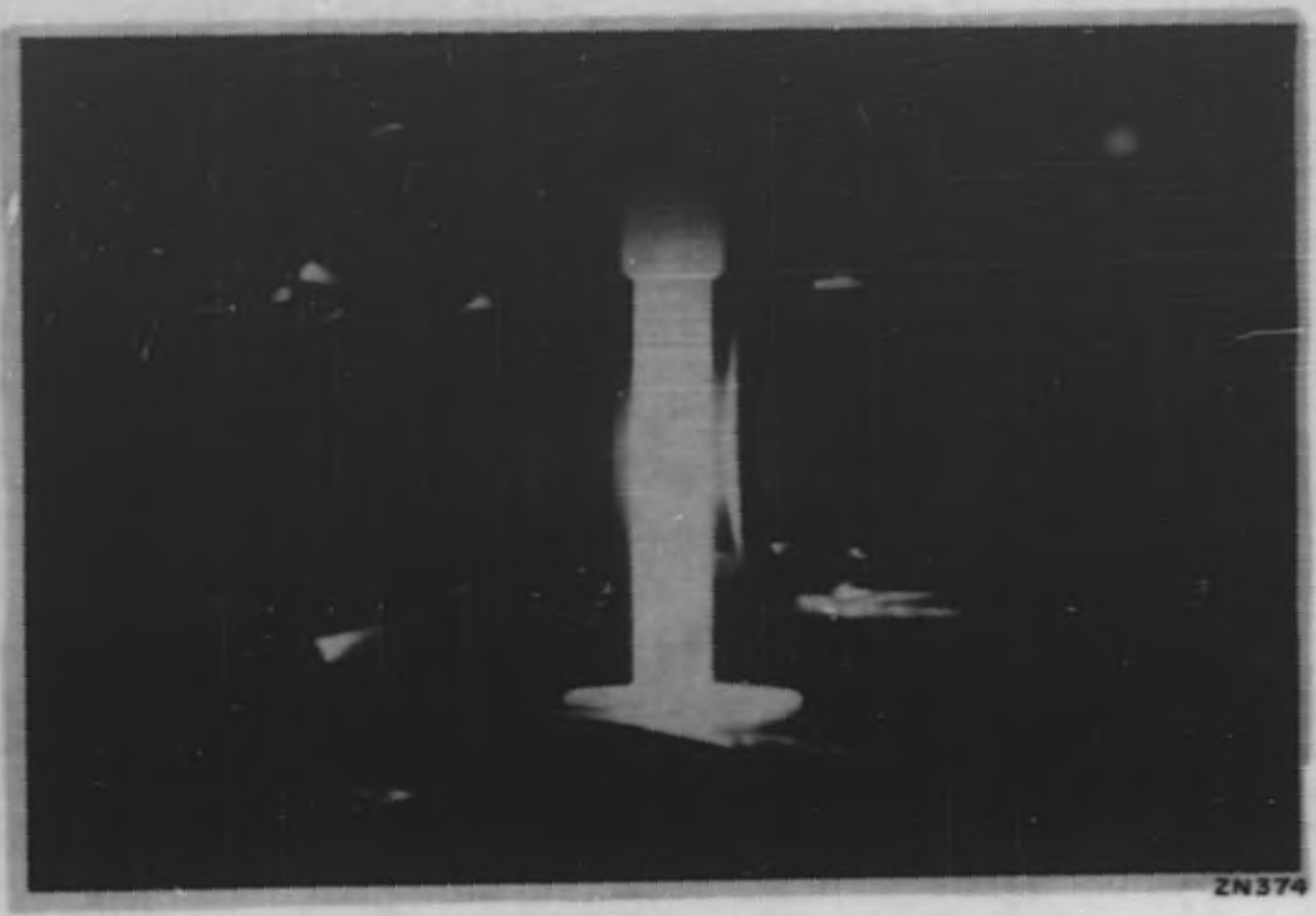

Fig. 1 Sec. 17

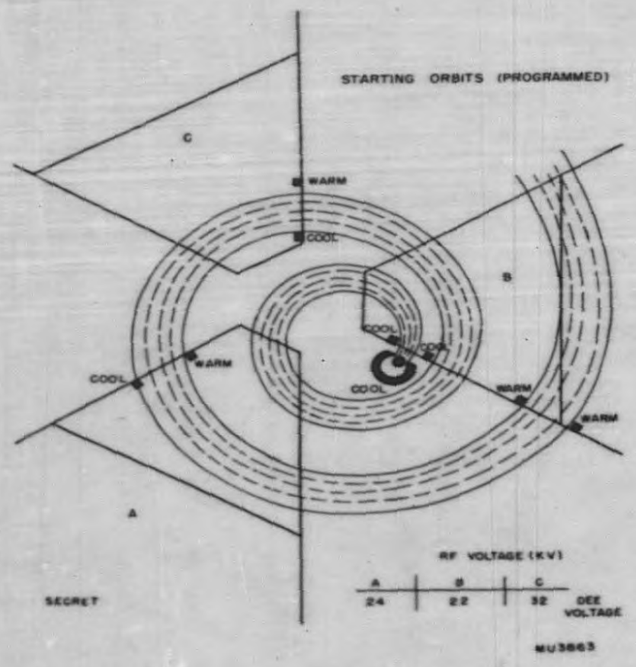

Fig. 2 Sec. 17

1903-183/182

END